People`s Democratic Republic of Algeria

Ministry of Higher Education and Scientific Resea

University of Echahid Hamma Lakhdar - El Oued

Faculty of Technology

Department of Electrical Engineering

Dissertation

ACADEMIC MASTER

Domain: Science and Technology

Department: Electrical Engineering

Specialty: Telecommunication

Presented by:

TLILI MOHAMED JAMALOUDDINE

Entitled:

Performance Investigation of Reconfigurable Intelligent Surfaces (RIS) in Wireless Communication Systems

Dissertation Submitted in Partial Fulfillment of the Requirements for the Master II Degree in Communication Systems

Publicly defended in: 29/05 /2025

Board of Examiners:

Dr. GHENDIR Said	**Chairman**
Dr.TOUHAMI Ridah	**Examiner**
Pr. KHELIL Abdelatif	**Supervisor**

Academic Year: 2024/2025

Abstract

This work explores the technical evolution of mobile networks from the first generation (1G) to the prospective seventh generation (7G), with a focus on Reconfigurable Intelligent Surfaces (RIS) and Non-Orthogonal Multiple Access (NOMA). It analyzes the performance of RIS-NOMA systems in complex wireless communication environments, comparing outage probability, system capacity, and bit error rate (BER) against decode-and-forward (DF) cooperative NOMA systems. The results demonstrate the superiority of RIS-NOMA, achieving an outage probability as low as $10^{-4.4}$ and a BER of $10^{-4.8}$ at 30 dB SNR, particularly with an increased number of RIS elements. This work highlights implementation challenges, such as interference cancellation complexity and energy consumption, and provides recommendations for design optimization and future research. This work offers valuable insights into the role of emerging technologies in shaping the future of wireless communications.

Keywords: Mobile Networks, Sixth Generation (6G), Seventh Generation (7G), Reconfigurable Intelligent Surfaces, Non-Orthogonal Multiple Access, Spectral Efficiency, Outage Probability, Bit Error Rate, Wireless Communications.

Résumé

Ce travail examine l'évolution technique des réseaux mobiles, de la première génération (1G) à la vision prospective de la septième génération (7G), en mettant l'accent sur les surfaces intelligentes reconfigurables (RIS) et l'accès multiple non orthogonal (NOMA). L'étude analyse les performances des systèmes RIS-NOMA dans des environnements de communication sans fil complexes, en comparant la probabilité d'interruption, la capacité du système et le taux d'erreur binaire (BER) avec les systèmes NOMA coopératifs avec relais de décodage et retransmission (DF). Les résultats montrent une supériorité des systèmes RIS-NOMA, avec une probabilité d'interruption réduite à $10^{-4.4}$ et un BER de $10^{-4.8}$ à 30 dB de SNR, particulièrement avec un nombre accru d'éléments RIS. Ce travail met en lumière les défis d'implémentation tels que la complexité de l'annulation des interférences et la consommation énergétique, tout en proposant des recommandations pour l'optimisation du design et les recherches futures. Ce travail constitue une contribution précieuse à la compréhension du rôle des technologies émergentes dans la transformation des communications sans fil.

Mots-clés : Réseaux mobiles,Sixième génération (6G),Septième génération (7G), Surfaces intelligentes reconfigurables, Accès multiple non orthogonal, Efficacité spectrale, Probabilité d'interruption, Taux d'erreur binaire, Communications sans fil.

الملخص

يستعرض هذا العمل التطور التقني لشبكات الهاتف المحمول من الجيل الأول (1G) إلى الرؤى المستقبلية للجيل السابع(7G) ، مع التركيز على تقنيات الأسطح الذكية القابلة لإعادة التهيئة (RIS) والوصول المتعدد غير المتعامد .(NOMA) يتناول العمل أداء أنظمة RIS-NOMA في بيئات الاتصالات اللاسلكية المعقدة، مع تحليل مقارن لاحتمالية الانقطاع، سعة النظام، ومعدل الخطأ في البت مقارنةً بأنظمة NOMA التعاونية بترحيل فك التشفير وإعادة الإرسال .(DF) أظهرت النتائج تفوق RIS-NOMA في تحسين الكفاءة الطيفية وتغطية الإشارة، خاصة مع زيادة عدد عناصرRIS ، حيث انخفضت احتمالية الانقطاع إلى $10^{-4.4}$ وسجل معدل الخطأ في البت $10^{-4.8}$ عند SNR=30 ديسيبل. يقدم العمل رؤى حول تحديات التنفيذ مثل تعقيد إلغاء التداخل واستهلاك الطاقة، مع توصيات لتحسين التصميم والبحث المستقبلي. يُعد هذا العمل مساهمة قيمة في فهم دور التقنيات الناشئة في تشكيل مستقبل الاتصالات اللاسلكية.

الكلمات المفتاحية :

شبكات المحمولة، الجيل السادس , الجيل السابع , الأسطح الذكية القابلة لإعادة التهيئة، الوصول المتعدد غير المتعامد الكفاءة الطيفية، احتمالية الانقطاع، معدل الخطأ البتي، الاتصالات اللاسلكية.

اهداء

أهدي هذا العمل إلى كل الباحثين والمبتكرين الذين يسعون لتطوير تقنيات الاتصالات اللاسلكية، وإلى أسرتي وأصدقائي الذين دعموني بلا كلل في هذه الرحلة شكرًا لجهود جميع الذين ساهموا في تحقيق هذا الإنجاز.

Acknowledgments

First and foremost, I express my gratitude to Almighty God for granting me the strength and guidance to complete this work.

I extend my deepest thanks to my supervisor,Pr.KHELIL Abdelatif, for their invaluable guidance, continuous support, and insightful feedback throughout this research journey.

I am also grateful to the faculty members of the Faculty of Technology for their knowledge and encouragement, which enriched my academic experience.

My heartfelt appreciation goes to my family for their unwavering support and endless encouragement.

Finally, I thank my colleagues and friends who provided inspiration and assistance along the way.

This work would not have been possible without their contributions.
With sincere gratitude,

TLILI MOHAMMED JAMALOUDDINE

List of Figures

List of Tables

List of Abbreviations

Abbreviation	Definition
1G	First Generation
2G	Second Generation
3G	Third Generation
4G	Fourth Generation
5G	Fifth Generation
6G	Sixth Generation
7G	Seventh Generation
AI	Artificial Intelligence
AMPS	Advanced Mobile Phone System
AUSF	Authentication Server Function
BCI	Brain-Computer Interface
BER	Bit Error Rate
BTS	Base Transceiver Station
CDMA	Code Division Multiple Access
CSK	Color Shift Keying
DF	Decode-and-Forward
eMBB	Enhanced Mobile Broadband
EDGE	Enhanced Data Rates for GSM Evolution
eURLLC	Enhanced Ultra-Reliable Low-Latency Communications
EPC	Evolved Packet Core
FDMA	Frequency Division Multiple Access
FR1	Frequency Range 1 (sub-6 GHz)
FR2	Frequency Range 2 (mmWave, 24-52 GHz)
GGSN	Gateway GPRS Support Node
GPRS	General Packet Radio Service
GSM	Global System for Mobile Communications
HAPS	High-Altitude Platform Systems
HLR	Home Location Register
HSPA	High-Speed Packet Access
IM/DD	Intensity Modulation/Direct Detection
IMT-2020	International Mobile Telecommunications 2020 (5G)
IMT-2030	International Mobile Telecommunications 2030 (6G)
IoT	Internet of Things
ISAC	Integrated Sensing and Communication
ITU	International Telecommunication Union
KPI	Key Performance Indicator
LEO	Low Earth Orbit
LiFi	Light Fidelity
LTE	Long-Term Evolution
MIMO	Multiple Input Multiple Output
mMTC	Massive Machine-Type Communications
MMSE	Minimum Mean Square Error
MSC	Mobile Switching Center
NGMA	Non-Orthogonal Grant-Free Multiple Access
NIM	Negative Index Material
NLoS	Non-Line-of-Sight
NOMA	Non-Orthogonal Multiple Access
NR	New Radio
OAM	Orbital Angular Momentum

List of Abbreviations

Abbreviation	Definition
OFDM	Orthogonal Frequency Division Multiplexing
OFDMA	Orthogonal Frequency Division Multiple Access
OOK	On-Off Keying
OWC	Optical Wireless Communication
Pbps	Petabit per Second
PLS	Physical Layer Security
PPM	Pulse Position Modulation
PSTN	Public Switched Telephone Network
QKD	Quantum Key Distribution
RAN	Radio Access Network
RIS	Reconfigurable Intelligent Surface
RNC	Radio Network Controller
RSMA	Rate-Splitting Multiple Access
SC-FDMA	Single Carrier Frequency Division Multiple Access
SCMA	Sparse Code Multiple Access
SDN	Software-Defined Networking
SGSN	Serving GPRS Support Node
SIC	Successive Interference Cancellation
SINR	Signal-to-Interference-plus-Noise Ratio
SMF	Session Management Function
SNR	Signal-to-Noise Ratio
Tbps	Terabit per Second
TDMA	Time Division Multiple Access
THz	Terahertz
UE	User Equipment
UM-MIMO	Ultra-Massive Multiple Input Multiple Output
UMTS	Universal Mobile Telecommunications System
UPF	User Plane Function
URLLC	Ultra-Reliable Low-Latency Communications
VLC	Visible Light Communication
VoLTE	Voice over LTE
WCDMA	Wideband Code Division Multiple Access
WRC	World Radiocommunication Conference

Chapter I

Technical Evolution of Mobile Networks

General Introduction

Wireless communication systems stand at the forefront of technological innovation, driving unprecedented connectivity and shaping the future of global communication networks. The rapid evolution of mobile networks, from the rudimentary analog systems of the first generation (1G) to the sophisticated, AI-empowered architectures of the fifth generation (5G), has transformed how societies interact, work, and access information. As the demand for higher data rates, ultra-low latency, and massive device connectivity continues to escalate, emerging technologies such as Reconfigurable Intelligent Surfaces (RIS) and Non-Orthogonal Multiple Access (NOMA) are poised to redefine the paradigms of wireless communications, particularly in the context of sixth-generation (6G) and prospective seventh-generation (7G) networks. These advancements promise to address critical challenges such as spectrum scarcity, interference management, and energy efficiency, paving the way for intelligent, immersive, and sustainable communication ecosystems.

This work aims to investigate the performance of RIS-aided NOMA systems in enhancing wireless communication in complex propagation environments. By leveraging the unique capabilities of RIS to dynamically optimize signal propagation and NOMA to improve spectral efficiency, this work seeks to provide a comprehensive analysis of key performance metrics, including outage probability, system capacity, and bit error rate (BER). Through a systematic exploration of mobile network evolution, theoretical foundations of RIS and NOMA, and rigorous performance evaluations using Nakagami-m fading channels, this work elucidates the transformative potential of these technologies in next-generation networks. The research compares RIS-NOMA systems against decode-and-forward (DF) cooperative NOMA systems, highlighting the scalability and efficacy of RIS in mitigating interference and enhancing connectivity, particularly in non-line-of-sight (NLoS) scenarios. Additionally, it addresses implementation challenges, such as interference cancellation complexity and energy consumption, and offers recommendations for design optimization and future research directions.

This work is structured into three main chapters. The first chapter traces the technical evolution of mobile networks from 1G to the envisioned 7G, providing a chronological analysis of advancements in radio access technologies, network architectures, and key performance indicators. The second chapter establishes the theoretical framework, delving into the principles of RIS, NOMA, and statistical fading models, with a focus on their roles in addressing spectrum and propagation challenges. The third chapter presents a detailed performance analysis of RIS-aided NOMA systems, deriving closed-form expressions for critical metrics and validating them through simulations. This work concludes with a synthesis of findings, underscoring the potential of RIS-NOMA systems to shape the future of wireless communications and identifying avenues for further investigation. Through this work, we aim to contribute to the academic conversation on intelligent and efficient communication systems, offering insights that bridge theoretical advancements with practical applications in the pursuit of next-generation connectivity.

I.1 Introduction

Mobile networks have revolutionized global communications, evolving from rudimentary analog systems (1G) to sophisticated digital architectures (5G) that interconnect billions of devices. This technical evolution represents one of the fastest and most significant technological transformations in modern history, fundamentally redefining how we communicate, work, and interact with the world around us [1].

Each generation of mobile networks has introduced significant technological advancements, enhancing data rates, reducing latency, and improving spectral efficiency. The first generation (1G) enabled basic mobile voice communications, while the second generation (2G) marked the transition to digital systems, introducing SMS and limited mobile data capabilities. The third generation (3G) truly marked the beginning of the mobile internet era, followed by the fourth generation (4G), which enabled high-definition video streaming and real-time applications. The fifth generation (5G), currently being deployed, offers unprecedented capabilities for the Internet of Things (IoT), ultra-reliable low-latency communications, and enhanced mobile broadband [2].

The sixth generation (6G), scheduled for deployment by 2030, promises intelligent connectivity through innovations such as terahertz (THz) frequency bands, reconfigurable intelligent surfaces (RIS), and integrated artificial intelligence (AI) [3]. Beyond that, the seventh generation (7G) envisions quantum and neuromorphic paradigms that could radically transform our conception of wireless communications [4].

This chapter examines the technical evolution of mobile networks, provides an in-depth analysis of 5G (including New Radio, NR), explores emerging 6G technologies (such as NOMA, RSMA, NGMA, QKD, ISAC), compares generational advancements, and outlines a prospective vision for 7G. This chronological exploration allows us to understand not only the technical progress made but also to anticipate the challenges and opportunities that will shape the future of mobile communications.

I.2 Fundamentals of Wireless Communications

Wireless communications facilitate data transmission through electromagnetic waves across allocated frequency bands, ranging from kilohertz (kHz) to terahertz (THz). Cellular networks partition geographic areas into cells, each served by base stations, to optimize coverage and capacity. Key performance indicators (KPIs) such as data rate, latency, spectral efficiency, connection density, and reliability are critical metrics for assessing network performance. Radio access technologies (e.g., FDMA, TDMA, CDMA, OFDMA, NOMA) and network architectures (centralized, distributed, virtualized) have evolved to meet escalating demands [5]. This chapter examines the technical evolution of mobile networks, providing comparative insights across generations.

I.3 Technical Evolution of Mobile Network Generations

I.3.1 First Generation (1G): Technologies and Performance

- **Technologies:** Launched in the 1980s, 1G networks employed analog systems, such as the Advanced Mobile Phone System (AMPS), with Frequency Division Multiple Access (FDMA). Channels were allocated at 30kHz bandwidth, using frequency modulation (FM) for voice transmission[6]
- **Performance:** Peak data rates reached 2.4kbps, with no support for digital data. Voice quality was susceptible to interference.
- **Technical Limitations:** Lack of encryption, poor spectral efficiency, and incompatibility among standards (e.g., AMPS, NMT, TACS).

I.3.1.1 1G Network Architecture

The architecture of a basic mobile telecommunications system is shown in Figure I.1. .

- **Public Communications Switching Network:** Connects the mobile network to the Public Switched Telephone Network (PSTN), enabling calls to be made to landline phones.
- **Mobile Telecommunications Switching Office:** Central hub for call routing between base stations and the public network.

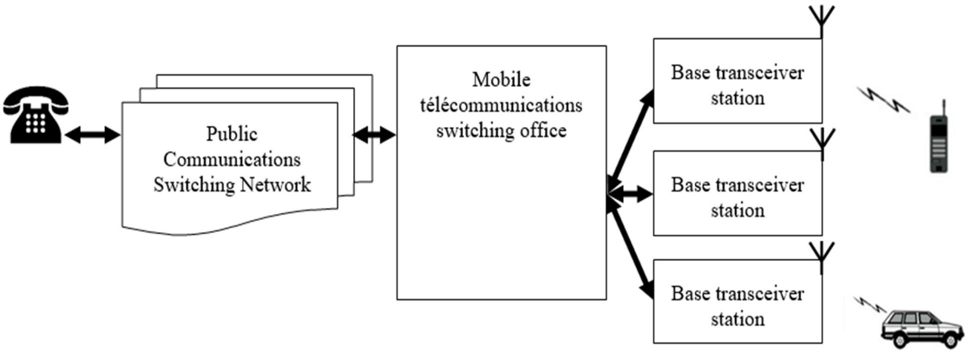

Figure I.1: 1G Cellular Network Architecture[6]

- **Base Transceiver Station (BTS):** Manages radio communication with mobile devices (e.g., phones, cars) over the air interface .

I.3.2 Second Generation (2G): Digitalization, GPRS, and EDGE

- **Technologies:** Introduced in 1991, 2G networks adopted digital transmission, utilizing Global System for Mobile Communications (GSM) with Time Division Multiple Access (TDMA) and IS-95 with Code Division Multiple Access (CDMA). Operating in 900/1800 MHz bands, channels were allocated a 200kHz bandwidth [7].

- **General Packet Radio Service (GPRS, 2.5G):** Deployed in 1997, GPRS enabled packet-switched data transmission using unused GSM time slots. Employing Gaussian Minimum Shift Keying (GMSK) modulation, it achieved theoretical peak data rates of 171.2kbps with four time slots [8].

- **Enhanced Data Rates for GSM Evolution (EDGE, 2.75G):** Introduced in 2003, EDGE utilized 8-Phase Shift Keying (8-PSK) modulation to achieve data rates up to 384kbps, enhancing spectral efficiency compared to GPRS [9].

- **Performance:** GSM offered data rates up to 64kbps, GPRS up to 171.2kbps, and EDGE up to 384kbps, with latency around 500 ms and spectral efficiency of approximately 0.5 bits/s/Hz [9].

- **Advancements:** Introduction of encryption (A5/1), Short Message Service (SMS), roaming, and initial data services (GPRS, EDGE).

- **Technical Limitations:** Insufficient data rates for multimedia applications and high latency.

I.3.2.1 GSM and GPRS architecture

The system supports both circuit-switched (voice via PSTN) and packet-switched (data via GPRS backbone) services, with the GGSN linking to the Internet or corporate networks. This architecture, as shown in Figure I.2, enables GSM for voice and GPRS for data, providing a foundation for later mobile technologies, such as 3G and 4G [10].

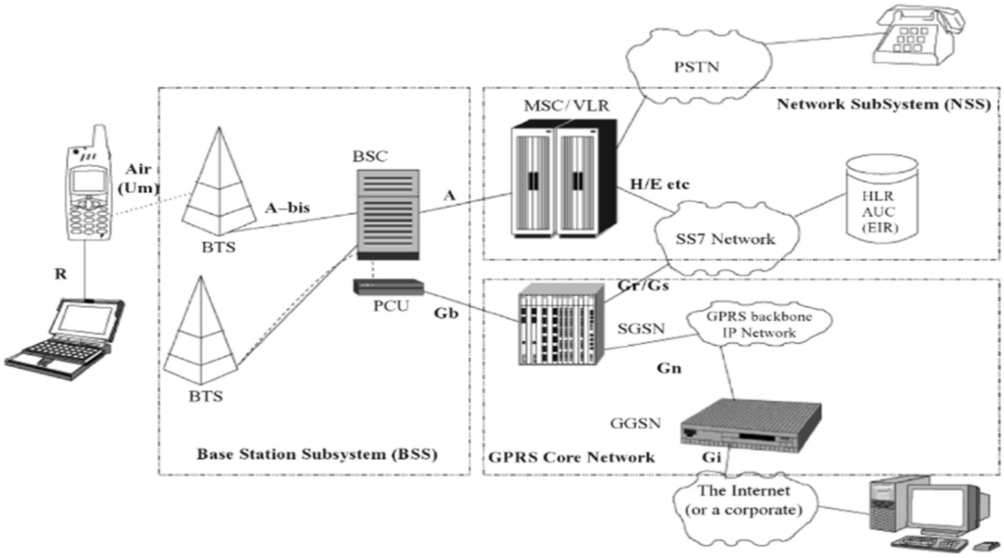

Figure I.2: GSM and GPRS architecture[10]

I.3.3 Third Generation (3G): Multimedia and Connectivity

- **Technologies:** Deployed in 2001, 3G networks utilized Universal Mobile Telecommunications System (UMTS) with Wideband Code Division Multiple Access (WCDMA) and CDMA2000, operating in 5MHz bands (1.9-2.1 GHz). High-Speed Packet Access (HSPA/HSPA+) further enhanced performance [11].

- **Performance:** Data rates reached 2Mbps (UMTS) and 14.4Mbps (HSPA), with a latency of $100 - 200$ ms and a spectral efficiency of $1 - 2$bits/s/Hz.

- **Advancements:** Support for video calls, mobile internet, and improved Quality of Service (QoS).

I.3.3.1 Comparison of 3G with 2G

- **Technologies:** Transition from TDMA/CDMA to WCDMA improved spectral efficiency and capacity. Wider 5MHz bands replaced 200kHz channels [11].

- **KPIs:** Data rates increased approximately 30-fold (2 Mbps vs. 64kbps), latency reduced (100 ms vs. 500 ms), and spectral efficiency doubled.
- **Advancements:** Multimedia support (video, web browsing) compared to voice/SMS in 2G.
- **Technical Limitations:** High energy consumption, uneven coverage, and elevated infrastructure costs.

I.3.3.2 3G network architecture

The UMTS network architecture, as shown in Figure I.3, is a 3G standard that comprises a Radio Access Network (RAN) with User Equipment (UE), Base Stations (Node B), and Radio Network Controllers (RNC), which manage radio resources and handovers. The 3G Core Network comprises the 3G-SGSN and 3G-GGSN for packet-switched data, the MSC and GMSC for circuit-switched voice, and the HLR for subscriber data, all of which connect to external networks, including the Public Switched Telephone Network (PSTN) and the Internet Protocol (IP) network. This structure supports enhanced data rates and seamless mobility compared to 2G systems [12].

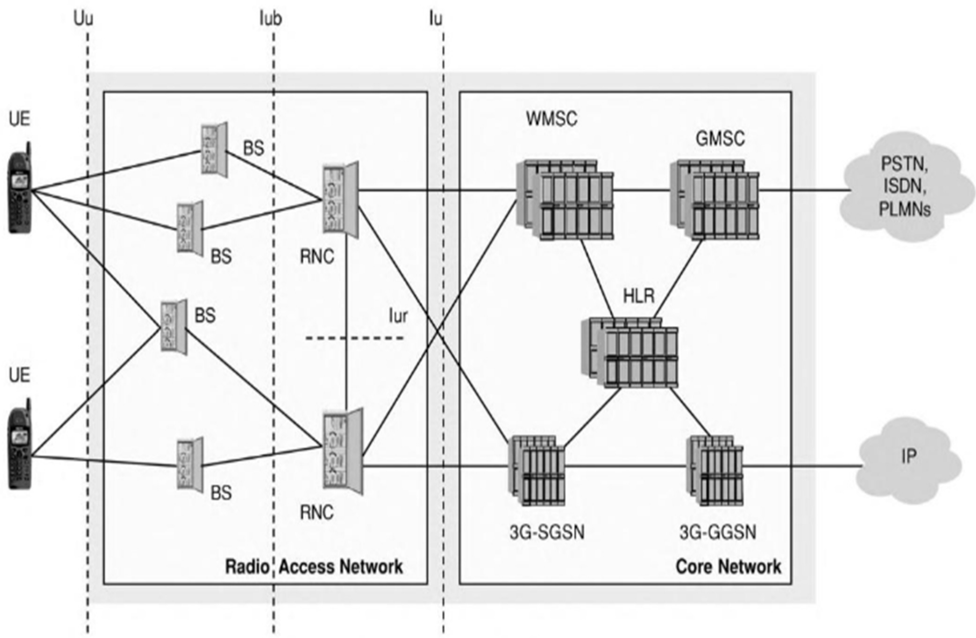

Figure I.3: UMTS Network architecture[12]

I.3.4 Fourth Generation (4G): High-Speed Mobile Broadband

- **Technologies:** Introduced in 2009, 4G networks leveraged Long-Term Evolution (LTE) and LTE-Advanced, employing Orthogonal Frequency Division Multiple Access (OFDMA) for downlink and Single Carrier FDMA (SC-FDMA) for uplink. Multiple Input Multiple Output (MIMO) configurations (2×2 and 4×4) and carrier aggregation were implemented, operating in the 700MHz to 2.6GHz frequency bands [13].
- **Performance:** Peak data rates reached 1 Gbps (stationary) and 100Mbps (mobile), with a latency of $20 - 50$ ms and a spectral efficiency of $5 - 10$bits/s/Hz.
- **Advancements:** All-IP architecture, high-definition (HD) streaming, and online gaming.

I.3.4.1 4G LTE architecture

The architecture, as shown in Figure I.4, uses an all-IP network, enabling high-speed data, voice (via VoLTE), and multimedia services with low latency. The eNode-B connects to the core network (EPC - Evolved Packet Core) via the S1 interface, while the MME, S-GW, and P-GW interact to manage connectivity and data transfer [14].

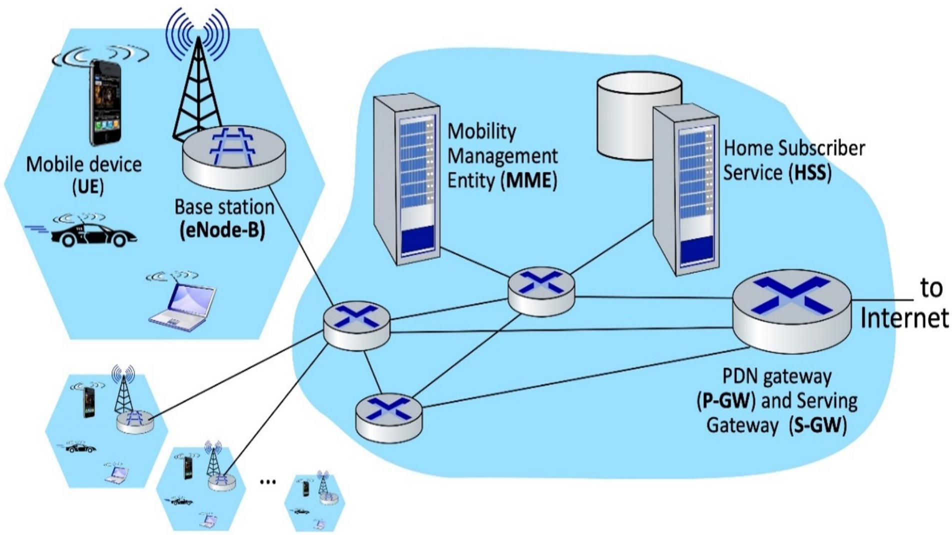

Figure I.4: 4G LTE Network Architecture [14]

I.3.4.2 Comparison of 4G with 3G

- **Technologies:** OFDMA replaced WCDMA, enabling flexible resource allocation. MIMO and carrier aggregation enhanced capacity [13].
- **KPIs:** Data rates increased 500-fold (1 Gbps vs. 2 Mbps), latency reduced fivefold (20 ms vs. 100 ms), and spectral efficiency improved 5-10 times.

- **Advancements:** High-speed mobile broadband and all-IP architecture compared to mixed circuit/packet switching in 3G.
- **Technical Limitations:** Spectral congestion and inter-cell interference.

I.3.5 Fifth Generation (5G): Ultra-Reliability, IoT, and New Radio

- **Technologies:** Launched in 2019, 5G employs 5G New Radio (NR). Operating in Frequency Range 1 (FR1, sub-6 GHz) and Frequency Range 2 (FR2, mmWave, 24-52 GHz), it incorporates
  - Massive MIMO (up to 256 antennas).
  - Flexible OFDMA (subcarrier spacing 15-240 kHz).
  - Beamforming for mmWave propagation.
  - Network slicing for dedicated services.
  - Edge computing for low latency [2].
- **Performance:** The 5G network is designed to deliver superior performance compared to previous generations, as shown in Figure I.5, with a focus on Key performance indicators
  - **Latency:** <1 ms (Ultra-Reliable Low-Latency Communications, URLLC).
  - **Peak data rate:** 20 Gbps; user-experienced: 100 Mbps.
  - **Connection density:** 1 million devices/km^2.
  - **Spectral efficiency:** 30bits/s/Hz.
  - **Reliability:** 99.999% [15].

I.3.5.1 Advancements

Support for enhanced Mobile Broadband (eMBB), massive Machine-Type Communications (mMTC), and URLLC. NR provides adaptive numerology and dynamic spectrum management [15].

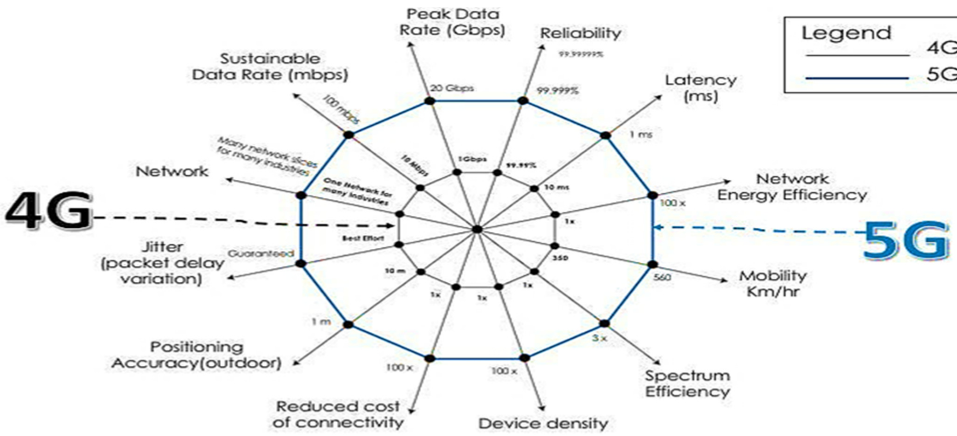

Figure I.5: Performance Comparison of 4G and 5G (IMT-2020) Networks: Key Metrics and Targets[15]

I.3.5.2 Comparison of 5G with 4G

- **Technologies:** NR introduces mmWave and Massive MIMO, unlike limited MIMO in 4G. Network slicing and edge computing are absent in 4G [2].
- **KPIs:** Data rates increased 20-fold (20 Gbps vs. 1 Gbps), latency reduced 20-fold (1 ms vs. 20 ms), connection density increased 1000-fold, and spectral efficiency tripled.
- **Advancements:** Massive IoT and mission-critical applications (e.g., autonomous vehicles) compared to general broadband in 4G.
- **Technical Limitations:** mmWave signal attenuation, high infrastructure costs, and security challenges in virtualized networks.

I.3.5.3 The 5G Core Network (5GC) architecture

The 5G Core Network (5GC) as shown in Figure I.6 architecture connects User Equipment (UE) via the Radio Access Network (RAN) to a service-based core, which includes functions such as the Access and Mobility Function (AMF) for mobility, the Session Management Function (SMF) for session management, and the User Plane Function (UPF) for data transfer. It includes AUSF for authentication, UDM for subscriber data, and PCF for policy control, alongside NEF, NRF, NSSF, and AF for network exposure, discovery, slicing, and application support. This setup ensures high-speed, low-latency connectivity to external data networks (DN) with separated control and user planes [16].

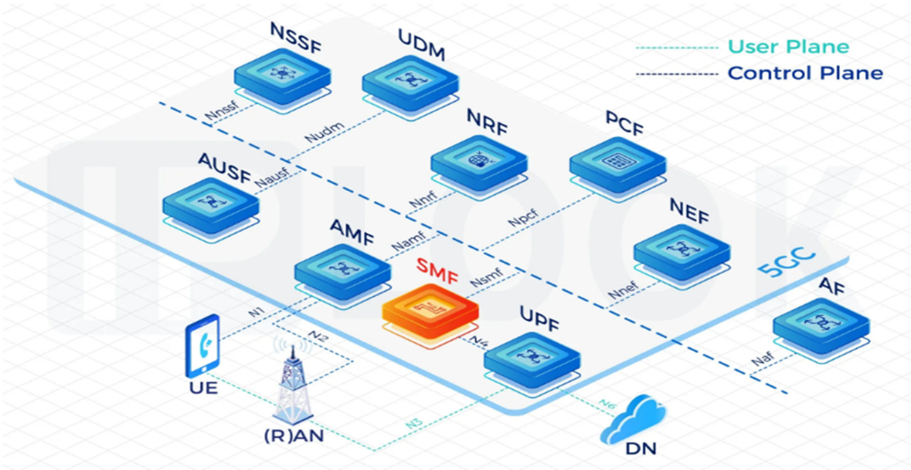

Figure I.6: Core Network Architecture for 5G[16]

I.4 Sixth Generation : In-Depth Technical Analysis

I.4.1 Timeline for 6G Development and Deployment

Outlines the key milestones for the evolution of 6G technology from 2023 to 2031 as shown in Figure I.7. It details the progression from 5G enhancements (Releases 18-20) to the initiation of 6G studies and the establishment of Release 21 specifications. The timeline includes critical events such as the TSG Workshop in March 2025 and ITU's IMT-2030 framework, culminating in commercial availability. This visual provides a structured roadmap for the global rollout of 6G technology.

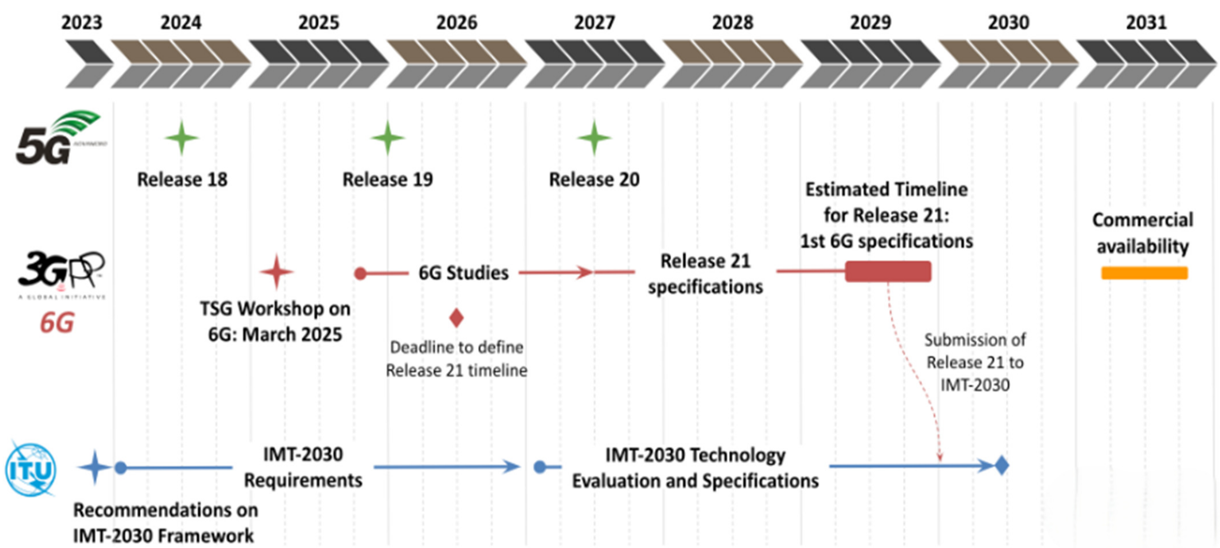

Figure I.7: Timeline for 6G Development and Deployment[17]

- **2020-2023: Early Research and Vision Definition**
  - Initial research on 6G began after 5G, focusing on use cases, requirements, and enabling technologies (e.g., terahertz bands and AI-driven networks) [3].
  - Global research initiatives, such as the ITU-R's Vision for 2030 and beyond and projects like Hexa-X in Europe, outlined 6G goals: terabit-per-second (Tbps) data rates, sub-millisecond latency, and massive connectivity [17].
  - Key activities: White papers published, academic and industry consortia formed (e.g., 6G Flagship in Finland) [18].
- **2024-2026: Technology Exploration and Standardization Kickoff**
  - Ongoing (as of May 2025): Researchers are exploring technologies like terahertz (THz) communication, reconfigurable intelligent surfaces (RIS), and integrated sensing and communication (ISAC) [19].
  - Standardization bodies, including 3GPP and ITU, begin defining 6G frameworks. 3GPP Release 19 (2024-2025) includes 6G study items, with formal specifications expected in Releases 20-21 (2026-2027) [20].
  - Prototyping of THz transceivers and AI-based network management systems intensifies [21].
- **2027-2029: Pre-Standardization and Trials**
  - Early 6G standards emerge, focusing on core technologies (e.g., THz bands, non-terrestrial networks) [22].
  - Field trials and testbeds expand, testing applications like holographic communication, digital twins, and ultra-reliable low-latency communications (URLLC) [23].
  - Global spectrum allocation discussions intensify, targeting the THz and sub-THz bands (e.g., 100-300 GHz) at events such as the World Radiocommunication Conference (WRC) 2027 [24].
- **2030-2032: Commercial Launch and Early Adoption**
  - Commercial 6G networks are projected to launch around 2030, starting in urban areas and developed markets [17].

  - Initial deployments focus on enhanced mobile broadband (eMBB), industrial Internet of Things (IIoT), and smart cities, leveraging artificial intelligence (AI) and integrating satellite and terrestrial technologies [22].
  - Early adopters include industries requiring high-bandwidth, low-latency applications (e.g., autonomous vehicles, extended reality) [23].

- **2033-2035: Widespread Adoption and Ecosystem Maturity**
  - 6G networks expand globally, improving coverage in rural and remote areas via non-terrestrial networks (e.g., satellites, high-altitude platforms) [19].
  - Full ecosystem maturity, with widespread availability of 6G-compatible devices and applications like immersive metaverse and integrated sensing [21].
  - Sustainability and energy efficiency become critical, with green technologies integrated into 6G infrastructure [25].

- **Post-2035: Evolution Toward 7G**
  - 6G networks continue to evolve, incorporating lessons learned to refine performance and address limitations.
  - Research into seventh-generation (7G) networks is accelerating, with a focus on quantum communication, bio-integrated networks, and molecular communication. A conceptual framework is expected to emerge by the late 2030s [4].

I.4.2 Technologies and Architectures

6G integrates terrestrial, aerial (High-Altitude Platform Systems, HAPS), and satellite (Low Earth Orbit, LEO) networks to achieve three-dimensional (3D) coverage. Key technologies include those shown in Figure I.8.

- **Terahertz Frequencies (THz):** 0.1-10 THz for ultra-high data rates [3].
- **Artificial Intelligence (AI):** Resource optimization and network management [22].
- **Integrated Sensing and Communication (ISAC):** Simultaneous sensing and communication using shared spectrum [26].
- **Cell-Free Networks:** Distributed access points for seamless connectivity [27].

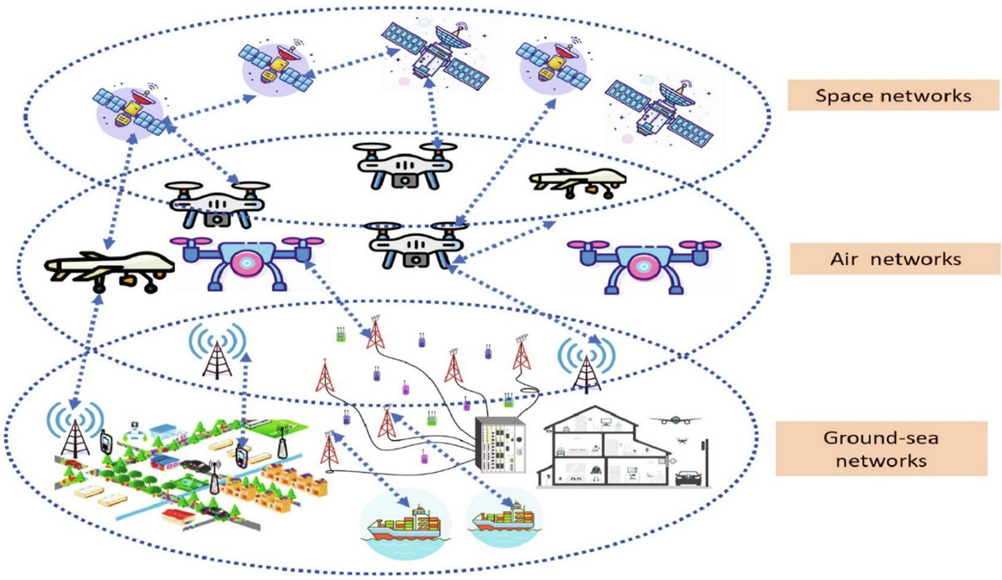

Figure I.8: The integrated Ground Sea Air Space 6G expected network[19]

- **Visible Light Communications (VLC/LiFi):** High-speed indoor data transmission [28].
- **Architecture:** Software-Defined Networking (SDN), Network Function Virtualization (NFV), and edge/cloud computing as shown in Figure I.9 [19].

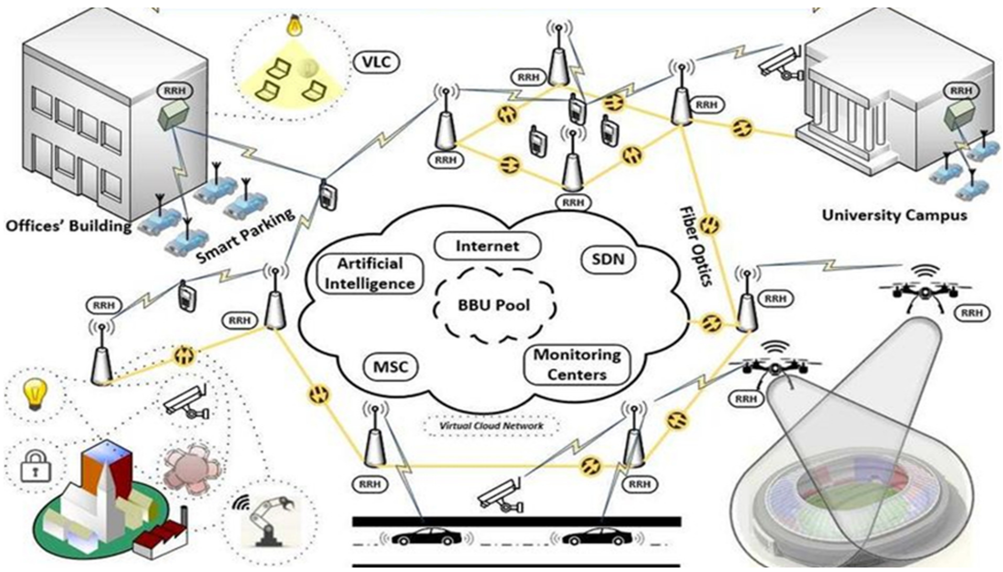

Figure I.9: Proposed Network level 6G architecture[19]

I.4.3 Signal Transmission Methods

I.4.3.1 Massive MIMO and Ultra-Massive MIMO

- **Massive MIMO:** Up to 512 antennas for THz/sub-THz bands, employing precoding techniques (e.g., zero-forcing, Minimum Mean Square Error, MMSE) [29].

- **Ultra-Massive MIMO (UM-MIMO):** Thousands of antennas (e.g., 1000x1000) using metamaterials/graphene, enabling extreme beam focusing and massive spatial multiplexing [21].
- **Principle:** AI-adjusted narrow beams maximize directional gain [22].

I.4.3.2 Reconfigurable Intelligent Surfaces (RIS): Principles and Technical Details

- **Principle:** Metasurfaces passively modify the phase/amplitude of incident waves, controlled by PIN diodes or digital circuits [30].
- **Structure:** Sub-wavelength elements (e.g., 64x64 arrays) using materials such as graphene or metamaterials.
- **Role:** Enhances THz coverage, spectral efficiency, and ISAC performance.
- **Modeling:** Reflected signal optimized via AI-driven phase adjustments [30].
- **Types:** Passive (energy-efficient) and active (amplified).
- **Challenges:** Calibration, channel modeling, and AI integration.

I.4.3.3 Visible Light Communication (VLC)

- **Principle:** Uses visible light (400-800 THz) to transmit data by modulating LED intensity, with photodiode receivers decoding signals via intensity modulation/direct detection (IM/DD) [28].
- **Structure:** Comprises LEDs or laser diodes as transmitters, photodiodes or CMOS sensors as receivers, and driver circuits for modulation (e.g., OOK, OFDM).
- **Role:** Enables high-speed, secure indoor communication, supports Li-Fi, indoor positioning, and Integrated Sensing and Communication (ISAC) with no electromagnetic interference (EMI).
- **Modeling:** Signal optimization via equalization and AI-driven interference mitigation; relies on line-of-sight (LOS) or reflected light paths [28].

- **Types:**
  - **Single-Carrier:** On-Off Keying (OOK), Pulse Position Modulation (PPM) for low/medium data rates.
  - **Multi-Carrier:** Orthogonal Frequency Division Multiplexing (OFDM), Color Shift Keying (CSK) for high data rates.
- **Challenges:** Line-of-sight dependency, ambient light interference, limited LED modulation bandwidth, and integration with RF networks for uplink.

I.4.4 Key Performance Indicators (KPIs)

- **Peak Data Rate:** 1 Tbps; user-experienced: 1 Gbps.
- **Latency:** $< 100\mu$s (enhanced URLLC, eURLLC).
- **Connection Density:** 10 million devices/km^2.
- **Spectral Efficiency:** 100bits/s/Hz.
- **Reliability:** 99.99999%.
- **Energy Efficiency:** 1 pJ/bit.
- **Coverage:** 99.9% (3D).
- **Mobility:** 1000 km/h [17].

I.4.5 Radio Access Methods: NOMA, RSMA, NGMA

- **Non-Orthogonal Multiple Access (NOMA):** Signal superposition with Successive Interference Cancellation (SIC), improving spectral efficiency over OFDMA **Ding201 broadcasts7**.
- **Rate-Splitting Multiple Access (RSMA):** Splits messages into common and private components, transmitted via superposition, enhancing interference management in dense environments [31].
- **Non-Orthogonal Grant-Free Multiple Access (NGMA):** Uncoordinated access for massive IoT and sporadic communications, reducing latency and signaling overhead [32].
- **Enhanced OFDMA:** Adaptive subcarrier allocation.

- **Sparse Code Multiple Access (SCMA):** Utilizes sparse codes for achieving massive connectivity [33].
- **Hybrid Access:** Combines NOMA, RSMA, NGMA, OFDMA, and SCMA.

I.4.6 Security and Privacy: QKD and Beyond

- **Quantum Key Distribution (QKD):** Utilizes quantum mechanics (e.g., BB84 protocol) for secure key distribution, resistant to quantum attacks [34].
- **Physical Layer Security (PLS):** Dynamic key generation using THz channels [35].
- **Blockchain:** Decentralized identity management [36].
- **AI for Cybersecurity:** Anomaly detection [37].
- **Challenges:** Satellite vulnerabilities, QKD complexity, and adversarial AI attacks.

I.4.7 Vision and Requirements

- **Vision:** An intelligent Internet of Everything, enabling immersive communications, ubiquitous AI, ISAC, and sustainability [17].
- **Requirements:** Data rates of 100-1000 Gbps, latency $< 100\mu$s, global coverage, and 10-100x energy efficiency over 5G.

I.4.8 Challenges and Opportunities

- **Challenges:** THz signal attenuation, infrastructure costs, RIS complexity, and QKD integration.
- **Opportunities:** Extended reality, smart cities, rural connectivity, and ISAC applications (e.g., surveillance, localization)[22].

I.5 Technical Comparison: 5G vs 6G (KPIs, New capability, Usage Scenarios)

I.5.1 Comparison of 5G and 6G Key Performance Indicators (KPIs)

The table I-1 compares the Key Performance Indicators (KPIs) of 5G, based on ITU IMT-2020 standards, with those of the anticipated 6G, based on ITU IMT-2030 standards, providing more detailed information as shown in Figure I.10.

Table I.1: Technical Comparison of 5G vs 6G

KPI	**5G**	**6G**
Peak Data Rate	20Gbps	1Tbps
User Data Rate	100Mbps	1Gbps
Latency	$<$ 1ms (URLLC)	$<$ 100μs (eURLLC)
Connection Density	1million/km^2	10million/km^2
Spectral Efficiency	30bits/s/Hz	100bits/s/Hz
Reliability	99.999%	99.9999%
Energy Efficiency	0.1μJ/bit	1pJ/bit
Coverage	Urban-focused	Global (3D)
Mobility	500 km/h	1000 km/h

- **Technological Comparison:** 6G introduces THz bands, UM-MIMO, RIS, NOMA /RSMA/NGMA,QKD, and ISAC, compared to 5G's mmWave, Massive MIMO, and OFDMA [3].
- **KPI Advancements:** 50x peak data rate, 10x latency reduction, 10x connection density, and 100x energy efficiency [17].
- **Functional Advancements:** 3D connectivity, integrated AI, and ISAC compared to 5G's IoT and URLLC focus [22].

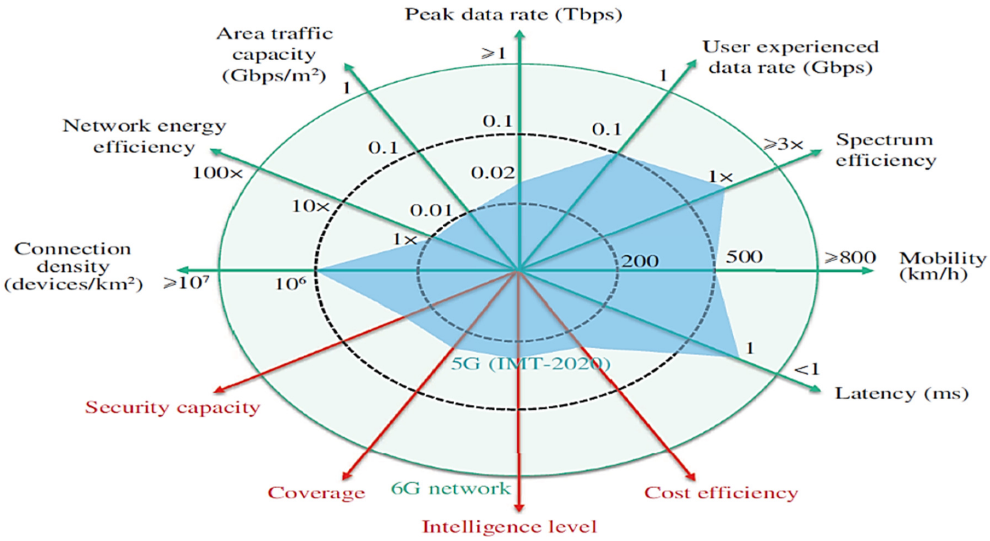

Figure I.10: : Performance Comparison of 5G (IMT-2020) and 6G Networks: Key Metrics and Targets[17]

I.5.2 Enhanced Performance of IMT-2020 and New Capabilities of IMT-2030

The International Mobile Telecommunications (IMT) standards, defined by the International Telecommunication Union (ITU), have played a pivotal role in shaping the evolution of mobile communication systems. IMT-2020, commonly associated with 5G technology, set a benchmark for enhanced performance in mobile networks by achieving significant improvements in key metrics such as latency (0.1 − 1 ms), reliability ($1-10^{-5}$ to $1-10^{-7}$ error rate), and connection density (10^5-10^6 devices/km^2). These advancements enabled a wide range of applications, from ultra-reliable low-latency communications (URLLC) to massive machine-type communications (mMTC) and enhanced mobile broadband (eMBB) [38]. Building on this foundation, IMT-2030, aligned with 6G visions, introduces a new set of capabilities to address emerging technological demands and societal needs. These include AI-related capabilities, sensing-related functionalities, interoperability, sustainability, and precise positioning (1-10 cm), alongside further improvements in coverage, security, and peak data rates [24]. To illustrate the transition and the expanded scope of these standards, as shown in Figure I.11, referred to as the "Palette Diagram," the enhanced performance metrics of IMT-2020 are visually compared with the new capabilities introduced by IMT-2030, providing a comprehensive overview of the evolution in mobile communication requirements.

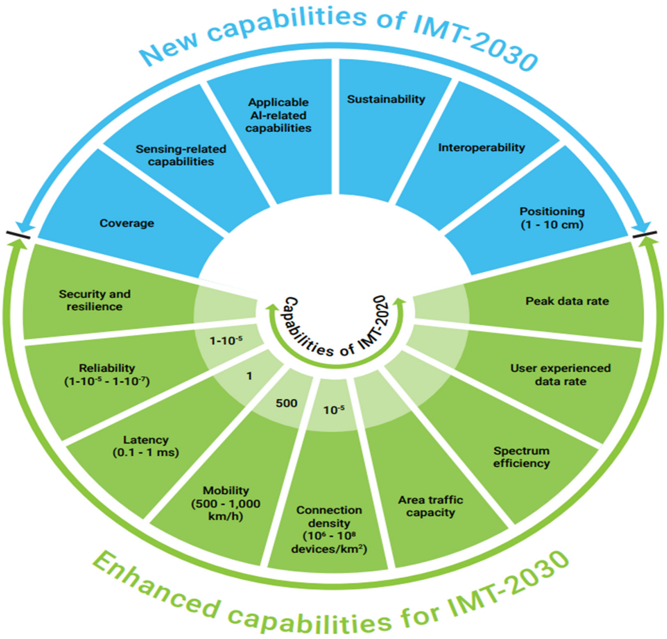

Figure I.11: IMT-2020 vs. IMT-2030: Enhanced Performance and New Capabilities[24]

I.5.3 Usage Scenarios

The progression of mobile communication technologies has been instrumental in shaping global connectivity, with the International Mobile Telecommunications (IMT) standards serving as a cornerstone for innovation. IMT-2020, which forms the basis of 5G networks, has delivered significant advancements in performance metrics, including Enhanced Mobile Broadband (eMBB), Massive Machine-Type Communications (mMTC), and Ultra-Reliable Low-Latency Communications (URLLC), thereby meeting the demands of an increasingly interconnected digital ecosystem [38]. As the telecommunications industry advances toward IMT-2030, anticipated to underpin 6G networks, the emphasis shifts toward visionary objectives that integrate cutting-edge technologies with societal imperatives. The NextG Alliance has proposed a forward-looking framework that prioritizes ubiquitous connectivity, integrated sensing and communication, artificial intelligence (AI) integration, sustainability, cost-efficiency, security, and resilience [39]. To elucidate this evolution, Figure I.12 encapsulates the foundational capabilities of IMT-2020 alongside the transformative usage scenarios and ambitious goals of IMT-2030, such as immersive communication, distributed cloud systems, and AI-enabled innovations, offering a detailed visual depiction of the future trajectory of mobile communication networks.

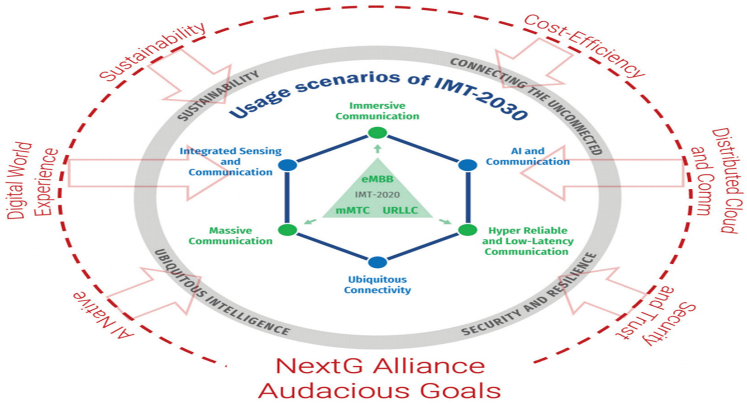

Figure I.12: IMT-2020 and IMT-2030 Usage Scenarios: NextG Alliance Goals Diagram[39]

I.6 Vision and Challenges for Seventh-Generation (7G) Wireless Networks

Exponential advancements in speed, latency, and connectivity have marked the evolution of wireless networks. While 6G is projected to launch commercially around 2030, offering terabit-per-second (Tbps) data rates and millisecond latencies [17], the conceptual framework for 7G is already taking shape. Envisioned for the 2040s, 7G aims to redefine communication by integrating quantum, biological, and nanoscale technologies, achieving unprecedented performance metrics, including petabit-per-second (Pbps) data rates and sub-microsecond latencies [4]. This article presents a forward-looking analysis of 7G, detailing its anticipated capabilities, transformative applications, and the multifaceted challenges that lie ahead.

I.6.1 Envisioned Capabilities of 7G

7G networks are expected to push the boundaries of wireless communication far beyond 6G, leveraging cutting-edge technologies to achieve the following capabilities:

- **Ultra-High Data Rates and Low Latency:** Operating in sub-millimeter wave and optical frequency bands (e.g., 400-700 THz), 7G aims to deliver data rates exceeding 10Pbps with latencies of less than 0.1μs, creating near-instantaneous communication [4].
- **Global Seamless Connectivity:** By integrating terrestrial, aerial, and satellite networks, 7G will ensure ubiquitous coverage, even in remote and underserved regions [19].
- **AI-Driven Network Management:** Advanced AI will enable self-organizing, self-healing, and self-optimizing networks, dynamically adapting to user demands and environmental conditions [22].

- **Quantum Communication:** Incorporating quantum entanglement and teleportation principles, 7G could offer unhackable communication channels and pave the way for a quantum internet [34].
- **Energy Harvesting:** 7G devices may harvest ambient energy (e.g., from thermal or biochemical sources), reducing reliance on traditional power sources [25].
- **Molecular and Nano-Scale Communication:** Utilizing biochemical signaling (e.g., calcium ions), 7G could enable communication at the molecular level, supporting applications in precision medicine and nanotechnology [40].

I.6.2 Potential Applications of 7G

The revolutionary capabilities of 7G are expected to unlock a wide range of transformative applications, including:

- **Neural Interfaces:** Brain-computer interfaces (BCIs) could enable direct neural communication, allowing thought-based device control and cognitive augmentation [41]. For instance, users may access cloud-based knowledge instantaneously.
- **Advanced AI Integration:** With ultra-high bandwidth and near-zero latency, 7G could support distributed AI systems that seamlessly integrate with physical environments, enhancing real-time decision-making [22].
- **Immersive Sensory Experiences:** Beyond 6G's holographic telepresence, 7G could transmit full sensory experiences, simulating physical presence with tactile and olfactory feedback [4].
- **Global Distributed Computing:** 7G could create a planet-wide computing network, enabling devices to access vast processing power on demand [19].
- **Swarm Robotics:** Massive swarms of nano-robots or drones could collaborate in real-time for tasks like environmental monitoring, disaster response, or space exploration [40].
- **Predictive Systems:** By combining big data, AI, and instantaneous communication, 7G could enable predictive analytics for events such as traffic congestion or health crises [22].

I.6.3 Development Timeline and Challenges

The development of 7G remains in its conceptual phase, with widespread adoption projected for the late 2030s to early 2040s, following the commercial rollout of 6G [4]. However, realizing 7G's vision will require overcoming significant challenges:

- **Technological Breakthroughs:** Achieving Pbps data rates and sub-microsecond latencies will necessitate advancements in materials science (e.g., graphene-based metasurfaces), quantum computing, and neuromorphic hardware [40].
- **Spectrum Management:** Operating in sub-millimeter and optical bands will require sophisticated spectrum allocation strategies to avoid interference [3].

I.6.4 Key Performance Indicators

- **Data Rate:** >10 Tbps.
- **Latency:** $< 10\mu$s.
- **Connection Density:** 100 million/km^2.
- **Energy Efficiency:** < 0.1pJ/bit.
- **Reliability:** 99.999999%.
- **Neuromorphic Computing:** Emulates neural architectures for ultra-low-latency brain-computer interfaces (BCIs), processing signals at femtojoule efficiencies, and is integrated with radio-frequency identification (RIS) for neural signal transmission over optical wireless communication (OWC) bands [41].
- **Molecular Communication:** Utilizes biochemical signals (e.g., calcium ions) for nanoscale networks, with RIS enhancing signal precision by focusing molecular propagation in complex biological environments [40].
- **Orbital Angular Momentum (OAM):** Exploits electromagnetic wave vorticity for ultra-high-capacity links, achieving Pbps rates in hybrid OWC-terahertz systems, complemented by RIS for dynamic beam steering [42].
- **Bio-Compatible RIS:** Employs organic metasurfaces (e.g., graphene-based) to interface with human tissue, enabling non-invasive bio-nano connectivity with minimal immunological impact [40].

I.7 Conclusion

This chapter provides a comprehensive overview of the technical evolution of mobile networks, tracing their development from the analog-based 1G systems of the 1980s to the ultra-reliable, AI-driven 5G networks of today. It also explores the emerging technologies and anticipated capabilities of 6G, expected around 2030, and offers a visionary outlook toward 7G, projected for the late 2030s and beyond .

Each generation has introduced significant improvements in key performance indicators (KPIs), including data rates, latency, connection density, spectral efficiency, and reliability. Starting with voice-only 1G, mobile networks have evolved through digitalization (2G), multimedia support (3G), high-speed broadband (4G), and finally ultra-reliable low-latency connectivity (5G). This chapter details the underlying technologies, network architecture, and limitations of each generation.

The discussion then transitions into 6G, which aims to deliver terabit-per-second data rates (less than 1 Tbps), sub-millisecond latencies (less than $100\mu s$), and massive device density (up to 10 million devices per square kilometer). It highlights enabling technologies such as terahertz communication, artificial intelligence (AI), integrated sensing and communication (ISAC), visible light communication (VLC), and, in particular, Reconfigurable Intelligent Surfaces (RIS), a transformative solution for enhancing signal propagation, coverage, and energy efficiency in high-frequency bands.

Looking ahead, 7G envisions a future where wireless communication integrates quantum mechanics, molecular signaling, and neuromorphic computing, potentially enabling brain-computer interfaces, ultra-secure quantum channels, and real-time sensory transmission. However, these advancements also present significant challenges related to spectrum management, infrastructure costs, energy sustainability, and technological feasibility.

In conclusion, the evolution of mobile networks reflects a continuous pursuit of faster and more innovative, and more reliable connectivity. As we move toward RIS-enabled environments and beyond, understanding this progression is crucial for shaping the next era of intelligent, immersive, and globally integrated communication systems.

Chapter II

RIS, NOMA, and Statistical Fading Models in Wireless Communications

II.1 Introduction

The rapid evolution of wireless communication systems has necessitated innovative approaches to address the challenges of spectrum scarcity, energy efficiency, and reliable signal propagation in complex environments. Among emerging technologies, Reconfigurable Intelligent Surfaces (RIS) have garnered considerable interest due to their potential to transform the landscape of wireless communications . By leveraging the unique properties of metamaterials, RIS enables dynamic manipulation of electromagnetic waves, thus offering a new paradigm for optimizing signal propagation and enhancing network performance. This chapter provides a comprehensive exploration of RIS, starting with the fundamental concepts of metamaterials and their electromagnetic properties. It also discusses the operational principles and architectural design of RIS, highlighting their role in creating intelligent communication environments . Furthermore, the chapter examines the integration of RIS with advanced multiple access techniques and statistical fading models, providing a holistic understanding of their impact on modern wireless systems. Through a detailed analysis of these elements, this chapter aims to lay the groundwork for understanding the transformative potential of RIS in meeting the demands of next-generation communication networks.

II.2 Definition and Fundamental Concepts of Metamaterials

Metamaterials, originating from the Greek term ”meta,” which translates to ”beyond,” and the Latin term ”materia,” meaning ”matter,” are artificially engineered substances designed to exhibit characteristics that are not present in naturally occurring materials [43]. The microstructure of metamaterials is carefully constructed to ensure that their effective macroscopic response to specific excitations is not typically observed in nature [44]. These materials can consist of metals, plastics, or semiconductors, and their periodic structures are defined by repeating units referred to as ”meta-atoms” [45]. For effective interaction with electromagnetic waves, the dimensions of these meta-atoms must be significantly smaller than the wavelength of the incident wave, generally adhering to the condition $p \leq \frac{\lambda}{4}$, where p denotes the size of the meta-atom and λ is the wavelength [46].

The interaction of metamaterials with electromagnetic waves is quantified by the refractive index n, which is derived from their constitutive parameters: relative permittivity ε and relative permeability μ. The relationship is expressed as $n = \pm\sqrt{\varepsilon\mu}$ [47].

Metamaterials constitute a novel class of artificial materials whose engineered microstructures allow them to display unique electromagnetic properties that were previously considered physically impossible [48]. Unlike natural materials, which have periodic structures formed by atoms, metamaterials feature an artificial periodic structure that is superimposed onto a host material [49]. This artificial structure comprises elements that are larger than the atoms of the host material, enabling it to dominate the natural response of the host to incoming electromagnetic waves. As a result, the ensuing penetration, reflection losses, and reflection angles are dictated by the artificial structure rather than the atomic configuration of the host material. In this paper, we will investigate the key characteristics of metamaterials, introduce the concept of Reconfigurable Intelligent Surfaces (RIS), and discuss the potential applications of RIS in contemporary wireless communications. Most naturally occurring materials exhibit positive permeability and permittivity, categorizing them as dielectrics. These materials facilitate forward electromagnetic wave propagation, where both group velocity and phase velocity move in the same direction, and energy flow aligns with the wave motion. In contrast, materials such as ferrites (with $\varepsilon > 0$ and $\mu < 0$) and plasmas (with $\varepsilon < 0$ and $\mu > 0$) exhibit a negative product of $\varepsilon\mu$, resulting in a purely imaginary refractive index and lossy propagation, commonly referred to as evanescent propagation.

The most intriguing scenario arises when both constitutive parameters are negative. In this case, despite each parameter being negative, their product remains positive, yielding a real refractive index. Such materials are classified as Negative Index Materials (NIM). NIMs are characterized by backward propagation, where group velocity and phase velocity move in opposite directions, and energy flows contrary to the wave motion[50]. Currently, no known natural materials exhibit negative index properties, making the synthesis of artificial NIMs a central focus of metamaterial research. The dynamics of forward, backward, and evanescent propagation are illustrated in Figure II.1 the accompanying $\mu\varepsilon$ diagram:

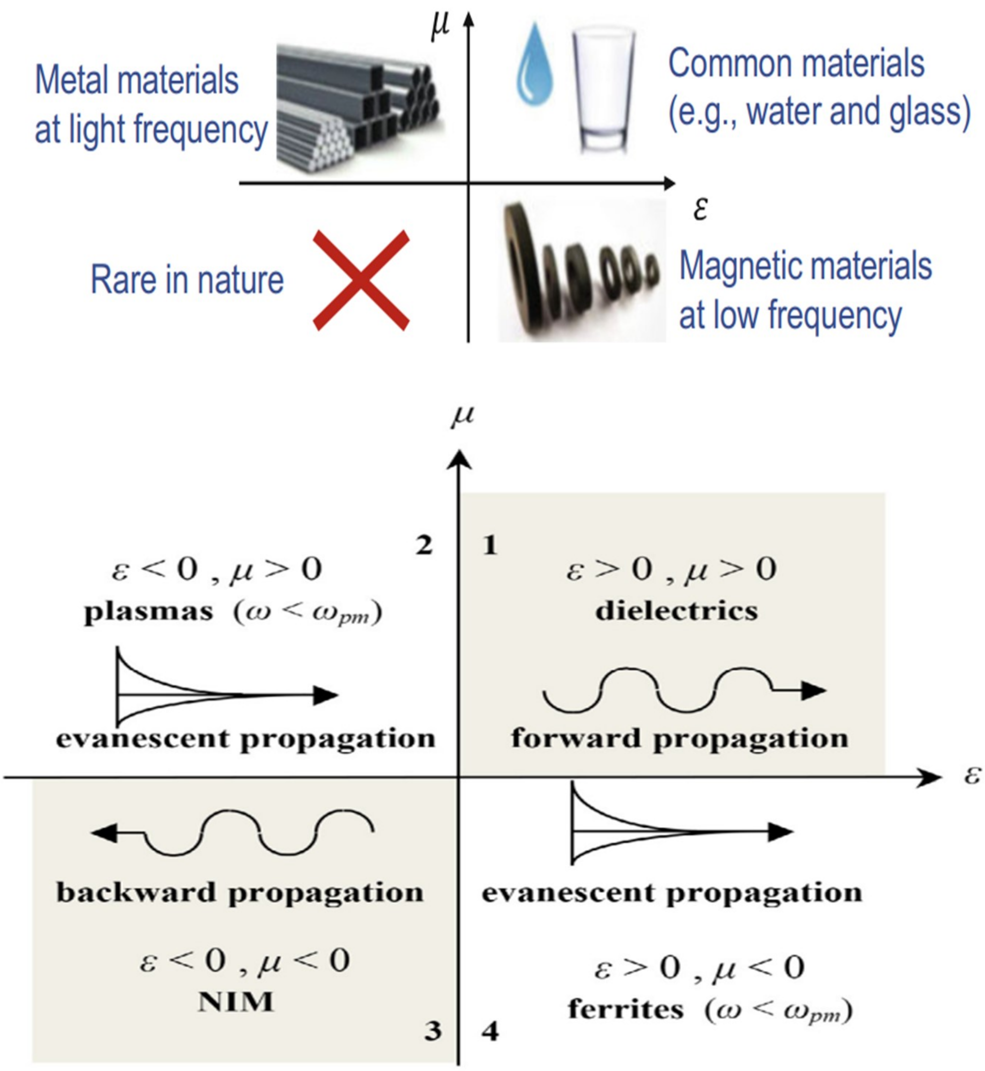

Figure II.1: Permittivity (ε) and permeability (μ) diagram[50]

II.2.1 Generalized Snell's & Reflection Laws

Snell's Law: Snell's law, also known as the Snell–Descartes law, describes how light or any other wave behaves when it transitions between two isotropic media with different refractive indices, it is expressed as[50]:

$$n_1 \sin \theta_1 = n_2 \sin \theta_2 \tag{II.1}$$

where:

- n_1 and n_2 are the refractive indices of the first and second media, respectively.
- θ_1 is the angle of incidence, and
- θ_2 is the angle of refraction measured from the normal.

During the study of metamaterials, this law was deemed inadequate for addressing the new variables encountered in the investigation of these materials, leading to the formulation of a new law in 2011, known as the generalized Snell's law was proposed. This law reveals that we can control the refraction direction by changing the phase gradient of the metasurface[50].

Generalized Law of Reflection: When an incident wave strikes an RIS, the reflected wave follows the generalized law of reflection shown in Figure II.2, which differs from conventional reflection due to the phase gradient introduced by the surface. For metasurfaces with a phase gradient $\nabla\Phi$, the relationship between the incident angle θ_i and the reflected angle θ_r is given by:

$$k_0 \sin \theta_r - k_0 \sin \theta_i = \nabla\Phi \tag{II.2}$$

where: k_0 is the wave number in free space.

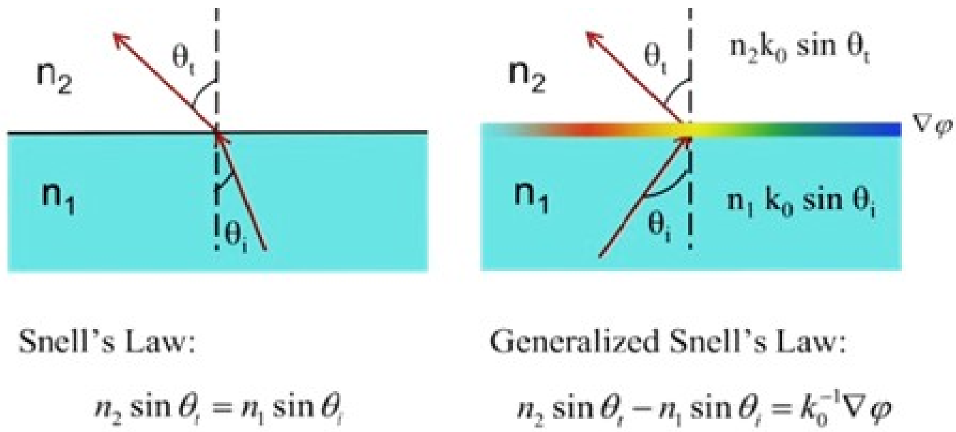

Figure II.2: Classical and Generalized Snell's Law at an Interface[50]

II.3 Definition and Fundamental Concepts of RIS

A Reconfigurable Intelligent Surface (RIS) is defined as a programmable planar array consisting of a multitude of individually controlled passive elements, as shown in Figure II.3, engineered to dynamically manipulate incident radio-frequency (RF) electromagnetic waves in real time [44], [51]. These elements, typically fabricated from metamaterials, possess the capability to adjust their electromagnetic properties—namely phase and amplitude—to facilitate the reflection or diffraction of signals toward designated directions [52].

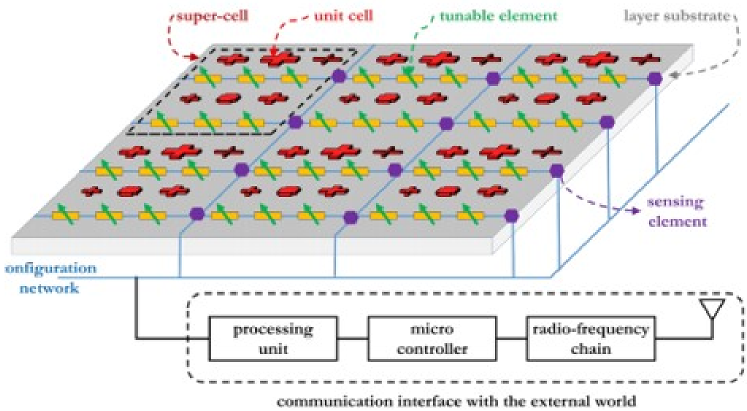

Figure II.3: Schematic Representation of the RIS Structure[30]

In essence, an RIS functions as a controllable surface that governs the reflection of electromagnetic (EM) waves by altering its electrical and magnetic characteristics [53]. Strategically deployed within the radio propagation channel between a transmitter and a receiver, an RIS enables precise management of signal reflection along the propagation path, thereby enhancing signal reception and improving the overall quality of the communication link.

In conventional wireless communication systems, the radio channel is typically regarded as an uncontrollable medium that introduces distortions to transmitted signals [54]. Such signals often interact with a diverse array of surfaces during propagation, resulting in random reflections that give rise to both constructive and destructive interference patterns. This is an environment defined by the Smart Environment 1.0. In contrast, an RIS provides a mechanism to regulate these interactions by directing reflected signals toward specific destinations. This controlled manipulation enhances the reliability and energy efficiency of wireless systems, mitigating the adverse effects of random scattering [53]. Furthermore, RIS technology elevates wireless communications to a new paradigm known as Smart Environment 2.0, where the physical environment itself becomes an intelligent, programmable component of the communication infrastructure [44]. In this advanced framework, surfaces and objects within the environment are transformed into active participants that can intelligently optimize signal propagation, creating a seamlessly integrated ecosystem where communication performance is enhanced through environmental intelligence.

Consequently, the deployment of RIS can extend the operational range of wireless networks and enable signal delivery to regions that are otherwise challenging to access due to physical obstructions or non-line-of-sight (NLoS) conditions [52].

Primary methodologies are employed to implement a RIS for the purpose of controlling signal characteristics, as shown in Figure II.4, including reflection, refraction, absorption, focusing, and polarisation [45]. These approaches include the utilisation of conventional antenna arrays and the adoption of metasurfaces.

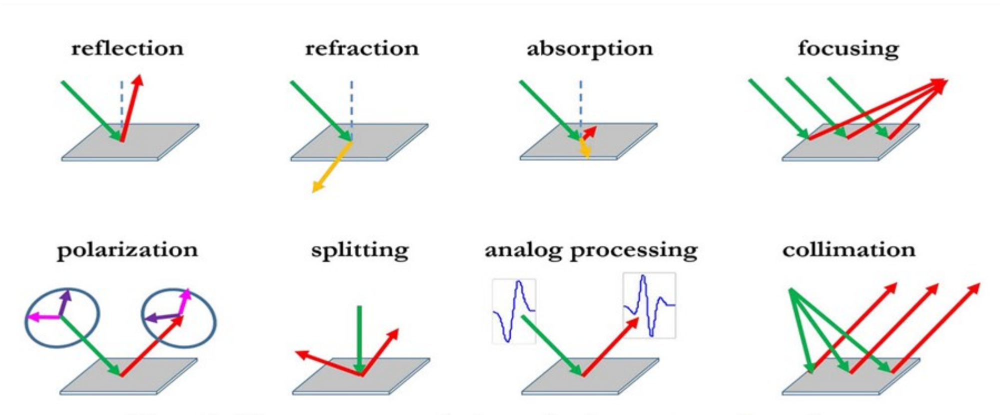

Figure II.4: Key Electromagnetic Wave Manipulation Functions of RIS[30]

Metasurfaces are characterized as electrically thin, densely packed two-dimensional arrays of structured elements that possess specific electromagnetic properties determined by their constituent components [46]. These components, commonly referred to as meta-cells, unit cells, or meta-atoms, have dimensions that are significantly smaller than the wavelength of the incident signal. In addition to their function in controlling electromagnetic wave propagation, metasurfaces facilitate complex operations, including data modulation and mathematical computations [47]. Moreover, experimental studies have shown their ability to temporarily store electromagnetic pulses for short durations. Due to these distinctive characteristics, Reconfigurable Intelligent Surfaces (RIS) have the potential to transform communication environments into intelligent systems, where signal propagation is dynamically optimized to meet the specific needs of users and applications [48].

II.4 Structure and Operation of a Reconfigurable Intelligent Surface

To facilitate precise manipulation of the electromagnetic propagation environment, a Reconfigurable Intelligent Surface (RIS) is engineered with a multilayered architecture, as depicted in Figure II.5, The constituent layers are delineated as follows [45]:

- The outermost layer comprises a two-dimensional array of RIS elements, configured to directly interact with incident electromagnetic signals.
- The intermediate layer consists of a copper substrate designed to mitigate signal energy leakage.
- The innermost layer incorporates a printed circuit board interfaced with the RIS controller, enabling precise modulation of the phase shifts exhibited by the RIS elements.

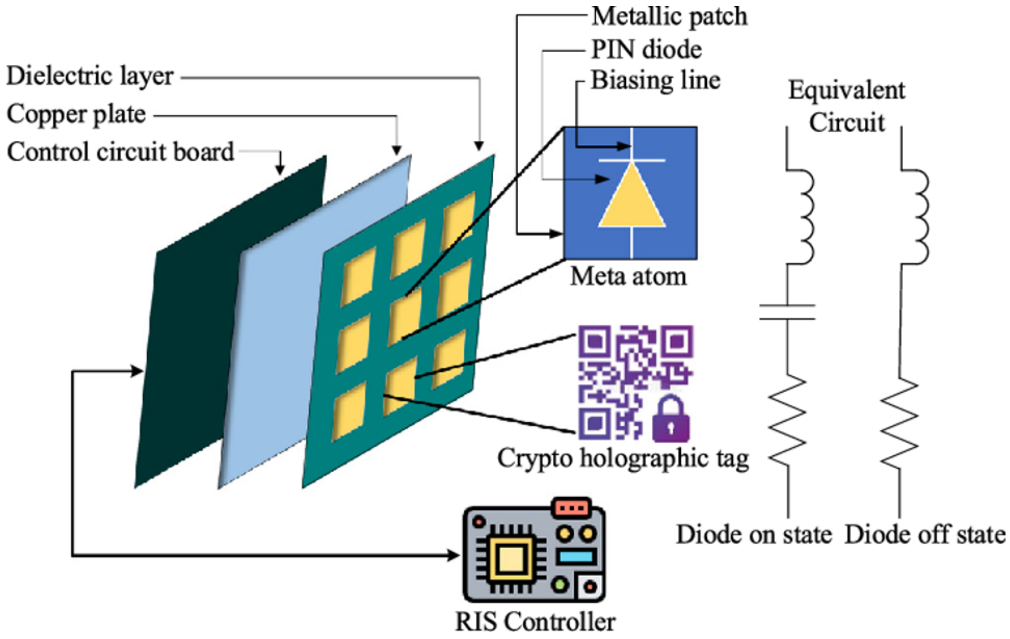

Figure II.5: System Overview of a Meta-Atom-Based RIS with PIN Diode Control[45]

Each RIS element is a cost-effective, sub-wavelength programmable metamaterial unit, operable across a frequency spectrum spanning sub-6 GHz to Terahertz bands [46]. Upon interaction with an incident electromagnetic wave, the RIS element induces an electric current, which subsequently generates secondary electromagnetic radiation. This radiation is governed by the permittivity (ε) and permeability (μ) characteristics of the RIS [47]. The operational principle of the RIS element in controlling wireless signal propagation is thus established. A representative schematic of a metamaterial particle is illustrated in Figure II.6

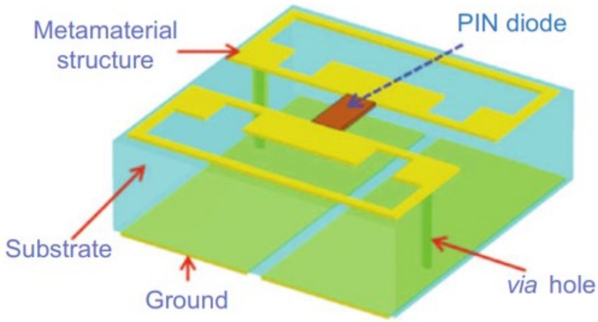

Figure II.6: An example of a programmable meta-material particle[45]

As shown, each element integrates PIN diodes, which are manipulated via biasing voltage applied through a via hole. This configuration enables the diodes to toggle between ”ON” and ”OFF” states, thereby altering the values of ε and μ. Consequently, the RIS element exhibits variable responses to incident signals, manifesting as distinct phase shifts and amplitude modulations [55]. it is pertinent to note that the amplitude associated with each phase shift is predetermined. Specifically, once a phase shift is selected, the corresponding amplitude is inherently fixed, ensuring consistent electromagnetic behavior, to support wireless communication applications.

- **Constituent Elements:** The individual reflecting units, commonly referred to as metasurfaces, are constructed from specialized materials engineered to manipulate electromagnetic waves with precision [45]. These materials enable the controlled reflection or diffraction of signals, optimizing their propagation characteristics.
- **Centralized Control Mechanism:** A dedicated control unit orchestrates the parameters of each reflecting element, ensuring that the signal transmission is optimized for the intended target receivers, thereby enhancing link reliability and system performance [55].

II.4.1 Operational Mechanism of a RIS in Wireless Communication

The functionality of a Reconfigurable Intelligent Surface (RIS) is grounded in the principle of controlled signal reflection modulation [53]. When a signal transmitted from a base station impinges upon the RIS, the surface dynamically adjusts its electromagnetic properties to redirect the signal toward a designated terminal, optimizing both signal strength and quality. This mechanism effectively mitigates the detrimental effects arising from interference, physical obstructions, and propagation losses in the wireless channel [52].

- **Channel Enhancement:** By precisely manipulating the phase and amplitude of the reflected signals, an RIS facilitates the creation of additional propagation paths [51]. This augmentation significantly enhances network coverage and capacity, enabling more robust communication links in challenging environments.
- **Interference Suppression:** The RIS's capability to steer signals toward specific receivers reduces co-channel interference among users. Consequently, this targeted signal delivery improves the overall quality of service (QoS) within the network, ensuring more reliable and efficient communication.
- **Enhanced System Capacity:** Through the optimization of signal propagation paths, RIS facilitate more effective utilization of available spectral resources, thereby increasing the overall capacity of the communication network [44].
- **Improved Energy Efficiency:** As RIS do not require active power sources for signal generation, they exhibit significantly lower energy consumption compared to conventional antenna systems, making them a sustainable choice for modern wireless networks [48].
- **Diverse Application Scenarios:** RIS can be deployed across a variety of contexts, including 5G and 6G networks, dense Internet of Things (IoT) ecosystems, and communication systems in challenging environments such as smart urban infrastructures [49].

Reconfigurable Intelligent Surfaces represent a transformative technology poised to revolutionize communication environments, enabling greater efficiency and adaptability. This advancement effectively addresses both present and anticipated challenges in the evolution of wireless networks [51].

II.4.2 Classification of Reconfigurable Intelligent Surfaces (RIS)

Reconfigurable Intelligent Surfaces (RIS) can be categorized based on their hardware architecture, operational modalities [55].

II.4.2.1 Based on Hardware Architecture

- **Passive RIS (P-RIS):** Passive RIS (PRIS) are artificial surfaces composed solely of passive elements as shown in Figure II.7 capable of manipulating incident electromagnetic waves without the use of active circuits or external energy injection [45]. These surfaces exclusively harness the energy of the received signals to dynamically adjust their electromagnetic properties, such as phase and amplitude, thereby redirecting or focusing the signals in specific directions.

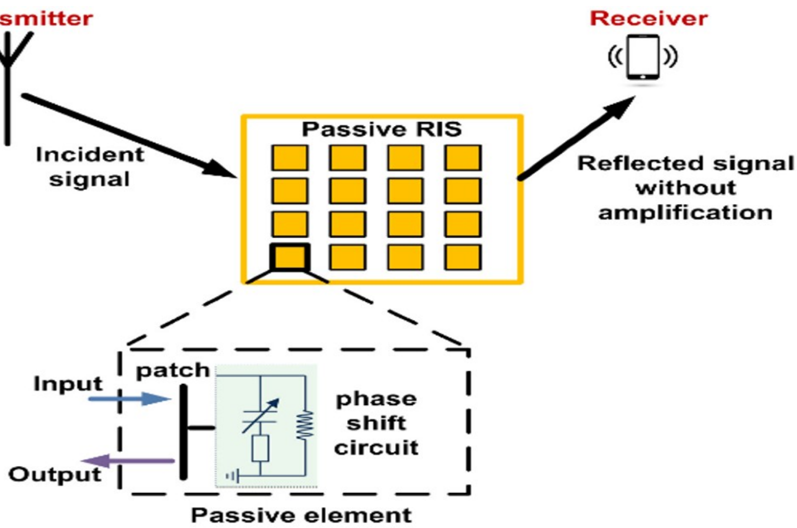

Figure II.7: Passive RIS Design for Reflecting Signals without Amplification[30]

- **Active RIS (A-RIS):** Active Reconfigurable Intelligent Surfaces (A-RIS) are engineered metasurfaces embedded with active components shown in Figure II.8, such as amplifiers or integrated electronic circuits, enabling advanced manipulation of incident electromagnetic waves, including radiofrequency signals [46]. Unlike their passive counterparts, A-RIS not only reflect or redirect these waves but also inject additional energy into the reflection or transmission process.

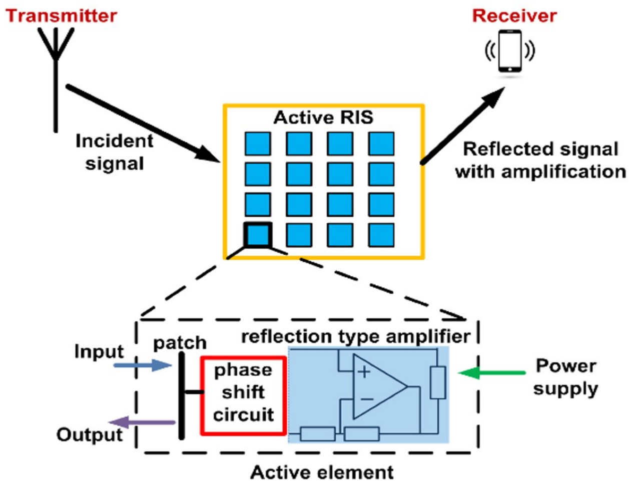

Figure II.8: Active RIS Design for Reflecting Signals with Amplification[30]

This capability facilitates signal amplification, modulation, or regeneration, thereby enhancing signal strength and quality prior to redirection toward intended receivers. The incorporation of active elements distinguishes A-RIS by enabling dynamic control over wave propagation characteristics, optimizing performance in wireless communication systems [47].

- **Hybrid RIS (H-RIS):** Hybrid Reconfigurable Intelligent Surfaces (H-RIS) represent a class of reconfigurable metasurfaces that integrate both passive and active elements to manipulate incident electromagnetic waves as shown in Figure II.9 [48]. Passive components enable energy-efficient reflection or redirection of signals without requiring external power, while active components, such as amplifiers or electronic circuits, introduce controlled energy to enhance the power or fidelity of transmitted signals. This hybrid architecture leverages the complementary strengths of passive and active RIS technologies, aiming to optimize energy efficiency, network coverage, and system capacity in wireless communication frameworks. By balancing passive and active functionalities, H-RIS provide a versatile solution for improving the performance of next-generation telecommunication networks.

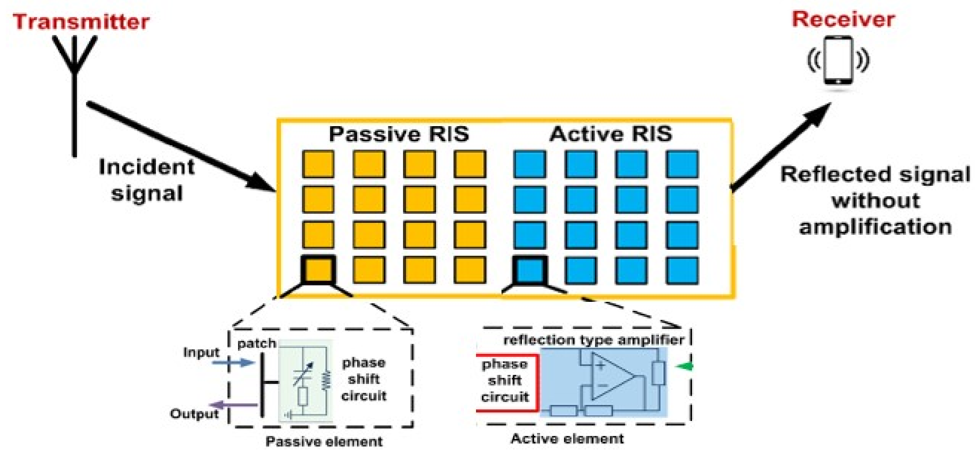

Figure II.9: Hybrid RIS Design for Incident Signal Reflection[30]

II.4.2.2 Based on Operational modalities

According to the implementation of the RIS, RISs can be categorized into three types: reflective, transmissive, and hybrid [49]. In the following, we will elaborate on these types. These three types of RISs are also illustrated in Figure II.10.

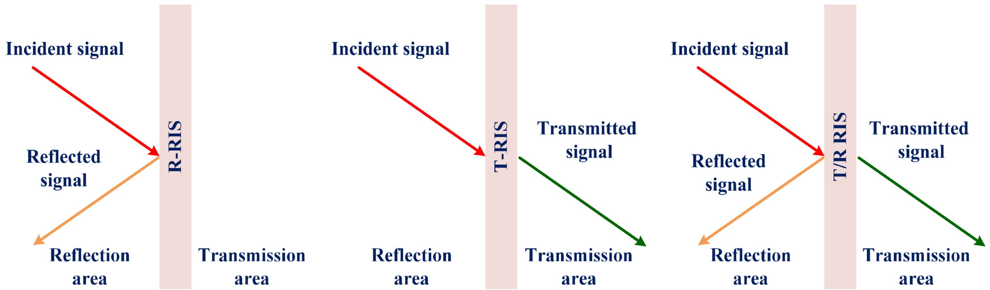

Figure II.10: R-RIS: Reflective RIS — T-RIS: Transmissive RIS — T/R-RIS[49]

- **Reflective Type:** In this type, the RIS only reflects incident signals towards the users on the same side of the BS. In the literature, this type of RIS is also referred to as intelligent reflecting surfaces (IRS).
- **Transmissive Type:** In this type, incident signals will penetrate the RIS and be transmitted towards users on the opposite side of the BS.
- **Hybrid Type:** This type of RIS enables the dual function of reflection and transmission. In other words, the incident signals will be split into two parts: one part is transmitted and the other is reflected. This type of RIS is also referred to as Intelligent Omni-Surface IOS. In the following chapters, the term ”RIS” typically refers to the reflective type RIS for brevity unless otherwise specified.

II.5 Comparison of P-RIS with Relay Systems (DF):

II.5.1 Decode-and-Forward (DF) Relays vs. RIS

Decode-and-Forward (DF) relays decode and re-encode signals before retransmission, which is completely different from the operation of RIS [55]:

- **Signal Processing:** DF relays perform complete decoding and re-encoding, eliminating noise from the first hop, but they require complex baseband processing [54]. In contrast, RIS performs no digital processing and operates purely in the analog domain [45].
- **Spectral Resources:** DF relays typically operate in half-duplex mode, requiring orthogonal time or frequency resources, which reduces spectral efficiency. RIS, however, operates in full-duplex mode without needing additional spectral resources [53].
- **Latency:** DF relays introduce a significant processing delay due to the decoding and re-encoding processes [54]. RIS introduces negligible delay, limited only by the electromagnetic propagation time [52].

II.5.2 Performance Trade-offs

The performance comparison reveals several trade-offs [55]:

1. **Multi-user Support:** RIS offers superior capabilities for simultaneously serving multiple users by creating multiple controllable paths [51], whereas conventional relays are limited in this aspect.
2. **Implementation Cost:** RIS typically offers significantly lower implementation and operational costs compared to relay systems, particularly when considering energy consumption over the system lifetime [48].

II.5.3 Amplify-and-Forward (AF) Relays vs. A-RIS

AF relays receive, amplify, and retransmit signals without decoding, which is similar to the reflection function of RIS but with active amplification. The key differences are as follows:

- **Signal Processing:** AF relays perform active amplification, which inherently amplifies both the signal and the noise [54]. In contrast, RIS reflects signals without amplification, thereby avoiding noise enhancement; however, RIS is subject to the ”double fading” effect [56].

- **Power Consumption:** AF relays require substantial power for reception, amplification, and retransmission. On the other hand, passive RIS consumes power only for its control circuitry, resulting in orders of magnitude lower energy consumption [48].
- **Hardware Requirements:** AF relays need complete RF chains and power amplifiers to perform their functions [54]. Conversely, RIS requires only low-power control circuits for its reconfigurable elements, simplifying the hardware architecture [55].

II.6 Non-Orthogonal Multiple Access (NOMA) Techniques

Orthogonal Multiple Access (OMA) techniques have been foundational to mobile communications since the 1980s, with implementations such as Time Division Multiple Access (TDMA) and Frequency Division Multiple Access (FDMA) in the Global System for Mobile Communications (GSM), followed by Code Division Multiple Access (CDMA) in third-generation (3G) networks, and subsequently Orthogonal Frequency Division Multiple Access (OFDMA) and Multiple Input Multiple Output (MIMO) in 4G-LTE systems [54]. However, the proliferation of connected devices and the exponential growth in demand for network capacity and spectral efficiency have exposed the limitations of OMA approaches, shown in FigureII.11.

To address these challenges, Non-Orthogonal Multiple Access (NOMA) has emerged as a promising paradigm, garnering significant attention from researchers and standardization bodies, such as the 3rd Generation Partnership Project (3GPP), particularly for massive Machine-Type Communications (mMTC) in 5G and beyond [57].are shown in Figure II.11 .

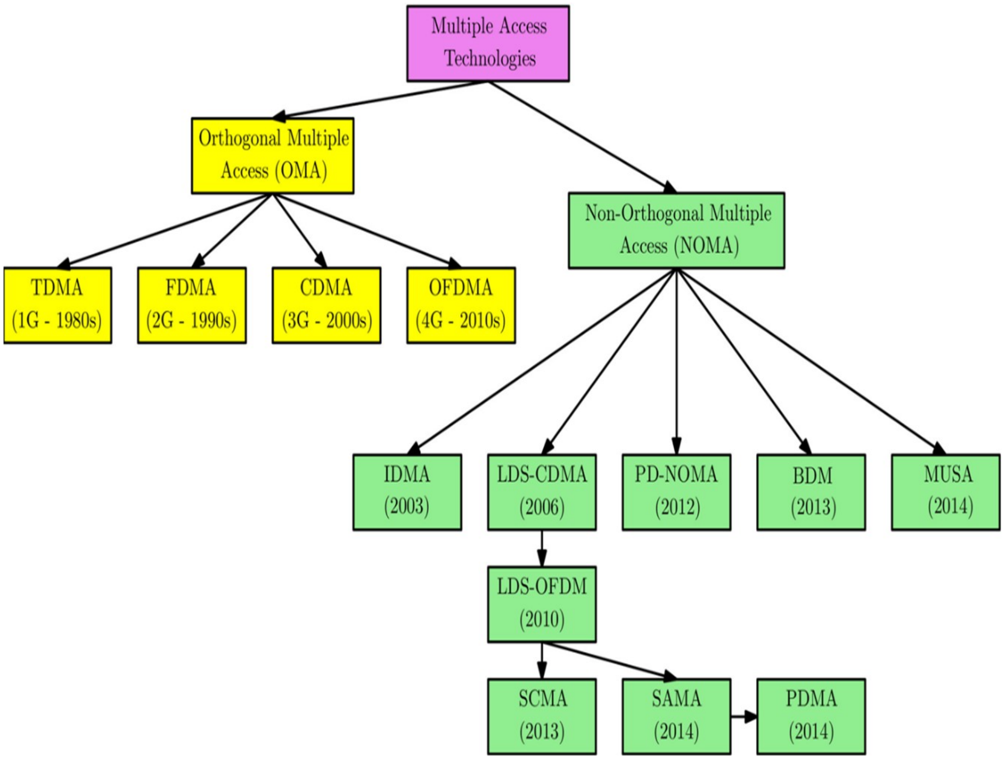

Figure II.11: Evolution of Multiple Access Technologies[32]

Non-Orthogonal Multiple Access (NOMA) involves a series of steps in both the transmission and reception processes to enable multiple users to share the same resource block effectively [57]. The fundamental stages:

1. **User Grouping and Channel Estimation:** Users are grouped based on their channel conditions, and channel state information (CSI) is estimated to facilitate informed power allocation [58].
2. **Power Allocation:** Based on the CSI and quality-of-service (QoS) requirements, distinct power allocation coefficients are assigned. Typically, users with poorer channel conditions receive higher power levels to ensure reliable decoding [57].
3. **Superposition Coding at the Transmitter:** The data signals from the grouped users are combined into a single composite signal using superposition coding. The signals are overlaid in the power domain according to the allocated power coefficients [57].
4. **Transmission Over the Wireless Channel:** The composite signal is then transmitted over the shared wireless channel, allowing multiple user signals to coexist on the same frequency-time resource.

5. **Reception and Successive Interference Cancellation (SIC):** At the receiver side, each user's device receives the composite signal. Through the application of SIC, the device sequentially decodes the overlaid signals [58]. It typically starts by decoding the strongest signal (usually allocated to the user with the weakest channel) and then subtracts this signal from the composite signal, progressively isolating and decoding the remaining signals.

6. **Data Decoding and Error Correction:** After SIC has separated the signals, each receiver decodes its respective data stream using appropriate error correction techniques to ensure data integrity.

   Research indicates that NOMA (b) achieves superior performance compared to OMA (a) in terms of outage probability and ergodic sum rate [59]. Nevertheless, its efficacy is contingent upon precise power allocation coefficients as shown (Figure II-12). Challenges persist, notably the increased computational complexity associated with Successive Interference Cancellation (SIC) and the potential for error propagation in the event of decoding failures, which may degrade transmission quality [58].

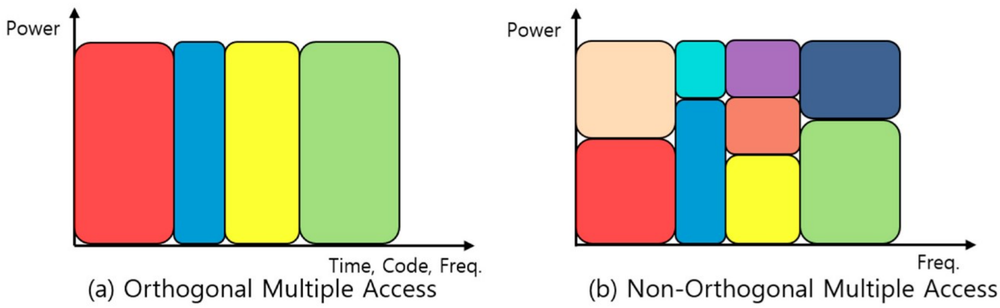

Figure II.12: Power allocation OMA vs NOMA[32]

To mitigate these limitations, a hybrid approach, termed Hybrid NOMA (H-NOMA), has been developed, integrating the strengths of TDMA and NOMA [60]. Through optimized algorithms for time and resource management, H-NOMA has demonstrated the potential to outperform both standalone NOMA and TDMA, achieving a reported 27%increase in throughput compared to OFDMA [60]. Unlike OMA, where each user is allocated a distinct resource block, NOMA enables multiple users to simultaneously utilize the same resource block, thereby enhancing user fairness and overall spectral efficiency within the network [57].

II.7 Overview of Fading Channels and Statistical Models

Fading channels constitute a critical aspect of wireless communication systems, characterized by stochastic fluctuations in the amplitude, phase, or power of the received signal [61]. These variations primarily arise from multipath propagation, wherein signals traverse multiple paths due to reflections, diffractions, and scattering within the propagation environment [62]. To characterize these intricate and random phenomena, statistical distributions have been developed [63]. The following sections elucidate the principal models employed to describe these effects.

II.7.1 Rayleigh Fading Model

The Rayleigh fading model is employed to characterize propagation environments lacking a direct line-of-sight (LoS) component between the transmitter and receiver [64]. In such scenarios, the in-phase and quadrature components of the received signal are modeled as zero-mean Gaussian processes. Consequently, the signal envelope adheres to a Rayleigh distribution [65].

- **Probability Density Function (PDF):**

$$f_\gamma(x) = \frac{1}{\Omega} \exp\left(-\frac{x}{\Omega}\right), \quad x \geq 0 \tag{II.3}$$

  where:

  - Ω denotes the average signal-to-noise ratio (SNR).

- **Applications:** This model is prevalent in urban environments characterized by dense multipath scattering, where no dominant LoS path exists [62].

II.7.2 Rician Fading Model

The Rician fading model extends the Rayleigh framework by incorporating a dominant LoS component alongside multipath contributions [66]. This model is suitable for scenarios where a strong direct signal coexists with scattered signals. The presence of the LoS component introduces a deterministic effect, mitigating the severity of signal fluctuations [67].

Probability Density Function (PDF):

$$f_\gamma(x) = \frac{(K+1)}{\Omega} \exp\left(-K - \frac{(K+1)x}{\Omega}\right) I_0\left(2\sqrt{\frac{K(K+1)x}{\Omega}}\right), \quad x \geq 0 \tag{II.4}$$

where:

- K represents the Rician factor, defined as the ratio of the power in the LoS component to that in the multipath components.
- $I_0(.)$ is the modified Bessel function of the first kind and zeroth order.
- **Special Case:** When $K = 0$, the Rician model degenerates to the Rayleigh model, indicating the absence of a dominant LoS component.

Applications: The Rician model is frequently utilized in suburban or rural settings, where a LoS path is more likely to be present [68].

II.7.3 Nakagami-m Fading Model

The Nakagami-m fading model provides a generalized framework for describing small-scale signal variations in environments with dense multipath scattering [69]. Its versatility stems from the fading severity parameter (m), which governs the characteristics of the fading process [63]. Key Characteristics:

- When ($m = 0.5$), the model corresponds to a one-sided Gaussian distribution.
- When ($m = 1$), it reduces to a Rayleigh distribution.
- For large values of (m), the channel approaches a deterministic state, indicating negligible fading.

Probability Density Function (PDF):

$$f_\gamma(x) = \frac{2m^m}{\Gamma(m)\Omega^m} x^{m-1} \exp\left(-\frac{mx}{\Omega}\right), \quad x \geq 0 \tag{II.5}$$

where:

- m: is the fading severity parameter, controlling the dispersion of the Nakagami-m distribution
- Ω: represents the average received signal power.
- $\Gamma(m)$: denotes the Gamma function.

Applications: The Nakagami-m model is extensively employed in both indoor and outdoor mobile communications, as well as in ionospheric radio communications, owing to its versatility in modeling various fading conditions [70].

In other words, the model's significant adaptability enables effective representation of diverse propagation environments [71].

It is utilized in performance analyses, including channel capacity, error probability, and coverage, and is compatible with simulations of advanced systems such as 5G/6G, RIS, and MIMO configurations [72].

Table II.1: Comparison of Wireless Fading Models Based on Principal

Model	**Principal Characteristics**	**Typical Applications**
Rayleigh	Non-line-of-sight (NLoS); characterized by multipath propagation exclusively	Urban environments, dense scattering scenarios
Rician	Dominant line-of-sight (LoS) component combined with multipath propagation	Suburban and rural areas, satellite communications
Nakagami-m	Generalized model with adjustable parameter (m) for flexible fading severity modeling	Indoor and outdoor mobile communications, ionospheric radio systems

II.8 Conclusion

This chapter has conducted a thorough analysis of Reconfigurable Intelligent Surfaces (RIS) and their crucial role in enhancing wireless communication systems [44]. By examining the foundational principles of metamaterials, the operational mechanisms of RIS, and their advantages over traditional relay systems, we have underscored the transformative potential of RIS in revolutionizing signal propagation and improving network efficiency [51]. The exploration of Non-Orthogonal Multiple Access (NOMA) and statistical fading models, including Rayleigh, Rician, and Nakagami-m, highlights the compatibility of RIS with advanced techniques designed to tackle the challenges faced in contemporary wireless environments [57]. The capability of RIS to dynamically manipulate electromagnetic waves not only boosts network coverage and capacity but also facilitates the creation of intelligent, programmable communication ecosystems [53]. Looking forward, Chapter III will build upon this analysis by assessing the integration of NOMA, RIS, and Nakagami-m fading models, comparing their combined performance with other information transfer techniques to further clarify their practical implications.

Chapter III

Performance Analysis of RIS-Aided NOMA Systems

III.1 Introduction

The rapid evolution of wireless communication systems demands innovative solutions to address challenges such as spectrum scarcity, coverage limitations, and energy efficiency in next-generation networks. Non-Orthogonal Multiple Access (NOMA) has emerged as a promising technique to enhance spectral efficiency by allowing multiple users to share the same frequency resources through power-domain multiplexing and successive interference cancellation (SIC) Simultaneously, Reconfigurable Intelligent Surfaces (RIS) have gained significant attention for their ability to manipulate the propagation environment, enabling enhanced signal coverage and quality in non-line-of-sight (NLoS) scenarios The integration of RIS with NOMA presents a transformative approach to improving system performance in dense urban environments, where traditional line-of-sight (LoS) communication is often obstructed This chapter delves into the performance analysis of RIS-aided NOMA systems, focusing on a dual-user scenario with near and far users under Nakagami-m fading channels By developing a comprehensive system model, we derive analytical expressions for key performance metrics, including outage probability, sum system capacity, and bit error rate (BER) Through rigorous simulations, we compare the proposed RIS-NOMA system with a benchmark Decode-and-Forward (DF) cooperative NOMA system, highlighting the advantages of RIS in enhancing system reliability and efficiency The primary objective is to evaluate the impact of RIS deployment, power allocation strategies, and channel characteristics on system performance, providing insights into practical implementation challenges and future research directions for RIS-enhanced NOMA systems

III.2 Our Study Scenario

III.2.1 Channel Model

This section elucidates the integration of a Reconfigurable Intelligent Surface (RIS) within the propagation environment for the formulation of a channel model. This integration is critical for evaluating the performance of RIS-aided communication networks [44], [73]. The analysis herein focuses exclusively on the reflective RIS configuration, with the channel models for alternative RIS types derivable through analogous methodologies. In an RIS-aided communication framework, the receiver acquires signals via two distinct pathways: the direct path from the transmitter and the reflective path mediated by the RIS [47]. Under the assumption of a narrowband flat-fading channel, the received signal can be mathematically expressed as:

$$Y = (H_{BS-RIS}\Phi H_{RIS-USER}) \cdot x + n \tag{III.1}$$

where x denotes the transmitted signal vector, and n represents the additive white Gaussian noise vector at the receiver. The term H_{BS-RIS} characterizes the direct channel matrix between the base station (transmitter) and the RIS, while $H_{RIS-USER}$ encapsulates the cascaded channel matrix from the transmitter to the receiver via the RIS.

In this investigation like Figure III.1, the focus is directed toward scenario (b), which delineates a configuration wherein communication between the base station (BS) and the user is facilitated through a non-line-of-sight (NLoS) link. This scenario holds particular significance, as it encapsulates real-world environments characterized by dense urban settings, where physical obstructions preclude a direct line-of-sight (LoS) connection between the base station and the user terminal [74].

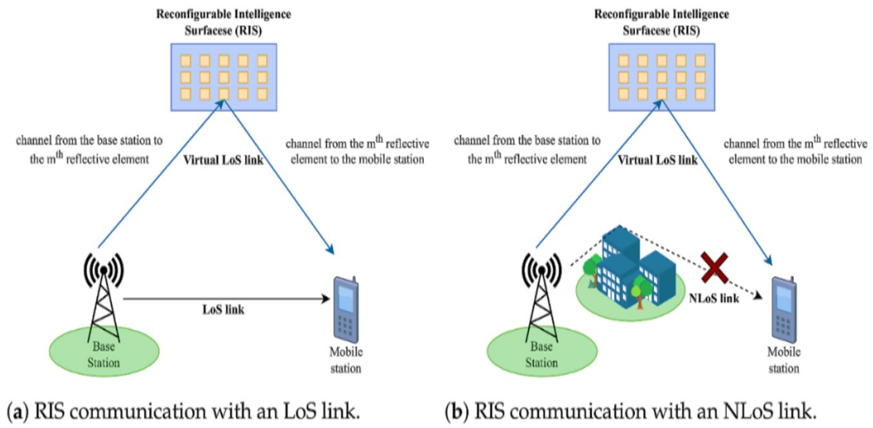

Figure III.1: Schematic Representation of RIS-Enabled Communication[30]

III.2.2 Context of the Study

This research investigates the performance of intelligent reconfigurable surface (RIS)-Aided wireless communication systems operating in a dual-user scenario, where users are positioned at varying distances from the base station, classified as near and far users . In the absence of a direct line-of-sight (LoS) propagation path between the base station and the users, communication relies entirely on the signal reflected by the RIS. The system under consideration employs either passive RIS elements to enhance signal propagation conditions . Performance evaluation is conducted within the framework of non-orthogonal multiple access (NOMA), enabling efficient resource allocation and user multiplexing [45], [71].

The study derives analytical expressions for several key performance metrics: Outage Probability, Sum System Capacity, and Bit Error Rate (BER) . To account for a range of fading environments with varying severity and multipath characteristics, the channel models are formulated using the Nakagami-m distribution, which provides a flexible and accurate representation of real-world propagation conditions [61], [67].

Computer simulations are carried out to corroborate the derived theoretical results and ensure their validity across different operational scenarios. The primary objectives of this work include: analyzing the outage behavior of both near and far users under NOMA-based RIS-Aided transmission [62], [75]; identifying critical system parameters that influence outage performance, such as RIS element configuration, channel fading characteristics, and power allocation strategies [70], [73]; and evaluating the impact of

RIS deployment design on overall system reliability and spectral efficiency [76].

Finally, the dissertation concludes with a comprehensive discussion on the practical implementation challenges and future research directions for RIS-enhanced NOMA systems, highlighting their potential to significantly improve coverage, connectivity, and energy efficiency in next-generation wireless networks [56], [77].

In the context of RIS-NOMA systems, the EC is computed for all users, considering the cascaded channel (base station to RIS to user), power allocation, and successive interference cancellation (SIC) [78].

III.2.3 NOMA Aided by RIS

The integration of Reconfigurable Intelligent Surfaces (RIS) with Non-Orthogonal Multiple Access (NOMA) represents a significant advancement in wireless communications, surpassing the constraints of both traditional Orthogonal Multiple Access (OMA) systems and standalone RIS deployments [44], [79]. By leveraging NOMA's spectral efficiency alongside RIS's capability to manipulate the propagation environment, this approach, whether implemented in passive or active configurations, substantially enhances performance metrics, including outage probability, system capacity, and user fairness [76], [80]. However, several challenges remain, including the complexity of SIC, optimal power allocation, and effective interference management, all of which must be addressed to realize the potential of this technology fully [81], [82].

Future research efforts should prioritize the optimization of beamforming techniques, the integration of multi-antenna configurations, and the development of energy-efficient solutions to ensure practical and scalable deployments in real-world scenarios [74], [83].

III.3 System Model for the Analysis of Passive RIS

III.3.1 System Model Description

The system model delineates a wireless communication framework augmented by a Passive Reconfigurable Intelligent Surface (Passive-RIS) within the context of Non-Orthogonal Multiple Access (NOMA) technology . The communication channels are characterized using the Nakagami-m distribution, facilitating the representation of various fading environments [61]. The model incorporates two users positioned at distinct distances: a Near user and a Far user, as shown in Figure III.2.

- **Base Station (BS):** Transmits signals to the users.
- **Passive-RIS:** A passive surface comprising reflective elements that manipulate the phase of incident signals to enhance transmission quality. The passive elements do not consume energy or amplify signals. Thermal noise generated by these elements is negligible [47].
- **Near User:** Located in close proximity to the Passive-RIS, benefiting from a stronger channel [59].
- **Far User:** Positioned farther away, experiencing significant path loss, and requiring higher power allocation [59].

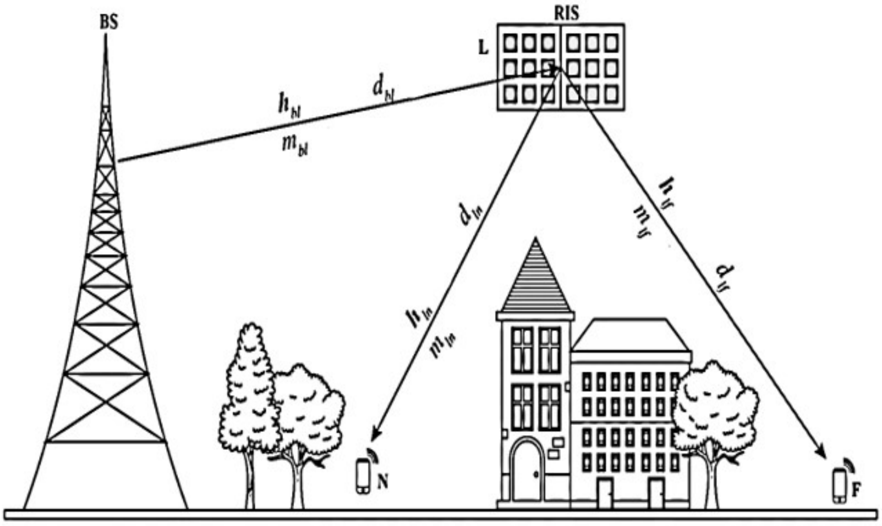

Figure III.2: System Model for Passive RIS-Aided Wireless Communication Network[84]

III.3.2 Non-Orthogonal Multiple Access (NOMA) Implementation in our System

The system employs Non-Orthogonal Multiple Access (NOMA) to facilitate concurrent sharing of spectral resources among multiple users, enhancing spectral efficiency through sophisticated signal processing techniques [45], [71].

(a) **Signal Superposition**

At the base station, signals intended for near and far users are superimposed, creating a composite signal that leverages the same frequency resources [85].

(b) **Power Allocation**

- **Far User (Weak Channel):** A higher power allocation coefficient, denoted as a_f, is assigned to ensure reliable signal detection despite channel impairments [82].
- **Near User (Strong Channel):** A lower power allocation coefficient, a_n, is allocated, where the constraint $a_n + a_f = 1$ ensures total power normalization [71].

(c) **Successive Interference Cancellation (SIC)**

The near user employs SIC to first demodulate the far user's signal, which is allocated higher power, before decoding its own signal, thereby mitigating interference [81].

(d) **Channel Power Characteristics**

The average channel power is determined by the path loss factor (α) and the physical distance between the communicating entities, influencing the overall signal quality [59].

III.4 Formulation of Transmitted and Received Signals

III.4.1 Transmitted Signal

The composite signal transmitted by the base station is expressed as:

$$x = \sqrt{a_n P_b} \cdot x_n + \sqrt{a_f P_b} \cdot x_f \tag{III.2}$$

- P_b: Total transmit power of the base station.
- a_n, a_f: Power allocation coefficients for the near and far users, respectively [71].
- x_n, x_f: Modulated signals intended for the near and far users, respectively.

III.4.2 Received Signal

(a) **Signal Received by the Near User** The signal received by the near user, Y_n, is given by:

$$Y_n = \sqrt{a_n P_b} \cdot (h_{b,l} \Phi h_{l,n}) x_n + \sqrt{a_f P_b} \cdot (h_{b,l} \Phi h_{l,n}) x_f + w_n \tag{III.3}$$

- $h_{b,l} \Phi h_{l,n}$: Composite channel gain between the base station, Passive Reconfigurable Intelligent Surface (RIS), and the near user [47].
- Φ: Diagonal matrix representing the reflection coefficients of the Passive RIS elements [73].
- w_n: Additive White Gaussian Noise (AWGN) at the near user.

(b) **Signal Received by the Far User**

The signal received by the far user, Y_f, is expressed as:

$$Y_f = \sqrt{a_n P_b} \cdot (h_{b,l} \Phi h_{l,f}) x_n + \sqrt{a_f P_b} \cdot (h_{b,l} \Phi h_{l,f}) x_f + w_f \tag{III.4}$$

- $h_{b,l} \Phi h_{l,f}$: Composite channel gain between BS, Passive RIS, and the far user [47].
- w_f: AWGN at the far user.

III.5 Reflection Coefficients of the Passive RIS

The reflection coefficients of the Passive Reconfigurable Intelligent Surface (RIS) govern the phase adjustment of incident signals without active amplification, playing a pivotal role in optimizing signal propagation [47], [73].

III.5.1 Definition of Reflection Coefficients

The reflection coefficients (Φ) are represented as a diagonal matrix:

$$\Phi = \mathrm{diag}(\delta_1 e^{j\theta_1}, \ldots, \delta_L e^{j\theta_L}) \tag{III.5}$$

Where:

- L: Total number of passive reflecting elements in the RIS.
- δ_l: Amplitude coefficient for the l-th element ($\delta_l = 1$ for a Passive RIS, as it does not alter signal amplitude) [73].
- θ_l: Phase shift applied by the l-th element to optimize signal propagation [47].

III.5.2 Role of Reflection Coefficients

- **Phase Control**
  The passive RIS elements adjust the phase of incident signals (θ_l) to maximize channel gain, enhancing communication quality by redirecting signals to circumvent obstacles and establish virtual line-of-sight (LoS) links in non-LoS environments [80].
- **Optimization of Reflection Coefficients**
  The primary objective is to maximize the received signal power by aligning the phases of reflected signals to minimize destructive interference and enhance constructive interference [73].
- **Phase Alignment**
  Optimal phase alignment is achieved by adjusting the phase shifts (θ_l) based on

channel conditions. The optimal phase angle for a given user is calculated as:

$$\text{angle}(\theta_l) = -\,\text{angle}(h_{b,l}) - \text{angle}(h_{l,n}) \tag{III.6}$$

Where:

– $h_{b,l}$: Channel between the base station and the Passive RIS.

– $h_{l,n}$: Channel between the Passive RIS and the near user [47].

- **Channel Gain Maximization**

  By optimizing the reflection coefficients, the Passive RIS enhances the composite channel gain ($h_{b,l}\Phi h_{l,n}$ or $h_{b,l}\Phi h_{l,f}$), thereby improving communication quality for both near and far users [80].

III.6 SINR for the Near User

III.6.1 SINR Without SIC

The SINR for the near user, without SIC, is defined as the ratio of the desired signal power to the sum of interference and noise power. The desired signal is $\sqrt{a_n P_b} \cdot (h_{b,l}\Phi h_{l,n})x_n$, while the far user's signal ($\sqrt{a_f P_b} \cdot (h_{b,l}\Phi h_{l,n})x_f$) contributes to interference. The SINR is expressed as:

$$\gamma_{n\to f} = \frac{a_n P_b |h_{b,l}\Phi h_{l,n}|^2}{a_f P_b |h_{b,l}\Phi h_{l,n}|^2 + \sigma_N^2} \tag{III.7}$$

Where:

- $|h_{b,l}\Phi h_{l,n}|^2$: Composite channel gain between the base station, P-RIS, and the near user [48].
- a_n, a_f: Power allocation coefficients for the near and far users [71].
- σ_N^2: Noise variance at the near user.

III.6.2 Simplified SINR

Introducing the signal-to-noise ratio (SNR) parameter $\zeta_N = \frac{P_b}{\sigma_N^2}$, the SINR becomes:

$$\gamma_{n\to f} = \frac{a_n \zeta_N |h_{b,l} \Phi h_{l,n}|^2}{a_f \zeta_N |h_{b,l} \Phi h_{l,n}|^2 + 1} \tag{III.8}$$

III.6.3 Application of SIC

- **Detection of the Far User's Signal**

  The near user first detects the far user's signal (x_f), which is allocated higher power ($a_f > a_n$) [81].

- **Interference Suppression**

  Upon successful detection, the far user's signal is subtracted from the received signal, yielding the interference-free signal for the near user:

$$Y_n^{\text{SIC}} = \sqrt{a_n P_b} \cdot (h_{b,l} \Phi h_{l,n}) x_n + w_n \tag{III.9}$$

- **SINR After Application of SIC**

  The SINR for the near user after SIC is given by:

$$\gamma_n = \frac{a_n P_b |h_{b,l} \Phi h_{l,n}|^2}{\sigma_N^2} \tag{III.10}$$

  Using the SNR parameter ζ_N, the SINR simplifies to:

$$\gamma_n = a_n \zeta_N |h_{b,l} \Phi h_{l,n}|^2 \tag{III.11}$$

The signal-to-interference-plus-noise ratio (SINR) for the far user in a non-orthogonal multiple access (NOMA) system without successive interference cancellation (SIC) is defined as the ratio of the desired signal power to the aggregate power of interference and noise [81]. For the far user, the desired signal is expressed as $\sqrt{a_f P_b} \cdot (h_{b,l} \Phi h_{l,f}) x_f$, where the signal intended for the near user, $\sqrt{a_n P_b} \cdot (h_{b,l} \Phi h_{l,f}) x_n$, is treated as interference [48].

The transmitted signal x, which encapsulates the superposed signals for both the near and far users under NOMA, yields the received signal at the far user as follows:

$$Y_f = \sqrt{a_n P_b} \cdot (h_{b,l}\Phi h_{l,f})x_n + \sqrt{a_f P_b} \cdot (h_{b,l}\Phi h_{l,f})x_f + w_f \tag{III.12}$$

The SINR for the far user is subsequently formulated as:

$$\gamma_f = \frac{\text{Power of Desired Signal}}{\text{Power of Interference} + \text{Power of Noise}} \tag{III.13}$$

Substituting the relevant terms, the SINR is expressed as:

$$\gamma_f = \frac{a_f P_b |h_{b,l}\Phi h_{l,f}|^2}{a_n P_b |h_{b,l}\Phi h_{l,f}|^2 + \sigma_F^2} \tag{III.14}$$

Where:

- $|h_{b,l}\Phi h_{l,f}|^2$: The composite channel gain from the base station to the far user via the passive reconfigurable intelligent surface (Passive-RIS) [48].
- a_n: The power allocation coefficient for the near user [71].
- a_f: The power allocation coefficient for the far user [71].
- σ_F^2: The noise variance at the far user.

- **Simplification of SINR**

  To facilitate analytical tractability, the SINR can be reformulated in a normalized form by introducing the following parameter:

  - $\zeta_F = \frac{P_b}{\sigma_F^2}$: The signal-to-noise ratio (SNR) at the far user.

  Consequently, the SINR is rewritten as:

$$\gamma_f = \frac{a_f \zeta_F |h_{b,l}\Phi h_{l,f}|^2}{a_n \zeta_F |h_{b,l}\Phi h_{l,f}|^2 + 1} \tag{III.15}$$

III.7 Conditions for Simplification of our Analysis

(a) **Idealized Passive-RIS Components**

The elements of the Passive Reconfigurable Intelligent Surface (Passive-RIS) are assumed to exhibit ideal phase-shifting capabilities without incurring losses or distortions, thereby maximizing their theoretical potential [73]. This assumption facilitates simplified modeling by neglecting material imperfections, thus establishing an optimal framework for evaluating theoretical performance benchmarks.

(b) **Perfect Channel State Information (CSI)**

Perfect CSI is presumed to be available at all network nodes, enabling optimal phase-shift adjustments to enhance system performance [47]. This idealized condition serves as a baseline for comparison with practical systems, where CSI may be subject to inaccuracies or incomplete knowledge [70].

(c) **Noise Modeled as Additive White Gaussian Noise (AWGN)**

The noise is characterized using a standard AWGN model, which streamlines analytical processes and provides a foundational reference for assessing system performance under typical operational conditions.

These conditions collectively delineate the theoretical performance boundaries of Passive-RIS, offering critical insights for practical system design and guiding future research endeavors [83].

III.8 Outage Probability

III.8.1 Near Users

The outage probability for the near user is expressed as:

$$P^{p}_{\mathrm{OUT}_n} = 1 - \Pr[\gamma_{n\to f} \geq \gamma_{\mathrm{th}_f}, \gamma_n \geq \gamma_{\mathrm{th}_n}] \tag{III.16}$$

where the threshold signal-to-noise ratios are defined as:

$$\gamma_{\mathrm{th}_f} = 2^{R_{\mathrm{th}}} - 1 \quad \text{and} \quad \gamma_{\mathrm{th}_n} = 2^{R_{\mathrm{th}_n}} - 1 \tag{III.17}$$

The outage probability is further formulated as:

$$P^p_{\mathrm{OUT}_n} = 1 - \Pr\left[\gamma_{n\to f} = \frac{a_n\zeta_N|h_{b,l}\Phi h_{l,n}|^2}{a_f\zeta_N|h_{b,l}\Phi h_{l,n}|^2+1} \geq \gamma_{\mathrm{th}_f}, \quad a_n\zeta_N|h_{b,l}\Phi h_{l,n}|^2 \geq \gamma_{\mathrm{th}_n}\right] \tag{III.18}$$

The channel power is:

$$|H_N|^2 = \left(\sum_{l=1}^{L}|h_{bl,l}||h_{ln,l}|\right)^2 \tag{III.19}$$

The outage probability is further formulated as:

$$P^p_{\mathrm{OUT}_n} = 1 - \Pr\left[|H_N|^2 \geq \max\left(\frac{\gamma_{\mathrm{th}_f}}{\zeta_N(a_n-\gamma_{\mathrm{th}_f}a_f)}, \frac{\gamma_{\mathrm{th}_n}}{a_n\zeta_N}\right)\right] \tag{III.20}$$

The parameters $Y_{BS} = \frac{m_{bl}}{\Omega_{bl}}$, $Y_N = \frac{m_{ln}}{\Omega_{ln}}$, with integer m_{bl}, m_{ln}, simplify the outage probability (OP) computation in RIS-NOMA by yielding a closed-form Gamma CDF with a finite sum [62]. The OP for user N is expressed as a function of the effective channel gain's CDF, which is computationally efficient due to the integer fading parameters [75].

Where: $h_M \sim \text{Nakagami}(m_{bl}, \Omega_M)$, $h_{ln} \sim \text{Nakagami}(m_{ln}, \Omega_{ln})$

The outage probability (P^p_{out}) for a passive Reconfigurable Intelligent Surface (RIS)-Aided system is given by the cumulative distribution function (CDF) of the effective channel gain $h_{bl}h_{ln}$, evaluated at a threshold related to the target SINR γ_{th} [67]. The expression is:

$$P^p_{\mathrm{out}} = \frac{(Y_{BS}Y_N\gamma_{\mathrm{th}_N})^{m_{ln}}}{\Gamma(m_{bl})\Gamma(m_{ln})(N^2\zeta_N)^{m_{ln}}} G^{2,1}_{1,3}\left(Y_{BS}Y_N\gamma_{\mathrm{th}_N} \;\middle|\; \begin{matrix} 0 \\ 0, m_{ln}, -m_{ln} \end{matrix}\right), \tag{III.21}$$

where:

- $G^{2,1}_{1,3}(\cdot)$: Meijer-G function with order (2,1;1,3) [62].
- $Y_S = \frac{m_{bl}}{\Omega_{bl}}$, $Y_N = \frac{m_{ln}}{\Omega_{ln}}$. Normalized fading parameters, with m_{bl}, m_{ln} as integer Nakagami-m fading parameters, and Ω_{bl}, Ω_{ln} as average channel powers.

- γ_{th_n}: SINR threshold, typically $\gamma_{\text{th}} = 2^{R_{\text{th}}} - 1$, where R_{th} is the target rate.
- ζ_N: Transmit SNR ($\zeta_N = \frac{P}{\sigma_N^2}$, where P is transmit power and σ^2 is noise variance).
- N: Number of RIS reflecting elements.
- $\Gamma(m) = (m-1)!$: Gamma function.

III.8.2 Far Users

The outage probability for the far user is expressed as:

$$P^p_{\text{OUT}_f} = \Pr[\gamma_f < \gamma_{\text{th}_f}] \tag{III.22}$$

$$\gamma_f = \frac{a_f \zeta_F |H_F|^2}{a_n \zeta_F |H_F|^2 + 1} \tag{III.23}$$

$$|H_F|^2 < \frac{\gamma_{\text{th}_f}}{\zeta_F (a_f - \gamma_{\text{th}_f} a_n)} \tag{III.24}$$

$$P^p_{\text{OUT}_f} = \Pr\left[|H_F|^2 < \frac{\gamma_{\text{th}_f}}{\zeta_F (a_f - \gamma_{\text{th}_f} a_n)}\right] \tag{III.25}$$

The parameters $Y_{BS} = \frac{m_{bl}}{\Omega_{bl}}$, $Y_F = \frac{m_{lf}}{\Omega_{lf}}$, with integer m_{bl}, m_{ln}, simplify the outage probability (OP) computation in RIS-NOMA by yielding a closed-form Gamma CDF with a finite sum [62]. The OP for user F is expressed as a function of the effective channel gain's CDF, which is computationally efficient due to the integer fading parameters [75].

Where: $h_{bl} \sim \text{Nakagami}(m_{bl}, \Omega_{bl})$, $h_{ln} \sim \text{Nakagami}(m_{lf}, \Omega_{lf})$

The outage probability (P^p_{out}) for a passive Reconfigurable Intelligent Surface (RIS)-Aided system is given by the cumulative distribution function (CDF) of the effective channel gain $h_{bl}h_{lf}$, evaluated at a threshold related to the target SINR γ_{th} [67]. The expression is:

$$P_{\text{out}}^{p} = \frac{(Y_{BS}Y_F\gamma_{\text{th}_f})^{m_{lf}}}{\Gamma(m_{bl})\Gamma(m_{lf})(N^2\zeta_F)^{m_{lf}}} G_{1,3}^{2,1}\left(Y_{BS}Y_F\gamma_{\text{th}_f} \mid \begin{array}{c} 0 \\ 0, m_{lf}, -m_{lf} \end{array} \right), \tag{III.26}$$

where:

- $G_{1,3}^{2,1}(\cdot)$: Meijer-G function with order (2,1;1,3) [62].
- $Y_S = \frac{m_{bl}}{\Omega_{bl}}$, $Y_F = \frac{m_{lf}}{\Omega_{lf}}$. Normalized fading parameters, with m_{bl}, m_{lf} as integer Nakagami-m fading parameters, and Ω_{bl}, Ω_{lf} as average channel powers.
- γ_{th_f}: SINR threshold, typically $\gamma_{\text{th}} = 2^{R_{\text{th}}} - 1$, where R_{th} is the target rate.
- ζ_F: Transmit SNR ($\zeta_F = \frac{P}{\sigma_F^2}$, where P is transmit power and σ_f^2 is noise variance).
- N: Number of RIS reflecting elements.
- $\Gamma(m) = (m-1)!$: Gamma function.

III.9 Bit Error Rate (BER)

The Bit Error Rate (BER) for the near user and far user in a Passive Reconfigurable Intelligent Surface (PRIS) system is derived using the general BER expression (equation III-27). Below are the final closed-form BER expressions, obtained by evaluating the integral involving the Meijer G-function [84].

The general expression for the Bit Error Rate (BER) in a communication system is given by:

$$\text{BER} = \int_{-\infty}^{\infty} P_e(x) f(x)\, dx \tag{III.27}$$

where:

- $P_e(x)$ is the conditional error probability given the received signal.
- $f(x)$ is the probability density function (PDF) of the received signal.

For AWGN channels, the BER for BPSK modulation is:

$$\text{BER} = Q\left(\frac{\sqrt{2E_b}}{\sigma}\right) \tag{III.28}$$

where:

- $Q(x) = \frac{1}{\sqrt{2\pi}} \int_x^\infty e^{-t^2/2} dt$ is the Q-function.
- E_b is the energy per bit.
- σ is the noise standard deviation.

III.9.1 Near Users

In Nakagami-m fading, the channel power gains H_n and H_f follow a Gamma distribution with PDF [61]:

$$f_{H_i}(x) = \frac{m_i^{m_i} x^{m_i-1}}{\Gamma(m_i)\Omega_i^{m_i}} e^{-\frac{m_i x}{\Omega_i}}, \quad x \geq 0, \quad i \in \{n, f\} \tag{III.29}$$

For the near user, $\gamma_n = a_n \zeta_N H_n$. Let $\bar{\gamma}_n = a_n \zeta_N \Omega_n$ be the average SNIR. The instantaneous SNIR is proportional to H_n, so:

$$\gamma_n = \bar{\gamma}_n \frac{H_n}{\Omega_n} \tag{III.30}$$

The BER is:

$$P_{b,n} = \int_0^\infty Q\left(\sqrt{2\bar{\gamma}_n \frac{x}{\Omega_n}}\right) \cdot \frac{m_n^{m_n} x^{m_n-1}}{\Gamma(m_n)\Omega_n^{m_n}} e^{-\frac{m_n x}{\Omega_n}} dx \tag{III.31}$$

Substitute $z = \frac{m_n x}{\Omega_n}$, so $x = \frac{\Omega_n z}{m_n}$, $dx = \frac{\Omega_n}{m_n} dz$, and the PDF becomes:

$$f_{H_n}(x)dx = \frac{m_n^{m_n} \left(\frac{\Omega_n z}{m_n}\right)^{m_n-1}}{\Gamma(m_n)\Omega_n^{m_n}} e^{-z} \cdot \frac{\Omega_n}{m_n} dz = \frac{z^{m_n-1}}{\Gamma(m_n)} e^{-z} dz \tag{III.32}$$

The argument of the Q-function becomes:

$$\sqrt{2\bar{\gamma}_n \frac{x}{\Omega_n}} = \sqrt{2\bar{\gamma}_n \frac{z}{m_n}} \tag{III.33}$$

Thus:

$$P_{b,n} = \int_0^\infty Q\left(\sqrt{\frac{2\bar{\gamma}_n z}{m_n}}\right) \cdot \frac{z^{m_n-1}}{\Gamma(m_n)} e^{-z} dz \tag{III.34}$$

This integral can be evaluated using the moment-generating function (MGF) approach. The MGF of the Q-function for Nakagami-m fading is [84]:

$$P_{b,n} = \frac{1}{\sqrt{\pi}\Gamma(m_n)} \int_0^{\pi/2} \left(\frac{m_n \sin^2\theta}{m_n \sin^2\theta + \bar{\gamma}_n}\right)^{m_n} d\theta \tag{III.35}$$

For integer m_n, this can be expressed in closed form using finite sums, or special functions. Alternatively, it can be represented using the Meijer G-function for general m_n:

$$P_{b,n} = \frac{1}{\sqrt{\pi}\Gamma(m_n)} G_{2,2}^{2,1}\left(\frac{\bar{\gamma}_n}{m_n} \;\middle|\; \begin{matrix} 1-m_n, 1 \\ 0, 1/2 \end{matrix}\right) \tag{III.36}$$

III.9.2 Far Users

For the far user, the SNIR is:

$$\gamma_f = \frac{a_f \zeta_F H_f}{a_n \zeta_F H_f + 1} \tag{III.37}$$

Let $\bar{\gamma}_f = a_f \zeta_F \Omega_f$, $\bar{\gamma}'_n = a_n \zeta_F \Omega_f$. Then:

$$\gamma_f = \frac{\frac{a_f \zeta_F}{\Omega_f} \cdot H_f}{\frac{a_n \zeta_F}{\Omega_f} \cdot H_f + \frac{1}{\Omega_f}} = \frac{\frac{\bar{\gamma}_f}{\Omega_f} \cdot H_f}{\frac{\bar{\gamma}'_n}{\Omega_f} \cdot H_f + \frac{1}{\Omega_f}} \tag{III.38}$$

The BER is:

$$P_{b,f} = \int_0^\infty Q\left(\sqrt{\frac{2\bar{\gamma}_f \frac{x}{\Omega_f}}{\frac{\bar{\gamma}'_n}{\Omega_f}\frac{x}{\Omega_f} + \frac{1}{\Omega_f}}}\right) \cdot \frac{m_f^{m_f} x^{m_f-1}}{\Gamma(m_f)\Omega_f^{m_f}} e^{-\frac{m_f x}{\Omega_f}} dx \tag{III.39}$$

Substitute $z = \frac{m_f x}{\Omega_f}$, so $x = \frac{\Omega_f z}{m_f}$, $dx = \frac{\Omega_f}{m_f} dz$:

$$P_{b,f} = \int_0^\infty Q\left(\sqrt{\frac{2\bar{\gamma}_f z}{\bar{\gamma}'_n z + m_f}}\right) \cdot \frac{z^{m_f-1}}{\Gamma(m_f)} e^{-z} dz \tag{III.40}$$

This integral is more complex due to the fractional SNIR. It can be evaluated numerically or approximated using the MGF approach for the transformed variable [84]. For high SNIR, approximate:

$$\gamma_f \approx \frac{a_f}{a_n}, \quad \text{if} \quad a_n \zeta_F H_f \gg 1 \tag{III.41}$$

This integral is challenging due to the fractional term. For integer m_f, it can be approximated or evaluated using the Meijer G-function after variable substitution [84]. Assuming the user's context (Meijer G-function for SER), we approximate the inner integral:

$$P_{b,f} \approx \frac{1}{\sqrt{\pi}\Gamma(m_f)} \int_0^{\pi/2} G_{2,2}^{2,1}\left(\frac{\bar{\gamma}_f}{\bar{\gamma}'_n \sin^2\theta + m_f} \;\middle|\; \begin{matrix} 1-m_f, 1 \\ 0, 1/2 \end{matrix}\right) d\theta \tag{III.42}$$

III.10 Ergodic Capacity (EC)

III.10.1 Near User

The SNIR for the near user is:

$$\gamma_n = a_n \zeta_N H_n \tag{III.43}$$

The ergodic capacity is:

$$C_n = \mathbb{E}\left[\log_2\left(1 + a_n \zeta_N H_n\right)\right] \tag{III.44}$$

To compute this, we use the PDF of H_n [78]:

$$C_n = \int_0^\infty \log_2\left(1 + a_n \zeta_N x\right) \cdot \frac{m_n^{m_n} x^{m_n - 1}}{\Gamma(m_n)\Omega_n^{m_n}} e^{-\frac{m_n x}{\Omega_n}} dx \tag{III.45}$$

This integral can be evaluated using the following result for the expectation of a logarithmic function over a Gamma distribution. For a Gamma-distributed random variable $X \sim \text{Gamma}(m, \theta)$ (where $\theta = \frac{\Omega_n}{m_n}$), the ergodic capacity is [78]:

Using the PDF of H_n:

$$C_n = \int_0^\infty \log_2\left(1 + a_n \zeta_N x\right) \cdot \frac{m_n^{m_n} x^{m_n - 1}}{\Gamma(m_n)\Omega_n^{m_n}} e^{-\frac{m_n x}{\Omega_n}} dx \tag{III.46}$$

Converting to natural logarithm for convenience ($\log_2(x) = \frac{\ln(x)}{\ln(2)}$):

$$C_n = \frac{1}{\ln 2} \int_0^\infty \ln\left(1 + a_n \zeta_N x\right) \cdot \frac{m_n^{m_n} x^{m_n - 1}}{\Gamma(m_n)\Omega_n^{m_n}} e^{-\frac{m_n x}{\Omega_n}} dx \tag{III.47}$$

For integer m_n, a closed-form expression exists using the exponential integral $E_1(z) = \int_z^\infty \frac{e^{-t}}{t} dt$ [78]:

$$C_n = \frac{1}{\ln 2} \sum_{k=1}^{m_n} \binom{m_n}{k} (-1)^{m_n-k} \left(\frac{m_n}{a_n \zeta_N \Omega_n}\right)^{m_n-k} E_1\left(\frac{m_n}{a_n \zeta_N \Omega_n}\right) \tag{III.48}$$

For non-integer m_n, the integral can be evaluated numerically or expressed using the Meijer G-function, but numerical integration is often preferred [78]:

$$C_n = \frac{1}{\ln 2} \int_0^\infty \ln\left(1 + a_n \zeta_N x\right) \cdot \frac{m_n^{m_n} x^{m_n-1}}{\Gamma(m_n)\Omega_n^{m_n}} e^{-\frac{m_n x}{\Omega_n}} dx \tag{III.49}$$

III.10.2 Far User

The SNIR for the far user is:

$$\gamma_f = \frac{a_f \zeta_F H_f}{a_n \zeta_F H_f + 1} \tag{III.50}$$

The ergodic capacity is:

$$C_f = \mathbb{E}\left[\log_2\left(1 + \frac{a_f \zeta_F H_f}{a_n \zeta_F H_f + 1}\right)\right] \tag{III.51}$$

This can be rewritten as:

$$C_f = \mathbb{E}\left[\log_2\left(\frac{1 + (a_f + a_n)\zeta_F H_f}{1 + a_n \zeta_F H_f}\right)\right] \tag{III.52}$$

$$= \mathbb{E}\left[\log_2\left(1 + (a_f + a_n)\zeta_F H_f\right)\right] - \mathbb{E}\left[\log_2\left(1 + a_n \zeta_F H_f\right)\right] \tag{III.53}$$

Using the PDF of H_f

$$C_f = \int_0^\infty \left[\log_2\left(1 + (a_f + a_n)\zeta_F x\right) - \log_2\left(1 + a_n\zeta_F x\right)\right] \cdot \frac{m_f^{m_f} x^{m_f-1}}{\Gamma(m_f)\Omega_f^{m_f}} e^{-\frac{m_f x}{\Omega_f}} dx \quad \text{(III.54)}$$

This splits into two integrals, each similar to the near user case [78]:

$$C_f = \frac{1}{\ln 2}\left[\int_0^\infty \ln\left(1 + (a_f + a_n)\zeta_F x\right) f_{H_f}(x)dx - \int_0^\infty \ln\left(1 + a_n\zeta_F x\right) f_{H_f}(x)dx\right] \quad \text{(III.55)}$$

Each term can be evaluated similarly to the near user case, using the Meijer G-function or numerical methods. For integer m_f [78]:

$$C_f = \frac{1}{\ln 2}\sum_{k=0}^{m_f-1} \frac{(-1)^k\binom{m_f-1}{k}\left[E_1\left(\frac{m_f}{(a_f+a_n)\zeta_F\Omega_f}\right)\left(\frac{m_f}{(a_f+a_n)\zeta_F\Omega_f}\right)^{m_f-k} - E_1\left(\frac{m_f}{a_n\zeta_F\Omega_f}\right)\left(\frac{m_f}{a_n\zeta_F\Omega_f}\right)^{m_f-k}\right]}{\left(\frac{m_f}{\Omega_f}\right)^{m_f-k}} \quad \text{(III.56)}$$

III.11 System Model for Simulation

Figure III.3 presents a downlink NOMA-Aided RIS system model. The considered system consists of a base station (BS), one RIS, and two users, namely a strong user (n) and a weak user (f). We assume that the direct links do not exist between the BS and users due to the obstacles. Therefore, users receive their signal only through RIS [80]. The Nakagami-m fading channel is assumed in all nodes [61].

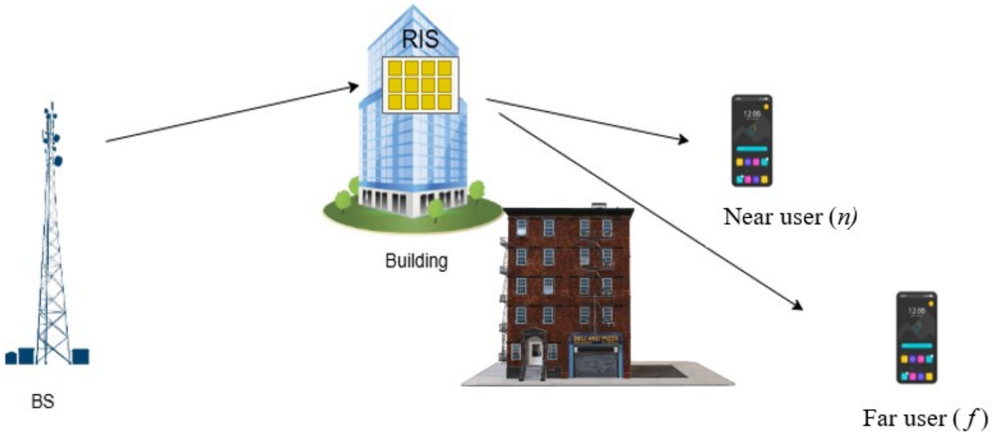

Figure III.3: NOMA-Aided RIS system model

The BS transmits a superposition coding (SC) signal consisting of Near User (n) and Far User (f) to the users through RIS with different power levels based on the channel gain $|h_{b,l}|^2\Phi|h_{l,f}|^2 < |h_{b,l}|^2\Phi|h_{l,n}|^2$ [71]. The received signal at users is given by:

$$y_i = \sqrt{P_S}\left(\sqrt{a_n X_n} + \sqrt{a_f X_f}\right) h_{b,l}\Phi h_{l,i} + w, \quad i = n, f \tag{III.57}$$

Where P_S is the total transmitting power by BS. $a_n + a_f = 1$. $a_n < a_f$. a_n and a_f are the power allocation coefficients of (n) and (f), respectively [71]. X_n and X_f are the signals of the (n) and (f), respectively. $h_{b,l}$ is the Nakagami-m fading channel between BS-RIS, where $h_{b,l} \in \mathbb{C}^{N\times 1} \sim \text{CN}(0, \sigma_l^2)$, $h_{l,n} \in \mathbb{C}^{N\times 1} \sim \text{CN}(0, \sigma_n^2)$, $h_{l,f} \in \mathbb{C}^{N\times 1} \sim \text{CN}(0, \sigma_f^2)$. $\sigma_l^2 = d_l^{-\alpha}$, $\sigma_n^2 = d_n^{-\alpha}$, $\sigma_f^2 = d_f^{-\alpha}$, where d_l, d_n, d_f denote the distances between the BS-RIS, RIS-n, and RIS-f, respectively, and α is the path loss exponent [59]. w is the additive white Gaussian noise (AWGN), where $w \sim \text{CN}(0, \sigma^2)$. $\Phi = \text{diag}(e^{j\Theta_1}, e^{j\Theta_2}, \ldots, e^{j\Theta_N})$ is the RIS phase shift matrix [73]. N is the number of RIS elements. To simplify calculations and simulations, we assume that the white Gaussian noise $w \sim \text{CN}(0, \sigma^2)$ is equal for both the near and far users, as well as for the channel, which means that the σ_f^2=σ_n^2=σ^2 value is the same for all parties, facilitating mathematical analysis and improving the accuracy of system performance evaluation.

The f decodes X_f first without SIC. The SINR at the f is given by:

$$\gamma_f^{\text{RIS}} = \frac{a_f P_b |h_{b,l}|^2 \Phi |h_{l,f}|^2}{a_n P_b |h_{b,l}|^2 \Phi |h_{l,f}|^2 + \sigma^2} \tag{III.58}$$

The n decodes X_f first without SIC. Then, it uses the SIC to decode X_n. The SINR at the n are given by:

$$\gamma_n^{\text{RIS}} = \frac{a_f P_b |h_{b,l}|^2 \Phi |h_{l,n}|^2}{a_n P_b |h_{b,l}|^2 \Phi |h_{l,n}|^2 + \sigma^2} \tag{III.59}$$

$$\gamma_n^{\text{RIS}} = \frac{a_n P_b |h_{b,l}|^2 \Phi |h_{l,n}|^2}{\sigma^2} \tag{III.60}$$

III.11.1 Benchmark: Cooperative NOMA

Figure III.4 presents a DF cooperative NOMA system as a benchmark to NOMA-Aided RIS [60]. The considered system consists of a BS, one relay, and two users, as follows: strong user (n) and weak user (f). We assume that the direct links do not exist between the BS and users due to the obstacles. Therefore, the users receive their signal through relay only [68]. The Nakagami-m fading channel is assumed in all nodes [61].

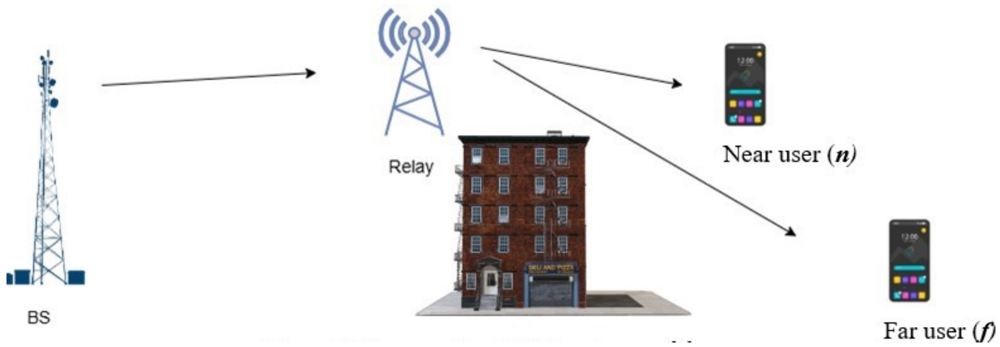

Figure III.4: Cooperative NOMA system model

The BS transmits an SC signal consisting of n and f to the relay with different power levels based on the channel gain $a_n < a_f$ [71]. The received signal at relay is given by:

$$y_{\text{relay}} = \sqrt{P_b}\left(\sqrt{a_n X_n} + \sqrt{a_f X_f}\right) h_{b,r} + w, \tag{III.61}$$

Where $h_{b,r}$ is the Nakagami-m fading channel between BS-relay such that, where $m = 1$

and $h_{b,r} \sim \text{CN}(0, \sigma_{b,r}^2)$, $\sigma_{b,r}^2 = d_{b,r}^{-\alpha}$, where $d_{b,r}$ denotes the distances between the BS-relay and α is the path loss exponent [59]. w is the additive white Gaussian noise (AWGN), where $w \sim \text{CN}(0, \sigma^2)$, and $\sigma_{b,r}^2 = \sigma^2$.

The relay decodes X_f first without SIC. Then, it uses the SIC to decode X_n. The SINR at the relay are given by:

$$\gamma_f^{\text{relay}} = \frac{a_f P_b |h_{b,r}|^2}{a_n P_b |h_{b,r}|^2 + \sigma^2} \tag{III.62}$$

$$\gamma_n^{\text{relay}} = \frac{a_n P_b |h_{b,r}|^2}{\sigma^2} \tag{III.63}$$

The relay re-encodes the X_n and X_f in an SC signal as in BS with different power levels based on the channel gain $|h_f|^2 < |h_n|^2$ [71]. The received signal at users is given by:

$$y_i = \sqrt{P_r}\left(\sqrt{a_n X_n} + \sqrt{a_f X_f}\right) h_{r,i} + w, \quad i = n, f \tag{III.64}$$

Where P_r is the relay transmitting power. $a_n + a_f = 1$. $a_n < a_f$. a_n and a_f are the power allocation coefficients of n and f, respectively [71]. X_n and X_f are the signals of the n and f, respectively. $h_{r,n}$ and $h_{r,f}$ are the Nakagami-m fading channel between relay-n and relay-f, where $h_{r,n} \sim \text{CN}(0, \sigma_n^2)$, $h_{r,f} \sim \text{CN}(0, \sigma_f^2)$. $\sigma_n^2 = d_n^{-\alpha}$, $\sigma_f^2 = d_f^{-\alpha}$, where d_n, d_f denote the distances between the relay-n, and relay-f, respectively, and α is the path loss exponent [59]. w is the additive white Gaussian noise (AWGN) where $\sigma_f^2 = \sigma_n^2 = \sigma^2$.

The f decodes X_f first without SIC. The SINR at the f is given by:

$$\gamma_{r,f} = \frac{a_f P_r |h_{r,f}|^2}{a_n P_r |h_{r,f}|^2 + \sigma^2} \tag{III.65}$$

The n decodes X_f first without SIC. Then, it uses the SIC to decode X_n. The SINR at the n are given by:

$$\gamma_{r,n}^{\mathrm{SIC}} = \frac{a_f P_r |h_{r,f}|^2}{a_n P_r |h_{r,n}|^2 + \sigma^2} \tag{III.66}$$

$$\gamma_{r,n}^{\mathrm{SIC}} = \frac{a_n P_r |h_{r,n}|^2}{\sigma^2} \tag{III.67}$$

III.12 Simulation and Results

In this section, simulation focuses on the comparative analysis of the performance of two systems: Reconfigurable Intelligent Surface Non-Orthogonal Multiple Access (RIS-NOMA) and Decode-and-Forward (DF) Relay NOMA, specifically in a Nakagami-m fading channel with $m = 1$, which is equivalent to a Rayleigh fading channel [61], [68]. The analysis will cover three essential performance metrics: Bit Error Rate (BER) [84], Outage Probability (OP) [62], [75], and Ergodic Capacity (EC) [78], all of which will be evaluated as functions of the Signal-to-Noise Ratio (SNR).

III.12.1 Simulation Parameters

In the simulations, we use the following parameters:

Table III.1: Simulation Parameters.

Parameters	**Notions**	**Values**
Distance between BS and RIS	$d_{b,l}$	1 m
Distance between RIS and n	$d_{l,n}$	1 m
Distance between RIS and f	$d_{l,f}$	2 m
Exponent of the path loss	α	1
Power allocation coeff of n	a_n	0.2
Power allocation coeff of f	a_f	0.8
Transmission rate of n	R_n	0.5 bps/Hz
Transmission rate of f	R_f	1 bps/Hz
Number of RIS elements	N	16, 32, 64
Channel Nakagami-m	m	1
Monte Carlo	ite	10^5

III.12.2 Capacity of System

In this subsection, we perform the capacity simulation of downlink NOMA-Aided RIS. we compare the capacity of our system with downlink cooperative NOMA. The capacity is the quantity of information that the channel can transmit, according to our system it is given by the following forms: The capacity of n and f for NOMA Aided RIS are given by:

$$C_n^{\text{RIS}} = \log_2(1 + \gamma_n^{\text{RIS}}) \tag{III.68}$$

$$C_f^{\text{RIS}} = \log_2(1 + \gamma_f^{\text{RIS}}) \tag{III.69}$$

The capacity of n and f for cooperative NOMA are given by:

$$C_f^{\text{RL}} = \frac{1}{2}\log_2\left(1 + \min\left(\frac{a_f P_b |h_{b,l}|^2}{a_n P_b |h_{b,l}|^2 + \sigma^2}, \frac{a_f P_r |h_{l,f}|^2}{a_n P_b |h_{l.f}|^2 + \sigma^2}\right)\right) \tag{III.70}$$

$$C_n^{\text{RL}} = \frac{1}{2}\log_2\left(1 + \min\left(\frac{a_n P_b |h_{b,l}|^2}{\sigma^2}, \frac{a_n P_r |h_n|^2}{\sigma^2}\right)\right) \tag{III.71}$$

Where P_r is the relay power in case of cooperative relay NOMA system model. The sum capacity is given by:

$$C_{\text{System}} = C_n + C_f \tag{III.72}$$

III.12.2.1 Simulation Results of Ergodic Capacity

Figure III.5 compares the ergodic capacity of Near and Far users in RIS-NOMA and DF Relay NOMA systems as a function of SNR. The x-axis represents SNR (dB), ranging from 0 to 30 dB, and the y-axis represents capacity (bits/sec/Hz), ranging from 0 to 12 bits/sec/Hz.

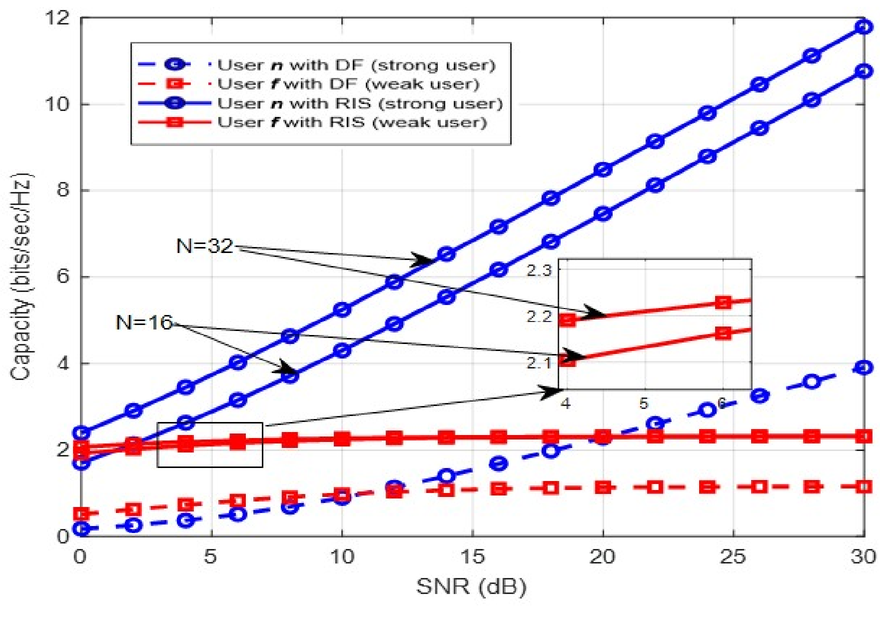

Figure III.5: Capacity of n and f for NOMA with RIS and DF cooperative NOMA.

1)-Key Observations for (Ergodic Capacity vs. SNR)

- **User n with RIS (strong user, solid blue line)**

  - For $N = 16$, the capacity starts at around 2 bits/sec/Hz at 0 dB SNR and increases steadily, reaching approximately 11 bits/sec/Hz at 30 dB SNR.

  - For $N = 32$, the capacity is higher, starting at around 2.5 bits/sec/Hz at 0 dB SNR and reaching around 12 bits/sec/Hz at 30 dB SNR.

- **User f with RIS (weak user, solid red line):**

  For $N = 16$, starting at around 2.1 bits/sec/Hz, the capacity is relatively flat, staying around 2.2 bits/sec/Hz across the SNR range.

  For $N = 32$, starting at around 2.2 bits/sec/Hz, the capacity is relatively flat, staying around 2.2 bits/sec/Hz across the SNR range.

- **User n with DF (strong user, dashed blue line):**
  The capacity starts at around 0.2 bit/sec/Hz at 0 dB SNR and plateaus at around 4 bits/sec/Hz beyond 30 dB SNR.

- **User f with DF (weak user, dashed red line):** The capacity starts at around 0.5 bit/sec/Hz at 0 dB SNR and plateaus at around 1.5 bits/sec/Hz beyond 30 dB SNR.

2)-Inset Graph (Zoomed View):

The inset graph zooms in on the capacity of the weak user (f), It highlights that the weak user's capacity in the RIS system (2.1–2.3 bits/sec/Hz) is consistently higher than weak users in the DF system (0.5–1.5 bits/sec/Hz).

3)-Analysis and Interpretation of Results

- **Effect of Number of RIS Elements (N):**
  - Increasing the number of RIS elements from $N = 16$ to $N = 32$ significantly improves the capacity for the strong user (n) in the RIS system, as seen in the steeper blue solid line for $N = 32$.
  - The weak user (f) in the RIS system sees a modest capacity increase (from 2.1 to 2.3 bits/sec/Hz) with more RIS elements, indicating that RIS benefits the strong user more prominently.

- **Comparison of RIS vs. DF Cooperative NOMA:**
  - The RIS system outperforms the DF cooperative NOMA system for both users across all SNR values.
  - For the strong user (n), the RIS system's capacity (blue solid lines) is significantly higher than the DF system (blue dashed line), especially at higher SNRs and with more RIS elements ($N = 32$).
  - For the weak user (f), the RIS system (red solid lines) achieves a capacity of around (2.1–2.3) bits/sec/Hz, which is much higher than the DF system's capacity of around (0.5 to 1.5 bits/sec/Hz) (red dashed line).
- **Superiority of RIS System:**
  - The NOMA-Aided RIS system significantly outperforms the DF cooperative NOMA system in terms of capacity for both the strong and weak users. This is primarily due to the RIS's ability to optimize the channel through phase shifts (Φ), enhancing the effective channel gain ($|h_{b,l}|^2\Phi|h_{l,i}|^2$).
  - The single-hop nature of the RIS system avoids the spectral efficiency loss ($\frac{1}{2}$ factor) inherent in the two-hop DF cooperative NOMA system, as seen in the capacity equations
  - RIS : $C_n^{\text{RIS}} = \log_2(1 + \gamma_n^{\text{RIS}})$, $C_f^{\text{RIS}} = \log_2(1 + \gamma_f^{\text{RIS}})$
  - DF: $C_n = \frac{1}{2}\log_2(1 + \min(\gamma_n^{\text{relay}}, \gamma_{r,n}^{\text{SIC}}))$, $C_f = \frac{1}{2}\log_2(1 + \min(\gamma_f^{\text{relay}}, \gamma_{r,f}^{\text{sic}}))$
- **Impact of N:**
  - Increasing the number of RIS elements (N) from 16 to 32 enhances the capacity of the strong user (n) dramatically, as more elements allow better beamforming and signal reflection, improving the SINR ($\gamma_n^{\text{RIS}} = \frac{N a_n P_b |h_{b,l}|^2\Phi|h_{l,n}|^2}{\sigma^2}$).
  - The weak user (f) benefits less from the increase in N, as its SINR ($\gamma_f^{\text{RIS}} = \frac{N a_f P_b |h_{b,l}|^2\Phi|h_{l,f}|^2}{a_n P_b |h_{b,l}|^2\Phi|h_{l,f}|^2 + \sigma^2}$) is limited by interference from the strong user's signal ($a_n P_b |h_{b,l}|^2\Phi|h_{l,f}|^2$).
- **Weak User's Performance:**
  - The weak user (f) in the RIS system maintains a relatively stable capacity (2.1–2.3 bits/sec/Hz) across SNR, which aligns with its SINR being interference-limited rather than noise-limited at higher SNRs.

  – In contrast, the weak user in the DF system has a very low capacity (around 0.5 bits/sec/Hz), likely due to the two-hop transmission and the relay's limited ability to mitigate interference.

III.12.2.2 Simulation Results of Sum Capacity

- In Figure III.6, a Sum Capacity vs. SNR is shown, the x-axis represents SNR (dB), ranging from 0 to 30 dB, and the y-axis represents sum capacity (bits/sec/Hz), ranging from 0 to 16 bits/sec/Hz.

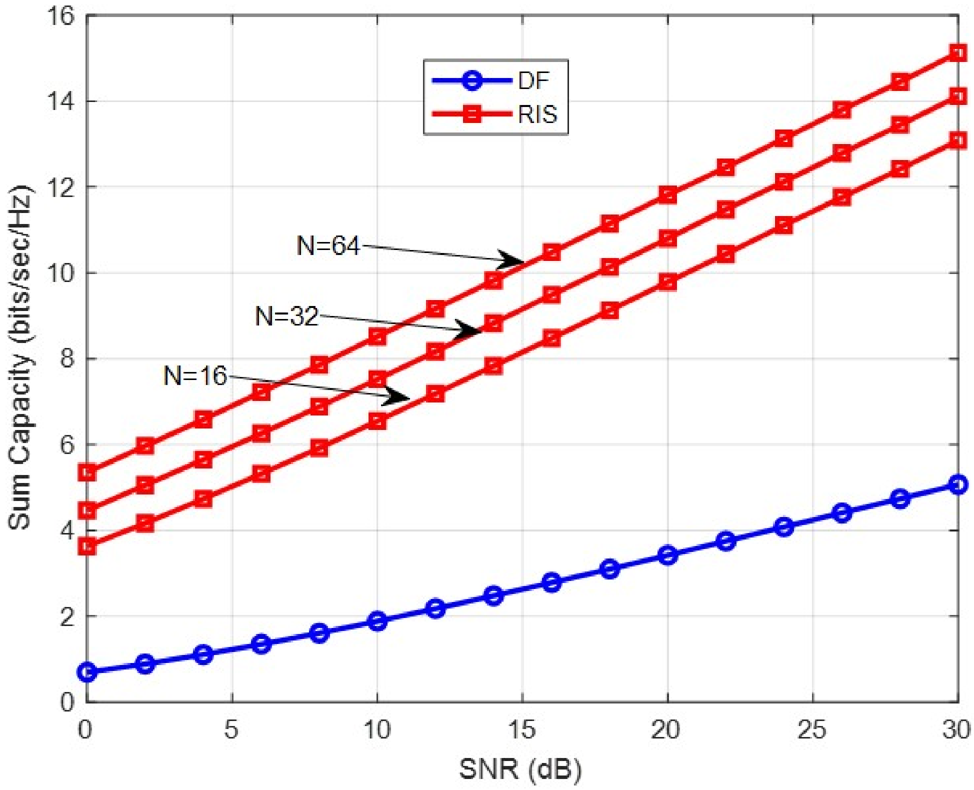

Figure III.6: Sum Capacity of NOMA with RIS and DF cooperative NOMA with different number of RIS elements (N=16, 32, 64).

1)-Key Observations for (Sum Capacity vs. SNR)

- **RIS System (red lines):**

  Three curves are shown for the RIS system in Figure III.6, corresponding to different numbers of RIS elements ($N = 16, 32, 64$):

  – For $N = 16$, the sum capacity starts at around 3.5 bits/sec/Hz at 0 dB SNR and increases to approximately 13 bits/sec/Hz at 30 dB SNR.

  - For $N = 32$, the sum capacity starts at around 4.5 bits/sec/Hz at 0 dB SNR and reaches around 14 bits/sec/Hz at 30 dB SNR.
  - For $N = 64$, the sum capacity is the highest, starting at around 5.5 bits/sec/Hz at 0 dB SNR and reaching approximately 15 bits/sec/Hz at 30 dB SNR.

- **DF Cooperative NOMA System (blue line):**
  - The sum capacity starts at around 1 bit/sec/Hz at 0 dB SNR and increases gradually, plateauing at around 5 bits/sec/Hz beyond 30 dB SNR.

2)- Analysis and Interpretation of Results

- **Effect of Number of RIS Elements (N):**
  - Increasing the number of RIS elements (N) from 16 to 64 significantly boosts the sum capacity of the RIS system.
  - The gap between the curves for $N = 16$, $N = 32$, and $N = 64$ widens as SNR increases, indicating that more RIS elements provide a greater capacity advantage at higher SNRs.
- **Comparison of RIS vs. DF Cooperative NOMA:**
  - The RIS system consistently outperforms the DF cooperative NOMA system across all SNR values and for all values of N.
  - At 30 dB SNR, the sum capacity of the RIS system with $N = 64$ (15 bits/sec/Hz) is nearly three times that of the DF system (5 bits/sec/Hz).
  - Even with $N = 16$, the RIS system's sum capacity (13 bits/sec/Hz at 30 dB SNR) is significantly higher than the DF system's (5 bits/sec/Hz), suggesting a limitation due to the DF two-hop transmission and interference constraints.
- **Superiority of RIS System:**
  - The NOMA-Aided RIS system achieves a much higher sum capacity than the DF cooperative NOMA system, primarily due to its ability to enhance the effective channel gain through the phase shift matrix Φ. The sum capacity for RIS is the sum of the individual user capacities: $C_{\text{System}}^{\text{RIS}} = C_n^{\text{RIS}} + C_f^{\text{RIS}}$, where $C_n^{\text{RIS}} = \log_2(1 + \gamma_n^1)$ and $C_f^{\text{RIS}} = \log_2(1 + \gamma_f^2)$.
  - In contrast, the DF system's sum capacity is limited by the two-hop transmission: $C_{\text{System}}^{\text{DF}} = C_n + C_f$, where $C_n = \frac{1}{2}\log_2(1 + \min(\gamma_{\text{relay}}^n, \gamma_{r,n}^n))$ and

$C_f = \frac{1}{2}\log_2(1+\min(\gamma^f_{\text{relay}}, \gamma^f_{r,f}))$. The $\frac{1}{2}$ factor reflects the spectral efficiency loss due to the two-phase transmission (BS to relay, relay to users).

- **Impact of N:**
  - The number of RIS elements (N) has a profound impact on the sum capacity. More elements allow better beamforming and signal reflection, increasing the SINR for both users (γ^n_{RIS} and γ^f_{RIS}) and thus boosting the overall capacity.
  - The capacity gain from increasing N is more pronounced at higher SNRs, as the RIS can more effectively mitigate interference and noise, leading to a steeper capacity curve.

III.12.3 Outage Probability

The outage defined the action that happened when the receiver cannot successfully decode the received signal. The outage is expressed when the capacity is less than the transmission rate. In this subsection, we perform the outage probability simulation of downlink NOMA Aided RIS. We compare the outage probability of our system with downlink DF cooperative NOMA. In case of NOMA Aided RIS, the OP of f is defined as own capacity C_f, which is less than the rate R_f:

$$P^f_{\text{out}} = P(\gamma^{\text{RIS}}_f < 2^{R_f} - 1) \quad ; \text{ when } \quad \gamma^f_{\text{th}} = 2^{R_f} - 1 \tag{III.73}$$

The OP of n is defined as the sum of: When X_f is detected erroneously and correctly. Then, the OP of n signal can be expressed by:

$$P^n_{\text{out}} = P(\gamma^{\text{RIS}}_n < \gamma^f_{\text{th}}, \delta^{\text{RIS}}_n < \gamma^f_{\text{th}}) \tag{III.74}$$

Likewise, in the DF cooperative NOMA system, the outage probability of n and f are defined as:

$$P^f_{\text{out}} = P\left(\min\left(\frac{a_f P_b |h_{b,r}|^2}{a_n P_b |h_{b,r}|^2 + \sigma^2}, \frac{a_f P_r |h_{r,f}|^2}{a_n P_r |h_{r,f}|^2 + \sigma^2}\right) < 2^{2R_f - 1}\right) \tag{III.75}$$

$$P^n_{\text{out}} = P(\psi_n < 2^{2R_f - 1}, \psi_f < 2^{2R_n - 1}) \tag{III.76}$$

Where $\psi_n = \min\left(\frac{a_f P_b |h_{b,r}|^2}{a_n P_b |h_{b,r}|^2 + \sigma_r^2}, \frac{a_f P_r |h_{r,n}|^2}{a_n P_r |h_{r,n}|^2 + \sigma_n^2}\right)$ and $\psi_f = \min\left(\frac{a_n P_b |h_{b,r}|^2}{\sigma_r^2}, \frac{a_n P_r |h_{r,n}|^2}{\sigma_f^2}\right) < 2^{2R_n - 1}$. R_n and R_f are the target rate of n and f, respectively, the outage probability of the system is given by:

$$P_{\text{out}}^{\text{Sys}} = 1 - (1 - P_{\text{out}}^{n})(1 - P_{\text{out}}^{f}) \tag{III.77}$$

III.12.3.1 Simulation Results of Outage Probability:

Analyze Figure III.7, which presents the outage probability of near user n and far user f for NOMA with RIS and DF cooperative NOMA systems as a function of SNR (dB). The figure uses a logarithmic scale for outage probability (y-axis, ranging from 10^{-5} to 10^{0}) and SNR (x-axis, ranging from 0 to 30 dB). The curves compare four scenarios: User n with DF (strong user), User f with DF (weak user), User n with RIS (strong user), and User f with RIS (weak user), with the number of RIS elements set to $N = 16$ and $N = 32$.

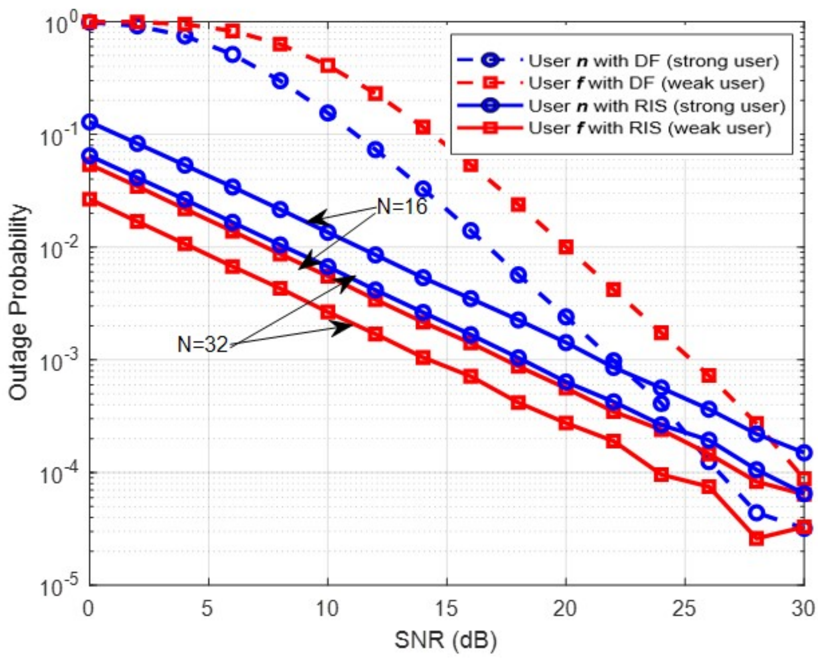

Figure III.7: outage probability of n and f for NOMA with RIS and DF cooperative NOMA.

1)- Key Observations for Outage Probability vs SNR

- **User n with RIS (strong user, solid blue line):**
  - For $N = 16$, the outage probability starts at around 10^{-1} at 0 dB SNR and decreases steadily, reaching approximately $10^{-3.8}$ at 30 dB SNR.
  - For $N = 32$, the outage probability improves, starting at around $10^{-1.4}$ at 0 dB SNR and dropping to around $10^{-4.2}$ at 30 dB SNR.

- **User f with RIS (weak user, solid red line):**
  - For $N = 16$, the outage probability starts at around $10^{-1.5}$ at 0 dB SNR and decreases to approximately $10^{-4.2}$ at 30 dB SNR.
  - For $N = 32$, the outage probability is better, starting at around $10^{-1.7}$ at 0 dB SNR and reaching around $10^{-4.6}$ at 30 dB SNR.
- **User n with DF (strong user, dashed blue line):**
  - The outage probability starts at around 10^0 (1) at 0 dB SNR and decreases gradually, reaching around 10^{-4} at 30 dB SNR.
- **User f with DF (weak user, dashed red line):**
  - The outage probability starts at around 10^0 (1) at 0 dB SNR and decreases slowly, reaching around $10^{-4.5}$ at 30 dB SNR.

2) - Analysis and Interpretation of Results

- **Effect of Number of RIS Elements (N)**
  Increasing the number of RIS elements from $N = 16$ to $N = 32$ significantly reduces the outage probability for both the strong user (n) and weak user (f). For the strong user, the outage probability improves from $10^{-3.8}$ to $10^{-4.2}$ at 30 dB SNR, while for the weak user, it improves from $10^{-4.2}$ to $10^{-4.6}$. This enhancement is due to better beamforming and signal reflection capabilities enabled by additional RIS elements, as described in Section III.5 (Page 53) with the phase shift matrix Φ. The stronger improvement for the weak user (a 0.4-log-unit decrease vs. 0.4 for the strong user) suggests that increasing N is particularly beneficial for mitigating the distance-related channel impairments ($d_{l,f} = 2\,\text{m}$).
- **Comparison of RIS vs. DF Cooperative NOMA**
  At low SNR (0 dB), DF starts with a higher outage probability (10^0) for both users compared to RIS (10^{-1} to $10^{-1.7}$), indicating RIS's initial advantage due to passive reflection in NLoS conditions (Page 48). At 30 dB SNR, the strong user with DF (10^{-4}) performs similarly to RIS with $N = 16$ ($10^{-3.8}$) but is outperformed by RIS with $N = 32$ ($10^{-4.2}$). The weak user with DF ($10^{-4.5}$) is comparable to RIS with $N = 32$ ($10^{-4.6}$), but RIS with $N = 16$ ($10^{-4.2}$) is slightly better than DF at lower N. DF's performance benefits from active relaying and SIC ($\gamma_n^{\text{relay}} = \frac{a_n P_b |h_{b,r}|^2}{\sigma^2}$), while RIS leverages scalable channel optimization (P_{OUT}^n, P_{OUT}^f).

- **Superiority of RIS System**

  The RIS-NOMA system demonstrates scalability with N, achieving outage probabilities as low as $10^{-4.2}$ for the strong user and $10^{-4.6}$ for the weak user at $N = 32$. This aligns with (Page 75-76's) sum capacity analysis, where increasing N enhances effective channel gain ($|h_{b,l}\Phi h_{l,i}|^2$). DF's two-hop transmission (Page 68) limits its ability to scale as effectively, with outage probabilities stabilizing at 10^{-4} and $10^{-4.5}$ for strong and weak users, respectively, due to relay-induced noise and interference.

- **Impact on Weak User (f)**

  The weak user's outage probability ($10^{-4.2}$ to $10^{-4.6}$ with RIS, $10^{-4.5}$ with DF) remains higher than the strong user's, reflecting its greater distance ($d_{l,f} = 2\,\text{m}$) and lower power allocation ($a_f = 0.8$).The improvement with $N = 32$ indicates RIS's ability to mitigate interference (γ_f^{RIS}), though it is still constrained by channel conditions.

III.12.3.2 Simulation Results of the Outage Probability in NOMA Systems:

Analyze the previously attached image, Figure III-8, which presents the outage probability of the NOMA-Aided RIS system compared to the DF cooperative NOMA system with different numbers of RIS elements ($N = 16, 32, 64$). The figure uses a logarithmic scale for outage probability (y-axis, ranging from 10^{-5} to 10^{0}) and SNR (x-axis, ranging from 0 to 30 dB).

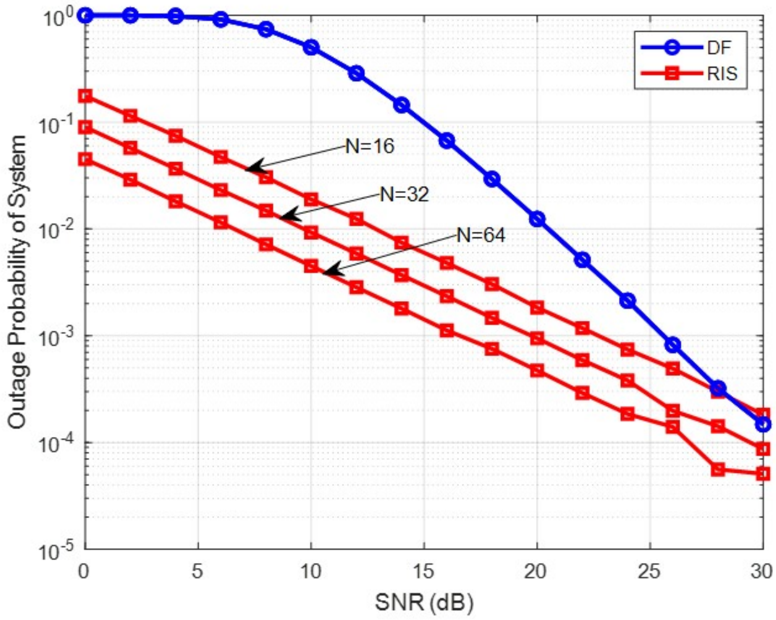

Figure III.8: Outage Probability of NOMA with RIS (16,32,64) elements and DF cooperative NOMA

1)- Key Observations for Outage Probability vs. SNR

- **RIS System (Red Lines)**:
  - For $N = 16$, the system outage probability starts at around $10^{-0.8}$ at 0 dB SNR and decreases steadily, reaching approximately $10^{-3.8}$ at 30 dB SNR.
  - For $N = 32$, the outage probability improves, starting at around $10^{-1.2}$ at 0 dB SNR and dropping to around $10^{-4.2}$ at 30 dB SNR.
  - For $N = 64$, the outage probability is the best among the RIS configurations, starting at around $10^{-1.4}$ at 0 dB SNR and reaching approximately $10^{-4.4}$ at 30 dB SNR.
- **DF Cooperative NOMA System (Blue Line):**
  - The system outage probability starts at around 10^{0} (1) at 0 dB SNR and decreases gradually, reaching around $10^{-3.8}$ at 30 dB SNR.

2)- **Analysis and Interpretation of Results**

- **Effect of Number of RIS Elements** (N)

  Increasing the number of RIS elements from $N = 16$ to $N = 64$ significantly reduces the system outage probability. At 30 dB SNR, the outage probability drops from $10^{-3.8}$ (for $N = 16$) to $10^{-4.4}$ (for $N = 64$), a notable improvement of nearly 0.6 log units. This enhancement aligns with the principles outlined in Section III.5 (Page 53), where the phase shift matrix Φ of the RIS optimizes the effective channel gain ($|h_{b,l}\Phi h_{l,i}|^2$) by adjusting the phase shifts of the reflected signals. More RIS elements enable finer beamforming and better signal reflection, which collectively enhance the SINR for both users (γ_n^{RIS} and γ_f^{RIS}), as seen in the SINR formulations (Pages 54-55). This results in a lower likelihood of outage, particularly at higher SNRs where noise becomes less dominant compared to interference.

- **Comparison of RIS vs. DF Cooperative NOMA**

  The RIS-NOMA system consistently outperforms the DF cooperative NOMA system across all SNR values and for all values of N. At low SNR (0 dB), the RIS system starts with a lower outage probability (10^{-1} to $10^{-1.5}$) compared to DF (10^0), reflecting the advantage of RIS's passive reflection in non-line-of-sight (NLoS) scenarios (Page 48). At 30 dB SNR, the RIS system with $N = 64$ achieves an outage probability of $10^{-4.4}$, which is better than DF's $10^{-3.8}$. Even with $N = 16$, the RIS system ($10^{-3.8}$) still slightly underperforms DF at high SNR (25 dB-30 dB), but the gap narrows as N increases. The DF system benefits from active relaying and successive interference cancellation (SIC), as seen in its SINR equations ($\gamma_n^{\text{relay}} = \frac{a_n P_b |h_{b,r}|^2}{\sigma^2}$), (Page 69), but it is constrained by the two-hop transmission, which introduces a spectral efficiency penalty and additional noise at the relay.

- **Superiority of RIS System**

  The superiority of the RIS-NOMA system is evident in its scalability with N. The outage probability of the system is defined as $P_{\text{out}}^{\text{Sys}} = 1 - (1 - P_{\text{out}}^n)(1 - P_{\text{out}}^f)$ (Page 78), and the improvement with increasing N reflects the enhanced effective channel gain for both near and far users. As noted in the sum capacity analysis (Page 75), the RIS system avoids the spectral efficiency loss inherent in DF's two-hop transmission (a factor of $\frac{1}{2}$, as seen in DF capacity equations on Page 74). Furthermore, the RIS's ability to create a virtual line-of-sight (LoS) link in NLoS environments (Page 52) provides a significant advantage, especially for the far user, who suffers from greater path loss ($d_{l,f} = 2\,\text{m}$). The DF system, while effective in decoding and forwarding, cannot match the RIS's ability to dynamically optimize the propagation environment, leading to higher outage probabilities at all SNRs.

- **Impact of SNR and System Design**

  At low SNRs, the outage probability is high for both systems due to the dominance of noise (σ^2) in the SINR denominators ($\gamma_f^{\text{RIS}} = \frac{a_f P_s |h_{b,l}|^2 \Phi |h_{l,f}|^2}{a_n P_s |h_{b,l}|^2 \Phi |h_{l,f}|^2 + \sigma^2}$) (Page 56). However, as SNR increases, the RIS system benefits more significantly due to its ability to scale with N, reducing the outage probability to as low as $10^{-4.4}$. The DF system, despite improvements at higher SNRs, plateaus around $10^{-3.8}$, limited by the relay's inability to mitigate interference as effectively as RIS. The power allocation strategy ($a_n = 0.2, a_f = 0.8$), (Table III-1, Page 71) also plays a role: the far user benefits from higher power allocation, but the interference term ($a_n P_s |h_{b,l}|^2 \Phi |h_{l,f}|^2$) in the far user's SINR limits further improvements, which RIS mitigates better through phase optimization.

III.12.4 Bit Error Rate:

BER is used to calculate errors that occur in a transmission system, BER is a key parameter used to evaluate systems that transmit digital data from one location to another. In this subsection, we perform the BER simulation of downlink NOMA Aided RIS we compare the BER of our system with downlink DF cooperative NOMA. The BER is obtained by the following formula:

$$\text{BER} = \frac{\text{Number of erroneous bits}}{\text{Number of total bits transmitted}} \tag{III.78}$$

III.12.4.1 Simulation Results of Bit Error Rate:

Figure III.9 the Bit Error Rate (BER) of near user n (strong user) and far user f (weak user) for both NOMA with RIS and DF cooperative NOMA systems as a function of Signal-to-Noise Ratio (SNR) in dB. The y-axis uses a logarithmic scale for BER, ranging from 10^{-5} to 10^{0}, and the x-axis represents SNR from 0 to 30 dB. The curves compare four scenarios: User n with DF, User f with DF, User n with RIS, and User f with RIS, with the number of RIS elements set to $N = 16$ and $N = 32$.

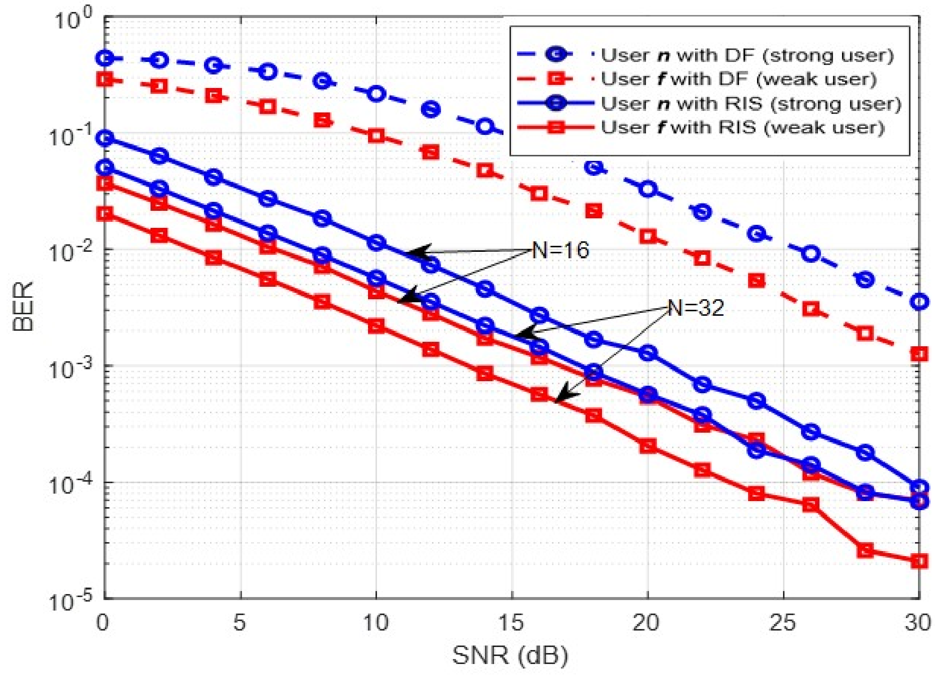

Figure III.9: BER of n and f for NOMA with RIS and DF cooperative NOMA.

1)- Key Observations for Bit Error Rate (BER) vs SNR

- **User n with RIS (strong user, solid blue line):**
  - For $N = 16$, the BER starts at around 10^{-1} at 0 dB SNR and decreases steadily, reaching approximately $10^{-4.1}$ at 30 dB SNR.
  - For $N = 32$, the BER improves, starting at around $10^{-1.3}$ at 0 dB SNR and dropping to around $10^{-4.3}$ at 30 dB SNR.
- **User f with RIS (weak user, solid red line):**
  - For $N = 16$, the BER starts at around $10^{-1.4}$ at 0 dB SNR and decreases to approximately $10^{-4.3}$ at 30 dB SNR.
  - For $N = 32$, the BER is better, starting at around $10^{-1.5}$ at 0 dB SNR and reaching around $10^{-4.6}$ at 30 dB SNR.
- **User n with DF (strong user, dashed blue line):**
  - The BER starts at around $10^{-0.4}$ at 0 dB SNR and decreases gradually, reaching around $10^{-2.4}$ at 30 dB SNR.
- User f with DF (weak user, dashed red line):
  - The BER starts at around $10^{-0.5}$ at 0 dB SNR and decreases slowly, reaching around $10^{-2.9}$ at 30 dB SNR.

2)-Analysis and Interpretation of Results

- **Effect of Number of RIS Elements (N):** Increasing the number of RIS elements from $N = 16$ to $N = 32$ significantly reduces the BER for both the strong user n and weak user f. For the strong user, the BER improves from $10^{-4.1}$ to $10^{-4.3}$ at 30 dB SNR, and for the weak user, it improves from $10^{-4.3}$ to $10^{-4.6}$. This improvement stems from the enhanced beamforming and signal reflection capabilities of the RIS, as additional elements allow better phase alignment (Section III.5, Page 53), increasing the composite channel gain $|h_{b,i}\Phi h_{i,n}|^2$.

- **Comparison of RIS vs. DF Cooperative NOMA:**
  - At low SNR (0 dB), the DF system exhibits a higher BER ($10^{-0.4}$) for strong user, is also outperformed compared to the RIS with $N = 16$ (10^{-1}) and $N = 32$ ($10^{-1.3}$)., for the weak user in (0 dB), the DF system exhibits a higher BER ($10^{-0.5}$) is also outperformed compared to the RIS with $N = 16$ ($10^{-1.4}$) and $N = 32$ ($10^{-1.5}$). highlighting the RIS's advantage in non-line-of-sight (NLoS) conditions through passive reflection (Page 53).
  - At 30 dB SNR, the strong user with DF ($10^{-2.4}$) is outperformed by RIS with $N = 16$ ($10^{-4.1}$) and $N = 32$ ($10^{-4.3}$). The weak user with DF ($10^{-2.9}$) is also outperformed by RIS with $N = 16$ ($10^{-4.3}$) and $N = 32$ ($10^{-4.6}$). The RIS system benefits from scalable channel optimization, while DF's performance is limited by two-hop transmission and relay-induced noise (Page 72).

III.12.4.2 Simulation Results of the Bit Error Rate in NOMA Systems:

Analyze the figure, which corresponds to Figure III-10; This figure presents the Bit Error Rate (BER) of the NOMA-Aided RIS system compared to the DF cooperative NOMA system with different numbers of RIS elements ($N = 16, 32, 64$). The figure uses a logarithmic scale for BER (y-axis, ranging from 10^{-5} to 10^{0}) and SNR (x-axis, ranging from 0 to 30 dB).

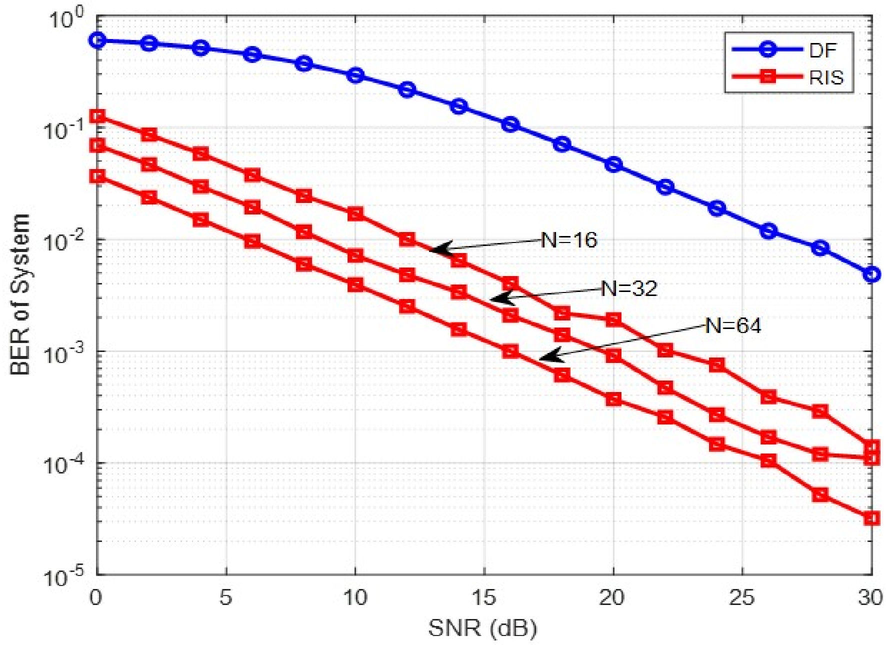

Figure III.10: BER of NOMA with RIS and DF cooperative NOMA with different number of RIS elements (N=16, 32, 64).

1)- **Key Observations for BER vs. SNR**

- **RIS System (Red Lines):**
  - For $N = 16$, the BER starts at around 10^{-1} at 0 dB SNR and decreases steadily, reaching approximately $10^{-3.9}$ at 30 dB SNR.
  - For $N = 32$, the BER improves, starting at around $10^{-1.2}$ at 0 dB SNR and dropping to around 10^{-4} at 30 dB SNR.
  - For $N = 64$, the BER is the best among the RIS configurations, starting at around $10^{-1.5}$ at 0 dB SNR and reaching approximately $10^{-4.8}$ at 30 dB SNR.
- **DF Cooperative NOMA System (Blue Line):**
  - The BER starts at around $10^{-0.3}$ at 0 dB SNR and decreases gradually, reaching around $10^{-2.5}$ at 30 dB SNR.

d) **Analysis and Interpretation of Results**

- **Effect of Number of RIS Elements** (N) Increasing the number of RIS elements from $N = 16$ to $N = 64$ significantly reduces the system BER. At 30 dB SNR, the BER improves from $10^{-3.9}$ (for $N = 16$) to $10^{-4.8}$ (for $N = 64$), a notable enhancement of nearly 0.9 log units. This improvement is consistent with the principles outlined in Section III.5 (Page 53), where the phase shift matrix Φ of the RIS optimizes the effective channel gain ($|h_{b,l}\Phi h_{l,i}|^2$) by adjusting the phase shifts of the reflected signals. More RIS elements enable finer beamforming and better signal reflection, which enhance the SINR for both near and far users (γ_n^{RIS} and γ_f^{RIS}), as derived in Sections III.6 (Pages 54-55). A higher SINR directly correlates with a lower BER, as the probability of erroneous bit detection decreases with improved signal quality.

- **Comparison of RIS vs. DF Cooperative NOMA** The RIS-NOMA system consistently outperforms the DF cooperative NOMA system in terms of BER across all SNR values and for all values of N. At low SNR (0 dB), the RIS system starts with a lower BER (10^{-1} to $10^{-1.5}$) compared to DF ($10^{-0.3}$), reflecting the advantage of RIS's passive reflection in non-line-of-sight (NLoS) scenarios . At 30 dB SNR, the RIS system with $N = 64$ achieves a BER of $10^{-4.8}$, significantly better than DF's $10^{-2.5}$. Even with $N = 16$, the RIS system ($10^{-3.9}$) outperforms DF, highlighting the scalability of RIS with increasing N. The DF system benefits from active relaying and successive interference cancellation (SIC), as seen in its SINR equations ($\gamma_n^{\text{relay}} = \frac{a_n P_b |h_{b,r}|^2}{\sigma^2}$), (Page 69), but it is limited by the two-hop transmission, which introduces additional noise and interference at the relay, degrading its BER performance compared to the single-hop RIS system.

- **Superiority of RIS System** The RIS-NOMA system demonstrates superior BER performance due to its ability to dynamically optimize the propagation environment. The BER is defined as $\text{BER} = \frac{\text{Number of erroneous bits}}{\text{Number of total bits transmitted}}$ (Page 60), and the analytical expressions for BER in Section III.9 (Pages 60-61) show that it is heavily influenced by the SINR. For the near user, the BER is derived as $P_{b,n} = \frac{1}{\sqrt{\pi}\Gamma(m_n)} \mathcal{G}_{2,2}^{2,1}\left(\frac{\bar{\gamma}_n}{m_n} \middle| \begin{matrix} 1-m_n, 1 \\ 0, 1/2 \end{matrix} \right)$, where $\bar{\gamma}_n = a_n \zeta_N \Omega_n$ (Page 62), and a similar approach applies to the far user. The RIS system's ability to enhance the effective channel gain through the phase shift matrix Φ (Page 53) directly improves $\bar{\gamma}_n$ and $\bar{\gamma}_f$, leading to a lower BER. In contrast, the DF system's two-hop transmission (Page 72) introduces a spectral efficiency penalty and additional noise, as reflected in its capacity equations , which indirectly impacts its BER performance by limiting the SINR.

- **Impact of SNR and System Design** At low SNRs, the BER is high for both systems due to the dominance of noise (σ^2) in the SINR denominators

($\gamma_f^{\text{RIS}} = \frac{a_f P_s |h_{b,l}|^2 \Phi |h_{l,f}|^2}{a_n P_s |h_{b,l}|^2 \Phi |h_{l,f}|^2 + \sigma^2}$), (Page 67). However, as SNR increases, the RIS system benefits more significantly due to its scalability with N, reducing the BER to as low as $10^{-4.8}$. The DF system, despite improvements at higher SNRs, plateaus around $10^{-2.5}$, limited by the relay's inability to mitigate interference as effectively as RIS. The power allocation strategy ($a_n = 0.2, a_f = 0.8$, Table III-1, Page 71) also influences BER: the far user benefits from higher power allocation, but the interference term ($a_n P_s |h_{b,l}|^2 \Phi |h_{l,f}|^2$) in the far user's SINR limits further improvements, which RIS mitigates better through phase optimization.

III.13 Conclusion

This chapter has provided a comprehensive performance analysis of RIS-aided NOMA systems, demonstrating their potential to significantly enhance wireless communication in challenging propagation environments. Through the development of a detailed system model incorporating Nakagami-m fading channels, we derived closed-form expressions for outage probability, sum system capacity, and bit error rate, validated by extensive computer simulations. The results reveal that the RIS-NOMA system consistently outperforms the benchmark DF cooperative NOMA system across all evaluated metrics, particularly as the number of RIS elements increases. The ability of RIS to optimize the propagation environment through phase shift adjustments enables substantial improvements in effective channel gain, leading to lower outage probabilities (down to $10^{-4.4}$ for $N = 64$ at 30 dB SNR), higher sum capacities (up to 15 bits/sec/Hz), and reduced bit error rates (down to $10^{-4.8}$). The scalability of RIS with increasing elements highlights its advantage over traditional relaying techniques, which are constrained by spectral efficiency losses in two-hop transmissions. However, challenges such as successive interference cancellation complexity, optimal power allocation, and practical RIS deployment remain critical areas for further investigation. These findings underscore the transformative potential of RIS-NOMA systems in improving coverage, connectivity, and energy efficiency, paving the way for their adoption in next-generation wireless networks. Future research should focus on optimizing beamforming techniques, integrating multi-antenna configurations, and developing energy-efficient RIS solutions to ensure scalable and practical deployments.

General Conclusion

This dissertation provided a comprehensive exploration of the technical evolution of mobile networks, tracing their progression from the rudimentary analog systems of the first generation (1G) to the sophisticated, AI-driven architectures of the fifth generation (5G), while also delving into the transformative potential of emerging sixth-generation (6G) and visionary seventh-generation (7G) networks. Through a systematic analysis, the study elucidated the advancements in key performance indicators (KPIs) such as data rates, latency, spectral efficiency, connection density, and reliability across each generation, highlighting the pivotal role of technological innovations in shaping modern wireless communications.

Chapter I meticulously chronicled the historical development of mobile networks, detailing the transition from analog voice-centric 1G systems to the high-speed, low-latency, and IoT-enabled 5G networks. It further provided an in-depth examination of 6G technologies, including terahertz (THz) communications, reconfigurable intelligent surfaces (RIS), integrated sensing and communication (ISAC), and advanced multiple access techniques such as non-orthogonal multiple access (NOMA). The chapter also offered a forward-looking perspective on 7G, envisioning quantum communication, molecular signaling, and neuromorphic computing as cornerstones of future networks. This chronological analysis underscored the relentless pursuit of enhanced connectivity and the challenges that accompany each generational leap, such as spectrum management, infrastructure costs, and energy efficiency.

Chapter II focused on the theoretical underpinnings of RIS, NOMA, and statistical fading models, emphasizing their significance in addressing the challenges of spectrum scarcity and signal propagation in complex environments. The exploration of metamaterials and their electromagnetic properties provided a foundation for understanding

RIS, which emerged as a transformative technology for optimizing signal propagation through dynamic phase adjustments. The integration of RIS with NOMA was analyzed, highlighting its potential to enhance spectral efficiency and connectivity in next-generation networks. Statistical fading models, such as Nakagami-m, were examined to provide insights into the stochastic nature of wireless channels, further enriching the theoretical framework. Chapter III presented a rigorous performance analysis of RIS-aided NOMA systems, employing Nakagami-m fading channels to derive closed-form expressions for outage probability, sum system capacity, and bit error rate (BER). The results demonstrated that RIS-NOMA systems consistently outperformed decode-and-forward (DF) cooperative NOMA systems across all evaluated metrics. Notably, increasing the number of RIS elements significantly enhanced channel gain, reducing outage probabilities to as low as $10^{-4.4}$ and BER to $10^{-4.8}$ at 30 dB SNR for $N = 64$, while achieving sum capacities up to 15 bits/s/Hz. These findings underscored the scalability and efficacy of RIS in mitigating interference and optimizing propagation environments, particularly in non-line-of-sight (NLoS) scenarios.

In conclusion, this dissertation highlighted the transformative impact of RIS and NOMA in advancing wireless communication systems, offering substantial improvements in performance metrics critical to next-generation networks. The study also illuminated the challenges that remain, including the complexity of successive interference cancellation, optimal power allocation, and practical RIS deployment. These findings pave the way for future research into scalable, energy-efficient solutions and the integration of multi-antenna configurations to realize the full potential of 6G and beyond. By providing a holistic understanding of mobile network evolution and the role of emerging technologies, this work contributed to the academic discourse on intelligent, immersive, and globally connected communication systems.

Bibliography

[1] J. G. Andrews, S. Buzzi, W. Choi, *et al.*, “What will 5G be?” *IEEE Journal on Selected Areas in Communications*, vol. 32, no. 6, pp. 1065–1082, Jun. 2014.

[2] M. Shafi *et al.*, “5G: A tutorial overview of standards, trials, challenges, deployment, and practice,” *IEEE Journal on Selected Areas in Communications*, vol. 35, no. 6, pp. 1201–1221, Jun. 2017.

[3] T. S. Rappaport, Y. Xing, O. Kanhere, *et al.*, “Wireless communications and applications above 100 GHz: Opportunities and challenges for 6G and beyond,” *IEEE Access*, vol. 7, pp. 78 729–78 757, 2019.

[4] S. J. Nawaz, S. K. Sharma, S. Wyne, M. N. Patwary, and M. Asaduzzaman, “Quantum machine learning for 6G communication networks: State-of-the-art and vision for the future,” *IEEE Access*, vol. 7, pp. 46 317–46 350, 2019.

[5] A. Goldsmith, *Wireless Communications*. Cambridge, UK: Cambridge University Press, 2005.

[6] T. S. Rappaport, *Wireless Communications: Principles and Practice*. Upper Saddle River, NJ, USA: Prentice Hall, 1996.

[7] A. F. Molisch, *Wireless Communications*, 2nd ed. Chichester, UK: Wiley, 2011.

[8] J. Cai and D. J. Goodman, “General packet radio service in GSM,” *IEEE Communications Magazine*, vol. 35, no. 10, pp. 122–131, Oct. 1997.

[9] A. Furuskär, S. Parkvall, M. Persson, and M. Samuelsson, “Performance of EDGE in various environments,” pp. 1413–1417, Apr. 2003.

[10] J. Eberspächer, H.-J. Vögel, and C. Bettstetter, *GSM: Architecture, Protocols and Services*. Chichester, UK: Wiley, 2001.

[11] H. Holma and A. Toskala, *WCDMA for UMTS: HSPA Evolution and LTE*, 4th ed. Chichester, UK: Wiley, 2007.

[12] H. Kaaranen, A. Ahtiainen, L. Laitinen, S. Naghi, and V. Niemi, *UMTS Networks: Architecture, Mobility and Services*, 2nd ed. Chichester, UK: Wiley, 2005.

[13] E. Dahlman, S. Parkvall, and J. Sköld, *4G: LTE/LTE-Advanced for Mobile Broadband*. Oxford, UK: Academic Press, 2011.

[14] S. Sesia, I. Toufik, and M. Baker, *LTE – The UMTS Long Term Evolution: From Theory to Practice*, 2nd ed. Chichester, UK: Wiley, 2011.

[15] S. Parkvall, E. Dahlman, A. Furuskär, and M. Frenne, "NR: The new 5G radio access technology," *IEEE Communications Standards Magazine*, vol. 1, no. 4, pp. 24–30, Dec. 2017.

[16] S. Rommer, P. Hedman, M. Olsson, L. Fridh, S. Sultan, and C. Mulligan, *5G Core Networks: Powering Digitalization*. London, UK: Academic Press, 2020.

[17] W. Saad, M. Bennis, and M. Chen, "A vision of 6G wireless systems: Applications, trends, technologies, and open research problems," *IEEE Network*, vol. 34, no. 3, pp. 134–142, May 2020.

[18] M. Katz, P. Pirinen, and H. Posti, "Towards 6G: Getting ready for the next generation," in *Proceedings of the 6G Wireless Summit*, Mar. 2019, pp. 1–5.

[19] P. Yang, Y. Xiao, M. Xiao, and S. Li, "6G wireless communications: Vision and potential techniques," *IEEE Network*, vol. 34, no. 4, pp. 70–75, Jul. 2020.

[20] 3GPP, "Release 19 overview," 3rd Generation Partnership Project, Tech. Rep., 2024. [Online]. Available: `https://www.3gpp.org/release-19`.

[21] J. Zhang, E. Björnson, M. Matthaiou, D. W. K. Ng, H. Yang, and D. J. Love, "Prospective multiple antenna technologies for beyond 5G," *IEEE Journal on Selected Areas in Communications*, vol. 38, no. 8, pp. 1637–1660, Aug. 2020.

[22] K. B. Letaief, W. Chen, Y. Shi, J. Zhang, and Y.-J. Zhang, "The roadmap to 6G: AI empowered wireless networks," *IEEE Communications Magazine*, vol. 57, no. 8, pp. 84–90, Aug. 2019.

[23] M. Chen, W. Saad, and C. Yin, "Liquid state machine learning for resource and power allocation in 6G networks," *IEEE Journal on Selected Areas in Communications*, vol. 39, no. 6, pp. 1717–1730, Jun. 2021.

[24] ITU-R, "Framework and overall objectives of the future development of IMT for 2030 and beyond," ITU-R, Tech. Rep. M.2516-0, Jun. 2023. [Online]. Available: `https://www.itu.int/pub/R-REP-M.2516`.

[25] M. Z. Chowdhury, M. Shahjalal, S. Ahmed, and Y. M. Jang, "6G wireless communication systems: Applications, requirements, technologies, challenges, and research directions," *IEEE Open Journal of the Communications Society*, vol. 1, pp. 957–975, 2020.

[26] F. Liu, Y. Cui, C. Masouros, *et al.*, "Integrated sensing and communications: Towards dual-functional wireless networks for 6G and beyond," *IEEE Journal on Selected Areas in Communications*, vol. 40, no. 6, pp. 1728–1767, Jun. 2022.

[27] H. Q. Ngo, A. Ashikhmin, H. Yang, E. G. Larsson, and T. L. Marzetta, "Cell-free massive MIMO versus small cells," *IEEE Transactions on Wireless Communications*, vol. 16, no. 3, pp. 1834–1850, Mar. 2017.

[28] H. Haas, L. Yin, Y. Wang, and C. Chen, "What is LiFi?" *Journal of Lightwave Technology*, vol. 34, no. 6, pp. 1533–1544, Mar. 2016.

[29] E. G. Larsson, O. Edfors, F. Tufvesson, and T. L. Marzetta, "Massive MIMO for next generation wireless systems," *IEEE Communications Magazine*, vol. 52, no. 2, pp. 186–195, Feb. 2014.

[30] E. Basar, M. Di Renzo, J. De Rosny, M. Debbah, M.-S. Alouini, and R. Zhang, "Wireless communications through reconfigurable intelligent surfaces," *IEEE Access*, vol. 7, pp. 116 753–116 773, 2019.

[31] Y. Mao, B. Clerckx, and V. O. Li, "Rate-splitting multiple access for downlink communication systems: Bridging, generalizing, and outperforming SDMA and NOMA," *EURASIP Journal on Wireless Communications and Networking*, vol. 2018, no. 1, pp. 1–33, May 2018.

[32] Y. Liu, Z. Qin, M. Elkashlan, Z. Ding, A. Nallanathan, and L. Hanzo, "Non-orthogonal multiple access for 5G and beyond," *Proceedings of the IEEE*, vol. 105, no. 12, pp. 2347–2381, Dec. 2017.

[33] H. Nikopour and H. Baligh, "Sparse code multiple access," in *Proceedings of the IEEE International Symposium on Personal, Indoor and Mobile Radio Communications*, Sep. 2013, pp. 332–336.

[34] N. Gisin, G. Ribordy, W. Tittel, and H. Zbinden, "Quantum cryptography," *Reviews of Modern Physics*, vol. 74, no. 1, pp. 145–195, Mar. 2002.

[35] N. Yang, L. Wang, G. Geraci, M. Elkashlan, J. Yuan, and M. Di Renzo, "Safeguarding 5G wireless communication networks using physical layer security," *IEEE Communications Magazine*, vol. 53, no. 4, pp. 20–27, Apr. 2015.

[36] I.-C. Lin and T.-C. Liao, "A survey of blockchain security issues and challenges," *International Journal of Network Security*, vol. 19, no. 5, pp. 653–659, Sep. 2017.

[37] A. L. Buczak and E. Guven, "A survey of data mining and machine learning methods for cyber security intrusion detection," *IEEE Communications Surveys Tutorials*, vol. 18, no. 2, pp. 1153–1176, 2016.

[38] ITU-R, "Minimum requirements related to technical performance for IMT-2020 radio interface(s)," ITU-R, Tech. Rep. M.2410-0, Nov. 2017. [Online]. Available: `https://www.itu.int/pub/R-REP-M.2410`.

[39] NextG Alliance, "6G roadmap: North american perspective," NextG Alliance, Tech. Rep., 2021. [Online]. Available: `https://www.nextgalliance.org/white-papers/`.

[40] I. F. Akyildiz, J. M. Jornet, and C. Han, "Terahertz band: Next frontier for wireless communications," *Physical Communication*, vol. 12, pp. 16–32, Sep. 2014.

[41] T. Nakamura, Y. Nagata, and M. Nakamura, "Brain-computer interfaces in the context of neurotechnology," *IEEE Transactions on Neural Systems and Rehabilitation Engineering*, vol. 25, no. 7, pp. 1132–1142, Jul. 2017.

[42] Y. Yan, G. Xie, M. D. Lavery, *et al.*, "High-capacity millimetre-wave communications with orbital angular momentum multiplexing," *Nature Communications*, vol. 5, no. 4876, Sep. 2014.

[43] S. Kinoshita, *Bionanophotonics - An Introductory Textbook*. Singapore: Pan Stanford, 2016. DOI: `10.1201/9780429068638`.

[44] M. D. Renzo, A. Zappone, M. Debbah, *et al.*, "Smart radio environments empowered by reconfigurable intelligent surfaces: How it works, state of research, and the road ahead," *IEEE Journal on Selected Areas in Communications*, vol. 38, no. 11, pp. 2450–2525, 2020. DOI: `10.1109/JSAC.2020.3007211`.

[45] M. Jian, G. C. Alexandropoulos, E. Basar, *et al.*, "Reconfigurable intelligent surfaces for wireless communications: Overview of hardware designs, channel models, and estimation techniques," *arXiv preprint arXiv:2203.03176*, 2022. DOI: 10.48550/arXiv.2203.03176.

[46] C. Huang, S. Hu, G. C. Alexandropoulos, *et al.*, "Holographic mimo surfaces for 6g wireless networks: Opportunities, challenges, and trends," *IEEE Wireless Communications*, vol. 27, no. 5, pp. 118–125, 2020. DOI: 10.1109/MWC.001.1900534.

[47] E. Björnson, H. Wymeersch, B. Matthiesen, P. Popovski, L. Sanguinetti, and E. de Carvalho, "Communication models for reconfigurable intelligent surfaces: From surface electromagnetics to wireless networks optimization," *Proceedings of the IEEE*, vol. 110, no. 9, pp. 1169–1190, 2022. DOI: 10.1109/JPROC.2022.3195506.

[48] H. Zhang, B. Di, L. Song, and Z. Han, *Reconfigurable Intelligent Surface-Empowered 6G*. Cham, Switzerland: Springer, 2021. DOI: 10.1007/978-3-030-73499-2.

[49] G. C. Alexandropoulos, D.-T. Phan-Huy, K. D. Katsanos, M. Crozzoli, and H. Wymeersch, "Ris-enabled smart wireless environments: Deployment scenarios, network architecture, bandwidth and area of influence," *EURASIP Journal on Wireless Communications and Networking*, vol. 2023, no. 1, pp. 1–38, 2023. DOI: 10.1186/s13638-023-02248-8.

[50] H. Zhang, B. Di, L. Song, and Z. Han, *Reconfigurable Intelligent Surface-Empowered 6G*. Cham, Switzerland: Springer, 2021. DOI: 10.1007/978-3-030-73499-2.

[51] Y. Liu, X. Liu, X. Mu, *et al.*, "Reconfigurable intelligent surfaces: Principles and opportunities," *IEEE Communications Surveys & Tutorials*, vol. 23, no. 3, pp. 1546–1577, 2021. DOI: 10.1109/COMST.2021.3077737.

[52] E. Basar, M. D. Renzo, J. de Rosny, M. Debbah, M.-S. Alouini, and R. Zhang, "Wireless communications through reconfigurable intelligent surfaces," *IEEE Access*, vol. 7, pp. 116 753–116 773, 2019. DOI: 10.1109/ACCESS.2019.2935192.

[53] Q. Wu and R. Zhang, "Towards smart and reconfigurable environment: Intelligent reflecting surface aided wireless network," *IEEE Communications Magazine*, vol. 58, no. 1, pp. 106–112, 2020. DOI: 10.1109/MCOM.001.1900107.

[54] H. Arslan, *Wireless Communication Signals*. Hoboken, NJ, USA: Wiley, 2021. DOI: 10.1002/9781119764441.

[55] A. M. T. Khel, "Design and analysis of next generation wireless communication networks," Ph.D. dissertation, The University of Manchester (United Kingdom), 2024.

[56] A. Maaref and S. Aissa, "Exact error probability analysis of orthogonal space-time block codes with arbitrary rectangular qam over mimo nakagami-m fading channels," in *2007 IEEE Wireless Communications and Networking Conference*, Kowloon, Hong Kong, 2007, pp. 445–450. DOI: 10.1109/WCNC.2007.88.

[57] Z. Ding, X. Lei, G. K. Karagiannidis, R. Schober, J. Yuan, and V. K. Bhargava, "A survey on non-orthogonal multiple access for 5g networks: Research challenges and future trends," *IEEE Journal on Selected Areas in Communications*, vol. 35, no. 10, pp. 2181–2195, 2017. DOI: 10.1109/JSAC.2017.2725519.

[58] X. Xie, "Optimisation in noma wireless communication networks," Ph.D. dissertation, The University of Manchester, Manchester, UK, 2024.

[59] S. Devipriya and J. M. L. Manickam, "Outage performance and ergodic capacity of user pairing in downlink mimo-noma systems with imperfect sic over nakagami-m fading channels," *IETE Journal of Research*, vol. 69, no. 12, pp. 8769–8783, 2023. DOI: 10.1080/03772063.2022.2136954.

[60] H. Marshoud, V. M. Kapinas, G. K. Karagiannidis, and S. Muhaidat, "Non-orthogonal multiple access for visible light communications," *IEEE Photonics Technology Letters*, vol. 28, no. 1, pp. 51–54, 2016. DOI: 10.1109/LPT.2015.2479600.

[61] A. Goldsmith, "Wireless communications," 2005.

[62] T. S. Rappaport, *Wireless Communications: Principles and Practice*, 2nd. Prentice Hall, 2002.

[63] M. K. Simon and M.-S. Alouini, *Digital Communication over Fading Channels*, 2nd. John Wiley & Sons, 2005.

[64] R. H. Clarke, "A statistical theory of mobile-radio reception," *Bell System Technical Journal*, vol. 47, no. 6, pp. 957–1000, 1968.

[65] W. C. Y. Lee, *Mobile Communications Engineering: Theory and Applications*, 2nd. McGraw-Hill, 1998.

[66] S. O. Rice, “Mathematical analysis of random noise,” *Bell System Technical Journal*, vol. 23, no. 3, pp. 282–332, 1944.

[67] A. Abdi and M. Kaveh, “A space-time correlation model for multielement antenna systems in mobile fading channels,” *IEEE Journal on Selected Areas in Communications*, vol. 20, no. 3, pp. 550–560, 2002.

[68] M. D. Yacoub, *Foundations of Mobile Radio Engineering*. CRC Press, 1993.

[69] M. Nakagami, “The m-distribution—a general formula of intensity distribution of rapid fading,” *Statistical Methods in Radio Wave Propagation*, pp. 3–36, 1960.

[70] M. K. Simon and M.-S. Alouini, *Digital Communication Techniques: Signal Design and Detection*. Prentice Hall, 2000.

[71] G. K. Karagiannidis, N. C. Sagias, and P. T. Mathiopoulos, “Nnakagami: A novel stochastic model for cascaded fading channels,” *IEEE Transactions on Communications*, vol. 55, no. 8, pp. 1453–1458, 2007.

[72] D. I. Laurenson, G. J. R. Povey, and P. M. Grant, “Nakagami-m approximations to the sum of m non-identical squared correlated nakagami-m variates and applications in wireless communications,” *IEEE Transactions on Communications*, vol. 56, no. 3, pp. 378–386, 2008.

[73] A.-T. Le, N.-D. X. Ha, D.-T. Do, A. Silva, and S. Yadav, “Enabling user grouping and fixed power allocation scheme for reconfigurable intelligent surfaces-aided wireless systems,” *IEEE Access*, vol. 9, pp. 92 263–92 275, 2021.

[74] C. Zhang, W. Yi, Y. Liu, K. Yang, and Z. Ding, “Reconfigurable intelligent surfaces aided multi-cell noma networks: A stochastic geometry model,” *IEEE Transactions on Communications*, vol. 70, no. 2, pp. 951–966, 2021.

[75] A. Hemanth, K. Umamaheswari, A. C. Pogaku, D.-T. Do, and B. M. Lee, “Outage performance analysis of reconfigurable intelligent surfaces-aided noma under presence of hardware impairment,” *IEEE Access*, vol. 8, pp. 212 156–212 165, 2020.

[76] S. Yang, J. Zhang, Y. Zhu, S. Jin, and C. Yuen, “The application of distributed ris to massive access miso systems: Noma or oma?” *IEEE Transactions on Wireless Communications*, 2024.

[77] C. Pan, H. Ren, K. Wang, J. F. Kolb, *et al.*, "Reconfigurable intelligent surfaces for 6g systems: Principles, applications, and research directions," *IEEE Communications Magazine*, 2021.

[78] M.-S. Van Nguyen, D.-T. Do, P. T. Tin, A. L. Imoize, and V. B. Kumaravelu, "Full duplex reconfigurable intelligent surfaces system relying on noma and wireless power transfer," *Wireless Networks*, vol. 30, no. 4, pp. 2127–2142, 2024.

[79] Y. Cheng, K. H. Li, Y. Liu, K. C. Teh, and H. V. Poor, "Downlink and uplink intelligent reflecting surface aided networks: Noma and oma," *IEEE Transactions on Wireless Communications*, 2021.

[80] J. Zuo, Y. Liu, and N. Al-Dhahir, "Reconfigurable intelligent surface assisted cooperative non-orthogonal multiple access systems," *IEEE Transactions on Communications*, vol. 69, no. 10, pp. 6750–6764, 2021.

[81] M. Jain, S. Soni, N. Sharma, and D. Rawal, "Performance analysis at far and near user in noma based system in presence of sic error," *AEU-International Journal of Electronics and Communications*, vol. 114, p. 152 993, 2020.

[82] S. Mounchili and S. Hamouda, "Pairing distance resolution and power control for massive connectivity improvement in noma systems," *IEEE Transactions on Vehicular Technology*, vol. 69, no. 4, pp. 4093–4103, 2020.

[83] M. Munochiveyi, A. C. Pogaku, D.-T. Do, A.-T. Le, M. Voznak, and N. D. Nguyen, "Reconfigurable intelligent surface aided multi-user communications: State-of-the-art techniques and open issues," *IEEE Access*, vol. 9, pp. 118 584–118 605, 2021.

[84] C. Kumaradasa, "Performance evaluation of hybrid ris-aided noma network," Master's thesis, University of Oulu, Oulu, Finland, Jun. 2024, p. 50.

[85] X. Zhu, C. Jiang, L. Kuang, N. Ge, and J. Lu, "Non-orthogonal multiple access based integrated terrestrial-satellite networks," *IEEE Journal on Selected Areas in Communications*, 2017.